AN EXPERIMENTAL INVESTIGATION OF LIQUID MIXING
ON A NONIDEAL SIEVE TRAY

763

by

TSUNG-WEN LEE

B. S., National Taiwan University, Taiwan, China, 1962

A MASTER'S THESIS

submitted in partial fulfillment of the

requirements for the degree

MASTER OF SCIENCE

Department of Chemical Engineering

KANSAS STATE UNIVERSITY
Manhattan, Kansas

1967

Approved by:

Major Professor

TABLE OF CONTENTS

CHAPTER I

INTRODUCTION

Problems related to liquid mixing in various systems have attracted the interest of many researchers. While the importance of the mixing mechanism has been recognized, knowledge of the mechanism has not been extensively developed. There has been great impetus for further study of liquid mixing, because a thorough understanding of the mixing mechanism within a system of mass transfer or chemical reaction is helpful in successful design, operation, and control. Liquid mixing on distillation trays is so important that neglecting it often brings about an appreciable error in the prediction of Murphree efficiency and thus leads to poor design of the distillation column.

This work, a continuation of previous work (1), presents results of a study of liquid mixing on a non-ideal sieve tray. The term "non-ideal sieve tray" is used here to distinguish it from a commercial sieve tray. This tray has fewer holes or a smaller percentage of free area than commercial ones. The use of such a tray may enable one to develop a clearer physical picture of fundamental mechanism of flow patterns.

Since Danckwerts (2) introduced the concept of age distribution analysis to the study of flow systems, much work has been based on this concept. Danckwerts originated the use of two probability functions, the exit age distribution and the internal age distribution function. The present study of liquid mixing on a distillation tray uses these two functions which are discussed in detail in Chapter 3. Noar and Shinnar (3) employed the intensity function, which represents another approach to the study of fluid mixing.

Due to the complexity of the distillation tray system, an analytic

solution of the governing equation for liquid mixing in the system is very difficult, if not impossible, to obtain. The approximate solution is based on the fact that the extent of actual mixing lies between two extreme modes. These two extreme modes are represented by the two models: the plug flow model and the backmix (completely stirred) model. The combined model which describes the actual mixing is made by series, parallel, or series-parallel combination of these two extreme models and is usually modified, for instance, by a bypassing stream or a dead region. The proposed models are developed in the above way to fit the experimental data.

The overall intent of this work was to lay the foundation for a comprehensive investigation of liquid mixing on the non-ideal sieve tray. The specific purposes of the work carried out here were the following:

(1) To develop an experimental procedure for the pulse testing technique by using the conductivity method.

(2) To develop flow patterns in order to obtain a qualitative picture of their effects on liquid mixing by means of a photographic technique and visual observation.

(3) To detect the possible existence of the stratification effect in the system and the extent to which it may disappear.

(4) To suggest a technique or new method of monitoring a tracer in case the stratification does exist.

The pulse testing technique measures mainly the concentration-time curves at the inlet and at the outlet of the system. The concentrations across the inlet and the outlet may be non-uniform due to the stratified streams which occur in the system. The nonuniformity of concentrations across any cross-sections may affect the degree of mixing and model

parameters. For this reason, the effect of those stratified streams or the effect of stratification (bulk segregation) on the degree of liquid mixing needs to be investigated. The detection of the stratification effect in the system was done qualitatively by photography and by visual observation. A quantitative measurement of this effect has been carried out experimentally.

In general, the major accomplishment of this research was the establishment of the equipment and instrumentation, followed by a primary detection of stratification effect; a minor contribution was a statistically designed plan to obtain experimentally the model parameters.

CHAPTER II

STRATIFICATION EFFECT

As has been pointed out by Bell and Babb (4), the effect of flow stratification is important in monitoring tracer experiments. There are two ways of monitoring tracer experiments. One of these is to place a detector either at the wall or in the inner part of the vessel in such a way that it monitors the average or mixing cup concentration of the vessel contents in some plane through the vessel. The other is to measure the mixing cup concentration of the effluent leaving a plane through the vessel. The first method was called "through the wall" and the second "in the effluent". Let one consider that the flow is made up of many stratified elements. Assuming that a pulse of tracer has been injected, each fluid element contains a certain quantity of that initial injection. The structure of the flow may appear as shown in Fig. 1 which represents a plane cut through the weir at the detection positions. The stratified elements are shown in Fig. 1, the length of each of the stratified elements being arbitrary. The velocities of the elements, v_i, the concentrations, c_i, and the areas, a_i, may all differ. The volumetric flow rate Q can be represented by

$$\Sigma_i \int_{a_i(t)} v_i \, da = Q \qquad (2\text{-}1)$$

If the concentration is monitored through the wall as a function of time, the contributions of each element to the monitored mean concentration are the cross-sectional area and concentration of the element. By denoting this mean concentration by $\overline{C}_1(t)$, one can write
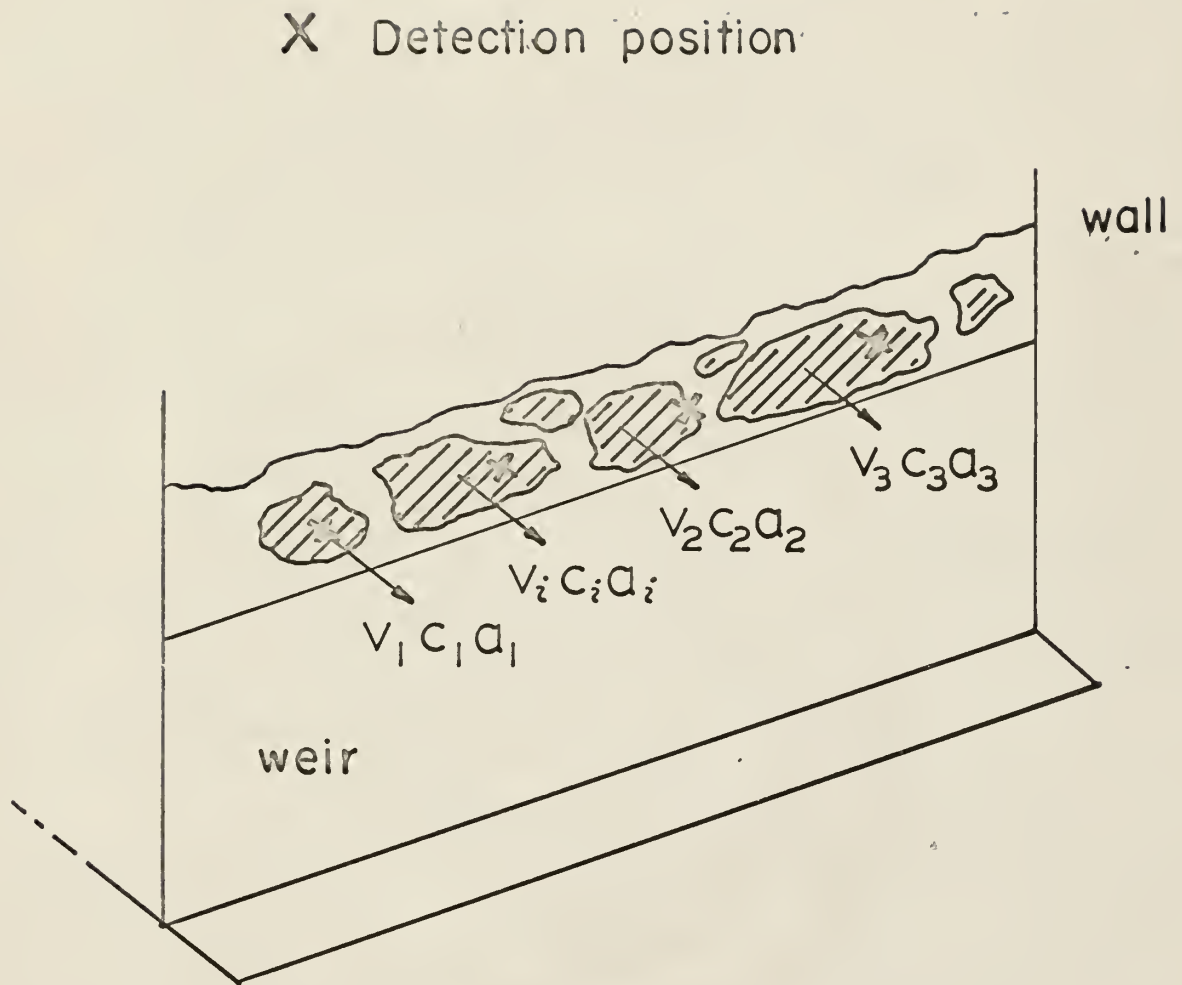
Fig. I. Schematic representation of
stratified flow of tracer
elements in a plane.

$$\bar{C}_1(t) = \frac{\sum_i \int_{a_i(t)} C_i(t)\,da}{\sum_i \int_{a_i(t)} da} = \frac{1}{A}\sum_i \int_{a_i} C_i(t)\,da \qquad (2\text{-}2)$$

where A denotes the cross-sectional area.

If the concentration is monitored in the effluent also as a time function, the contributions of each element to the mean concentration are the area, concentration, and the velocity of the element. By denoting this mean concentration by $\bar{C}_2(t)$, one has

$$\bar{C}_2(t) = \frac{\sum_i \int_{a_i(t)} C_i(t)\,v_i\,da}{\sum_i \int_{a_i(t)} v_i\,da} = \frac{1}{Q}\sum_i \int_{a_i(t)} C_i(t)\,v_i\,da \qquad (2\text{-}3)$$

It can be seen that the two monitoring techniques must be identical in the case that there is no concentration gradient or no velocity gradient across the cross-section, and thus $\bar{C}_1(t) = \bar{C}_2(t)$. Actual situations in liquid mixing do not correspond to these two extreme conditions of no concentration gradient and no velocity gradient. Therefore, the effect of stratification or bulk-segregation on the degree of liquid mixing needs to be investigated.

Let us consider the detection of the stratification effect on a specific system in which pulse testing is carried out with the use of two probes, one located upstream and the other downstream. To employ the pulse testing technique to measure the stratification effect only two probes have been used simultaneously in this work because:

(1) The stratification may occur either upstream or downstream.

(2) A small number of probes minimizes disturbance of the flow pattern by the probes being used.

CHAPTER III

AGE DISTRIBUTION

Knowledge of the complete flow pattern of fluid passing through a vessel can be obtained in different ways. A straightforward way would be to tag and follow each individual molecule as it passes through the vessel. In this approach a complete velocity distribution of the fluid within a vessel could be obtained. However, the attendant complexities make it impossible to use this approach.

An alternate approach is based on the concept of age distribution analysis (2). This concept can provide information concerning the fraction of fluid that resides for a certain time in the vessel. The details of the exact path history or where the particle has been during its stay are not considered. Therefore, information about the point to point changes of the variables is not obtainable from this approach. However, the concept of age distribution can provide us with the exit age distribution function. A mathematical model based on this function and related to the physical situation is then set up to fit experimental data.

Due to the linearity of the stimulus-response of the mixing behavior, an injected tracer (assuming no absorption at the walls and no disappearance by reaction) will pass through the vessel with the rest of the fluid. The age distribution of the tracer, therefore, represents the distribution of the fluid elements of the system. Due to this property, the age distribution can be used to understand the flow pattern.

It is necessary to define the mean residence time and the reduced time before proceeding to the discussion of the age distribution (3).

Definition of the mean residence time

The mean residence time, $\bar{t}$, is defined as

$$\bar{t} = \frac{V}{v} = \frac{\text{Volume of the vessel available for flow}}{\text{Volumetric flow rate of fluid through the vessel}} \qquad (3\text{-}1)$$

The reduced time, θ, is defined as

$$\theta = \frac{t}{\bar{t}} \qquad (3\text{-}2)$$

The discussion following is based on the work of Levenspiel (8).

Internal age distribution (2)

A vessel contains, in general, fluid elements of varying ages, age being the time a fluid element has spent in the vessel. Let the symbol, $I(\theta)$, be the measure of the distribution of the ages of the fluid in the vessel defined in such a manner that $I(\theta)\,d\theta$ is the fraction of fluid elements in the vessel between the ages θ and $\theta + d\theta$. A typical plot of the $I(\theta)$ against θ is given in Fig. 2. Since the sum of all the fractions of the fluid elements in the vessel is unity, this sum must also be the total area under the $I(\theta)$ vs. θ curve. Thus

$$\int_0^\infty I(\theta)\,d\theta = 1 \qquad (3\text{-}3)$$

The fraction of the fluid elements with the ages younger than a certain value, say θ_1, is shown in Fig. 2 as the shaded area and is given by

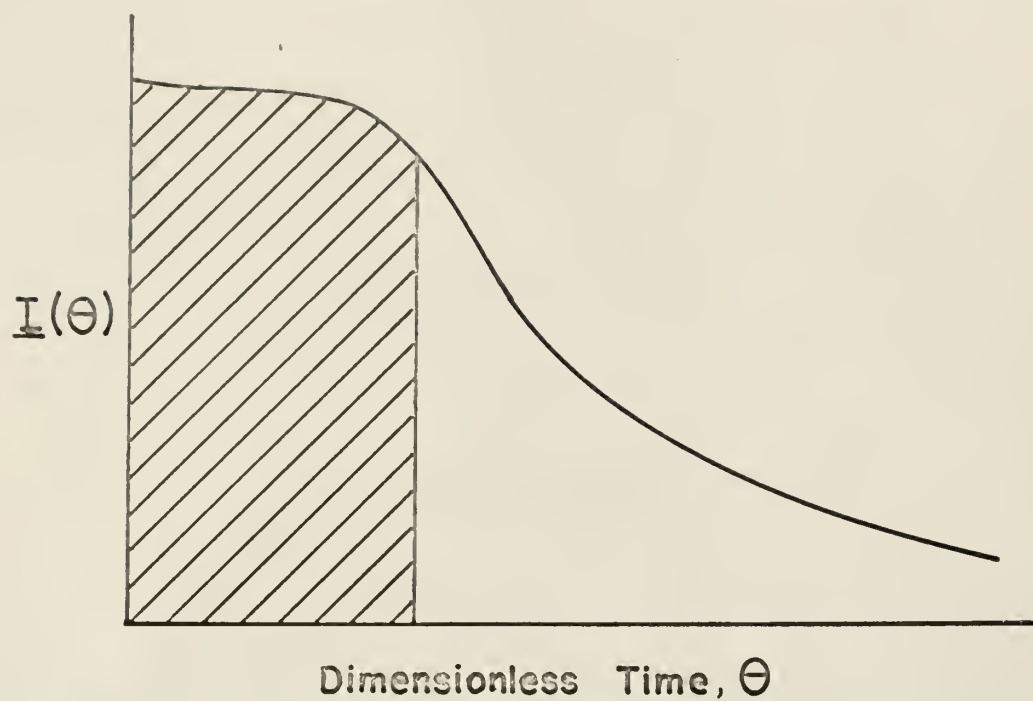$$\int_0^{\theta_1} I(\theta)\,d\theta \qquad (3\text{-}4)$$

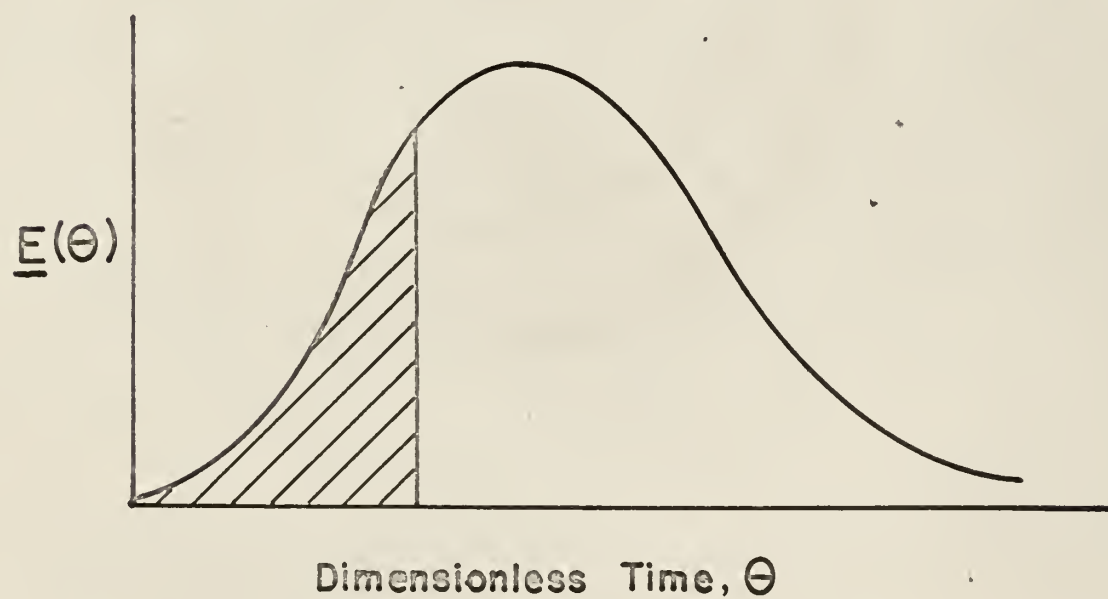Fig. 2. A typical internal age distribution curve.

Fig. 3. A typical exit age distribution curve.

The fraction of the fluid elements with ages older than θ_1 is

$$\int_{\theta_1}^{\infty} \underline{I}(\theta)\,d\theta \;=\; 1 - \int_{0}^{\theta_1} \underline{I}(\theta)\,d\theta \tag{3-5}$$

The internal age distribution $I(t)$ based on actual time rather than reduced time is related to $\underline{I}(\theta)$ as

$$\underline{I}(\theta) \;=\; \bar{t}\,I(t) \qquad \text{with} \qquad \int_{0}^{\infty} I(t)\,dt \;=\; 1 \tag{3-6}$$

Exit age distribution (2)

In a manner similar to the internal age distribution function, let $\underline{E}(\theta)$ denote the distribution of age of all fluid elements leaving the vessel. $\underline{E}(\theta)$ is defined in such a manner that $\underline{E}(\theta)\,d\theta$ is the fraction of fluid elements in the exit stream between the ages of θ and $\theta + d\theta$. It follows that

$$\int_{0}^{\infty} \underline{E}(\theta)\,d\theta \;=\; 1 \tag{3-7}$$

A typical $\underline{E}(\theta)$ vs. θ curve is given in Fig. 3. The fraction of fluid elements in the exit stream with ages younger than age θ_2 is

$$\int_{0}^{\theta_2} \underline{E}(\theta)\,d\theta \tag{3-8}$$

The fraction of fluid elements with ages older than θ_2 is then

$$\int_{\theta_2}^{\infty} \underline{E}(\theta)\,d\theta \;=\; 1 - \int_{0}^{\theta_2} \underline{E}(\theta)\,d\theta \tag{3-9}$$

$\underline{E}(\theta)$ is variously referred to as the exit age distribution function or the exit residence time distribution or simply the residence time distribution function (r. t. d. f.). If actual time t is used instead of dimensionless or reduced time θ,

$$\underline{E}(\theta) \ = \ \bar{t}\,E(t) \qquad \text{with} \qquad \int_0^\infty E(t)\,dt \ = \ 1$$

Intensity function (3)

Another method for representing residence time variability in continuous flow systems is based on the use of the intensity function (3). The advantage of this method is that it allows a physical insight into the mixing processes within the system and enhances the interpretability of experimental curves.

The intensity function $\underline{\lambda}(\theta)$ is defined in such a manner that $\underline{\lambda}(\theta)\,d\theta$ represents the fraction of fluid elements in a vessel of age θ that will leave at a time between θ and $\theta + d\theta$.

The physical meaning of the three probability functions

The amount of material leaving in time less than θ is

$$v \int_0^\theta \underline{E}(\theta)\,d\theta \tag{3-10}$$

where v = volumetric flow rate. Thus, the amount of fluid not leaving the vessel (i.e. remaining in vessel) is

$$v\,\underline{I}(\theta) \ = \ v \ - \ v \int_0^\theta \underline{E}(\theta)\,d\theta \tag{3-11}$$

and thus

$$\underline{I}(\theta) = 1 - \int_0^\theta \underline{E}(\theta)\, d\theta \tag{3-12}$$

Consequently, one can write

$$\underline{E}(\theta) = - \frac{d\underline{I}(\theta)}{d\theta} \tag{3-13}$$

The amount of material leaving the vessel between θ and $\theta + d\theta$ can be written as a product of the amount not leaving before θ and the fraction of fluid of age θ that will leave between θ and $\theta + d\theta$. In other words,

$$v\,\underline{E}(\theta)\, d\theta = \left[v\,\underline{I}(\theta)\right]\left[\underline{\lambda}(\theta)\, d\theta\right]$$

or

$$\underline{\lambda}(\theta) = \frac{\underline{E}(\theta)}{\underline{I}(\theta)} = - \frac{1}{\underline{I}(\theta)} \frac{d\underline{I}(\theta)}{d\theta} = - \frac{d \ln \underline{I}(\theta)}{d\theta} \tag{3-14}$$

The F curve (2)

With no tracer initially present in the entering stream, let a step of tracer signal of concentration C_o be introduced into the fluid entering the system in such a manner that the volumetric flow rate to the vessel remains constant. Then the concentration-time curve for the tracer in the exit fluid stream, measuring tracer concentration in terms of inlet tracer concentration and measuring time in reduced units, is called the F-curve. As shown in Fig. 4 the F-curve rises from 0 to 1.

The C curve (2)

The curve that describes the concentration-time function of tracer in the exit stream of a vessel in response to an idealized delta function of
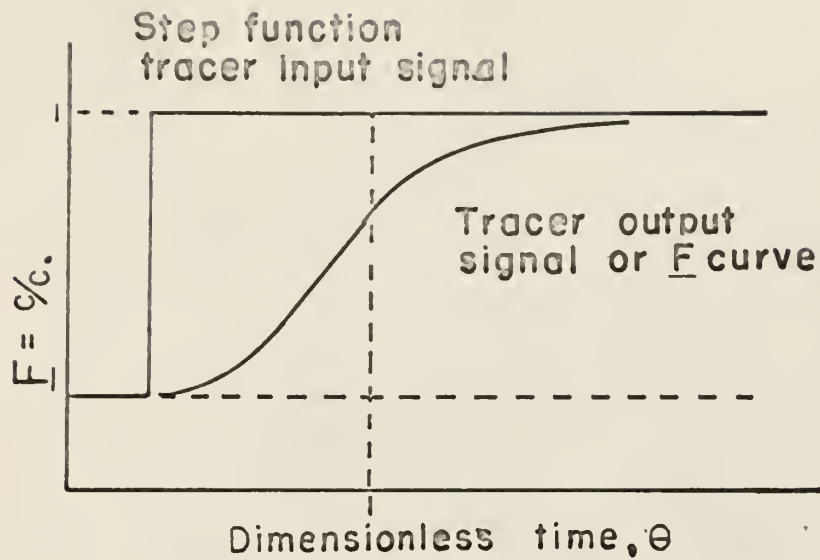
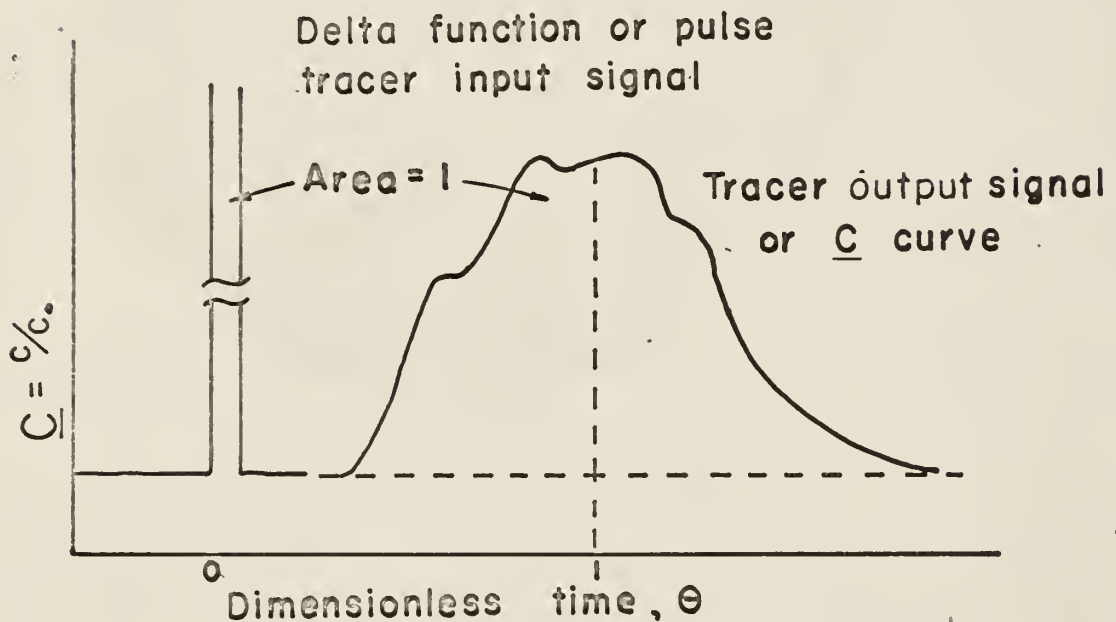Fig. 4. Typical downstream signal, the F curve, in response to an upstream step input signal.

Fig. 5. Typical downstream signal, the C curve, in response to an upstream delta-function tracer input signal.

unit impulse input is called the $\underline{C}$-curve if, as in the case of the $\underline{F}$ curve, dimensionless coordinates are chosen. Concentrations are measured in terms of the initial concentration of injected tracer, C_o, as if it were evenly distributed throughout the vessel, and time is measured in reduced units. The area under the C-curve always be unity, that is,

$$\int_0^\infty \underline{C}(\theta)\, d\theta = \int_0^\infty \frac{C}{C_o}\, d\theta = 1, \quad \text{where} \quad C_o = \frac{V}{V}\int_0^\infty \c(t)\, dt = \frac{1}{\bar{t}}\int_0^\infty C(t)\, dt$$

Relation between the $\underline{F}$, $\underline{C}$, $\underline{I}$, and $\underline{E}$ curves in closed vessels (8)

By material balance the following relationships can be obtained.

$$\underline{F}(\theta) + \underline{I}(\theta) = 1$$

$$\underline{C}(\theta) = \underline{E}(\theta) = \frac{d\underline{F}(\theta)}{d\theta} = -\frac{d\underline{I}(\theta)}{d\theta} \tag{3-15}$$

$$\underline{F}(\theta) = 1 - \underline{I}(\theta) = \int_0^\theta \underline{E}(\theta)\, d\theta = \int_0^\theta \underline{C}(\theta)\, d\theta$$

CHAPTER IV

SYSTEM AND TRACER TECHNIQUE

<u>Type of flow</u>

There are two extreme modes of mixing, micromixing and macromixing. The former is mixing on the microscopic scale (mixing of individual molecules), while the latter is mixing on the macroscopic scale (mixing of clumps, groups, or aggregates of molecules). An actual mixing condition of a fluid usually is found to be between the two extreme cases and is called a partially segregated fluid. A microfluid exhibits no segregation and a macrofluid, hence, exhibites complete segregation. The degree of segregation is of importance in analyzing the actual conversion of the reactions in nonlinear rate processes (5). However, while most of the mass transfer processes are linear processes, mixing on a distillation plate can be treated from either point of view (9).

The pulse testing technique used in detecting the residence time distribution has been extended to a two phase and even to a three phase system (two phase flow in fluidized beds) (10). The treatment of residence time distribution in a two phase system (for instance, a distillation plate) can be simplified by independent treatment of each individual phase because the mixing process is a linear process. The first phase (the gas phase) offers an additional source of kinetic energy as well as an additional impediment to the flow of the second phase (the liquid phase) (11).

<u>Open and closed systems</u>

An open system is essentially a system with no discontinuity in the type of flow at the point of tracer injection or at the point of tracer

measurement, i.e. diffusion and dispersion have to be taken into consideration in addition to bulk flow at the points of injection and measurement. On the other hand, a closed system is defined as one in which a fluid enters and leaves by bulk flow alone. When either the entrance or exit alone satisfies the closed system requirements, the system is said to be closed-open or open-closed.

A distillation system can be considered to be a closed system. This is based on the assumption that diffusion and dispersion are negligibly small at the downcomers as compared with that on the active zone of the tray. Therefore, the transport of the tracer at both entrance and exit can be considered to be due to the bulk flow only.

Tracer technique

The use of tracer experiments for characterizing flow patterns in process equipment has become a subject of much interest. The system is perturbed with the different kinds of tracer (dye stuffs, electrolytes, and radioactive isotopes), and the concentration-time curve at the exit point or at both entrance and exit points is analyzed. There are several methods extensively used for the system excitation: step input of tracer (or heaviside step function input), delta function input of tracer, sinusoidal input of tracer, and arbitrary input of tracer.

The first two methods of tracer input for the system excitation are directly related to the responses which give rise to the F-curve and the C-curve shown in Figs. 4, 5. That is to say, the F-curve and the C-curve can be obtained by measuring only the concentration-time curves of the output responses. However, the techniques using the definite shapes of tracer input signals have their difficulties and inaccuracies. While the sinusoidal input

of tracer is usually used for the frequency response analysis, there are also several difficulties and disadvantages associated with the method (1, 12, 13, 14).

Pulse testing technique

In the pulse testing method, the tracer is injected in a very arbitrarily manner at a convenient point upstream from the system of interest. Since the input is arbitrary, an arbitrary response signal is obtained, and thus the measurement of the concentration-time curve is no longer limited to the outlet of the system only. In many situations the measuring points are located at the inlet and at the outlet, and the measured curves are denoted as $X(t)$ and $Y(t)$ respectively. Their shapes are apparently arbitrary, but their magnitudes are greater than zero during the measuring period. Typical input and output concentration-time curves are shown in Fig. 6.

The dimensionless variables corresponding to $X(t)$ and $Y(t)$ can be defined as

$$X(\theta) = \frac{\bar{t} X(t)}{A_x}$$

$$Y(\theta) = \frac{\bar{t} Y(t)}{A_y}$$

(4-1)

where

$$\bar{t} = \frac{V}{v}$$

$$\theta = \frac{t}{\bar{t}}$$

and

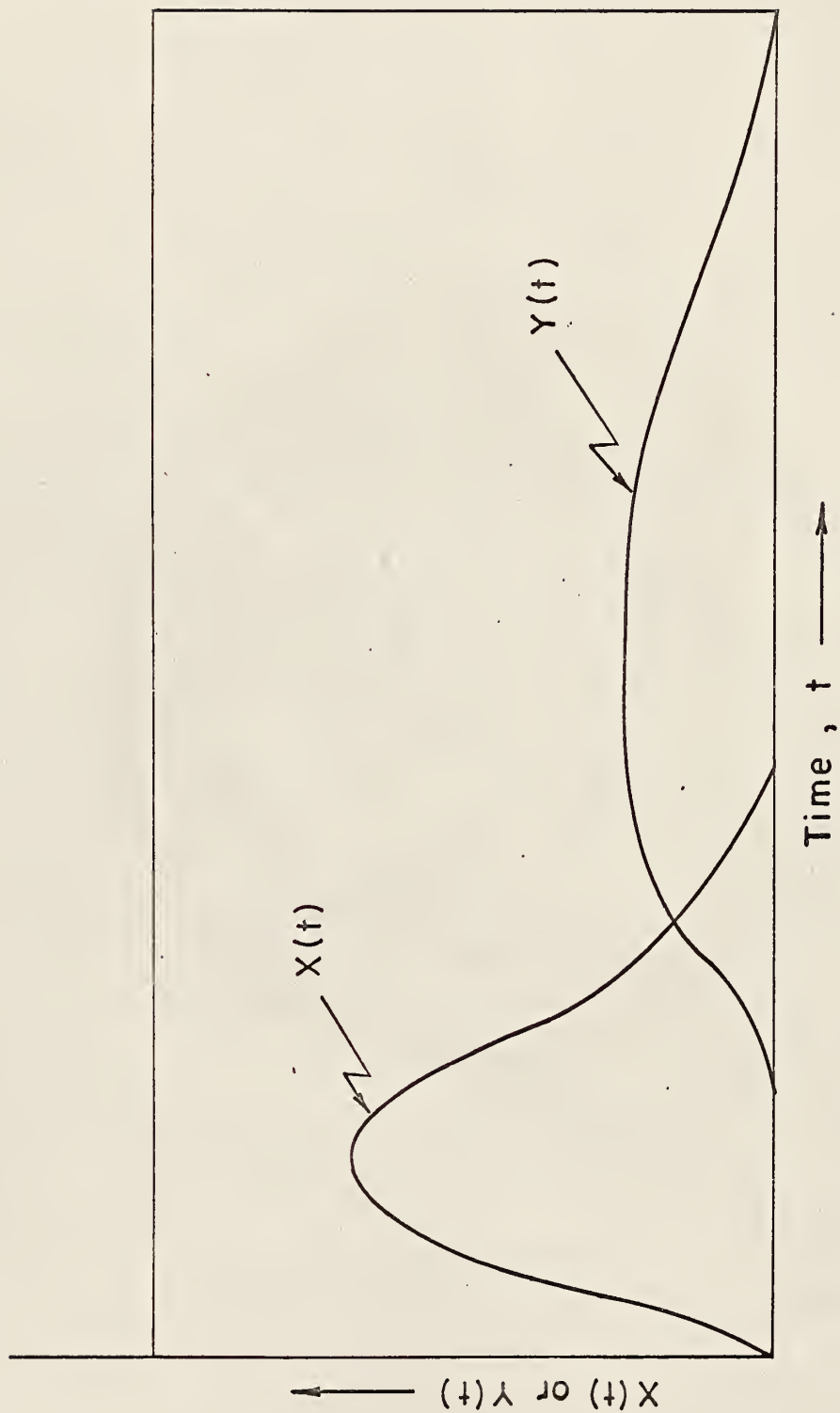$$A_x = \int_0^\infty X(t) \, dt$$

$$A_y = \int_0^\infty Y(t) \, dt$$

Fig.6. Typical input and output traces from a pulse testing experiment.

CHAPTER V

THE MOMENTS METHOD OF ANALYSIS

The interesting properties of the moments method of analysis have been pointed out by several authors (10, 15). This method is particularly well adapted to the description of the quality of mixing in a continuous mixing vessel. It is possible to describe numerically the process dynamics without the necessity of a specific model. On the other hand, if a system model is presumed, the system moments can be used to determine coefficients without the use of curve fitting techniques. The characteristics of the residence time distribution function can be represented by a set of moments and consequently by a set of numbers.

The first moment, or mean, of the residence time distribution function, $\underline{E}(\theta)$, is given by

$$\mu_\theta = M_1 = \int_0^\infty \theta \, \underline{E}(\theta) \, d\theta \tag{5-1}$$

The second moment about the mean, commonly called the variance, measures the spread of the distribution about the mean and is equivalent to the square of the radius of gyration of the distribution. It is defined for a continuous distribution as

$$\sigma_\theta^2 = M_2 = \int_0^\infty (\theta - \mu_\theta)^2 \, \underline{E}(\theta) \, d\theta \tag{5-2}$$

The third moment about the mean, commonly called the skewness, is obtained as

$$\tau_\theta^3 = M_3 = \int_0^\infty (\theta - \mu_\theta)^3 \, \underline{E}(\theta) \, d\theta \tag{5-3}$$

The exit age distribution function, $\underline{E}(\theta)$, is a mathematical representation of a model derived from a physical system. In the model there exist some parameters which we have to be determined experimentally. In order to determine the model parameters and fit the distribution curve to the experimentally collected input and output data, $X(\theta)$ and $Y(\theta)$, the transfer function, $\overline{H}(s)$, of a mixing system has to be introduced. It is defined as

$$\overline{H}(s) = \frac{\overline{Y}(s)}{\overline{\overline{X}}(s)} \qquad (5\text{-}4)$$

where

$$\overline{Y}(s) = \text{Laplace transform of } Y(\theta) = \int_0^\infty Y(\theta) e^{-s\theta} d\theta$$

$$\overline{X}(s) = \text{Laplace transform of } X(\theta) = \int_0^\infty X(\theta) e^{-s\theta} d\theta$$

If $X(\theta)$ is the delta function, then

$$\overline{X}(s) = 1 \qquad (5\text{-}5)$$

and

$$\overline{Y}(s) = \underline{\overline{C}}(s) = \underline{\overline{E}}(s) \qquad (5\text{-}6)$$

Thus it is evident that

$$\underline{\overline{E}}(s) = \overline{H}(s) \qquad (5\text{-}7)$$

that is, the Laplace transform of the residence time distribution function is equal to the transfer function of the system. From this identity the following relationships will be developed:

(1) The relationship between the residence time distribution function and the moments.

(2) The relationship between the transfer function and the moments.

(3) The relationship between the moments from case 1 and from case 2.

One defines the Laplace transform of the residence time distribution function as

$$\bar{E}(s) = \int_0^\infty E(\theta) e^{-s\theta} d\theta \qquad (5\text{-}8)$$

Upon successive differentiation of Equation (5-8), one has

$$\frac{d\bar{E}(s)}{ds} = -\int_0^\infty \left[\theta \underline{E}(\theta)\right] e^{-s\theta} d\theta \qquad (5\text{-}9a)$$

$$\frac{d^2\bar{E}(s)}{ds^2} = +\int_0^\infty \left[\theta^2 \underline{E}(\theta)\right] e^{-s\theta} d\theta \qquad (5\text{-}9b)$$

and

$$\frac{d^3\bar{E}(s)}{ds^3} = -\int_0^\infty \left[\theta^3 \underline{E}(\theta)\right] e^{-s\theta} d\theta \qquad (5\text{-}9c)$$

Taking the limit on both sides of Equations (5-9a), (5-9b) and (5-9c), one obtains

$$\lim_{s\to 0} \frac{d\bar{E}(s)}{ds} = -\int_0^\infty \left[\theta \underline{E}(\theta)\right] d\theta \qquad (5\text{-}10a)$$

$$\lim_{s\to 0} \frac{d^2\bar{E}(s)}{ds^2} = +\int_0^\infty \left[\theta^2 \underline{E}(\theta)\right] d\theta \qquad (5\text{-}10b)$$

and

$$\lim_{s\to 0} \frac{d^3\bar{E}(s)}{ds^3} = -\int_0^\infty \left[\theta^3 \underline{E}(\theta)\right] d\theta \qquad (5\text{-}10c)$$

Substituting Equation (5-10a) into Equation (5-1) yields

$$\mu_\theta = -\lim_{s\to 0} \frac{d\bar{E}(s)}{ds} \tag{5-11a}$$

Substituting Equations (5-10a) and (5-10b) into Equation (5-2) and making

$$\sigma_\theta^2 = \int_0^\infty (\theta - \mu_\theta)^2 \, \underline{E}(\theta) \, d\theta$$

$$= \int_0^\infty \theta^2 \, \underline{E}(\theta) \, d\theta - 2\mu_\theta \int_0^\infty \theta \, \underline{E}(\theta) \, d\theta + \mu_\theta^2 \int_0^\infty \underline{E}(\theta) \, d\theta$$

$$= \lim_{s\to 0} \left[\frac{d^2\bar{E}(s)}{ds^2} - 2\left(\frac{d\bar{E}(s)}{ds}\right)^2 + \left(\frac{d\bar{E}(s)}{ds}\right)^2 \cdot 1 \right]$$

$$= \lim_{s\to 0} \left[\frac{d^2\bar{E}(s)}{ds^2} - \left(\frac{d\bar{E}(s)}{ds}\right)^2 \right] \tag{5-11b}$$

Similarly, making use of Equations (5-3), (5-1), (5-2), (5-10a), (5-10b), and (5-10c) yields

$$\tau_\theta^3 = -\lim_{s\to 0} \left[\frac{d^3\bar{E}(s)}{ds^3} - 3\frac{d\bar{E}(s)}{ds}\frac{d^2\bar{E}(s)}{ds^2} + 2\left(\frac{d\bar{E}(s)}{ds}\right)^3 \right] \tag{5-11c}$$

Now, let us establish the relationship between the transfer function and the moments.

Differentiation of Equation (5-4) yields

$$\frac{d\bar{H}(s)}{ds} = \frac{\bar{X}(s)\,\bar{Y}'(s) - \bar{Y}(s)\,\bar{X}'(s)}{\bar{X}(s)^2} \tag{5-12}$$

By taking the limits of Equations (5-13), (5-14), and (5-15) and making use of Equations (5-16), (5-17), and (5-18), one has

$$\lim_{s \to 0} \frac{d\bar{H}(s)}{ds} = \lim_{s \to 0} \left[\frac{d\bar{Y}(s)}{ds} - \frac{d\bar{X}(s)}{ds}\right] \tag{5-19}$$

$$\lim_{s \to 0} \left[\frac{d^2\bar{H}(s)}{ds^2} - (\frac{d\bar{H}(s)}{ds})^2\right] = \lim_{s \to 0} \left[\frac{d^2\bar{Y}(s)}{ds^2} - (\frac{d\bar{Y}(s)}{ds})^2\right]$$

$$- \lim_{s \to 0} \left[\frac{d^2\bar{X}(s)}{ds^2} - (\frac{d\bar{X}(s)}{ds})^2\right] \tag{5-20}$$

$$\lim_{s \to 0} \left[\frac{d^3\bar{H}(s)}{ds^3} - 3 \frac{d\bar{H}(s)}{ds} \frac{d^2\bar{H}(s)}{ds^2} + 2(\frac{d\bar{H}(s)}{ds})^3\right]$$

$$= \lim_{s \to 0} \left[\frac{d^3\bar{Y}(s)}{ds^3} - 3 \frac{d\bar{Y}(s)}{ds} \frac{d^2\bar{Y}(s)}{ds^2} + 2(\frac{d\bar{Y}(s)}{ds})^3\right]$$

$$- \lim_{s \to 0} \left[\frac{d^3\bar{X}(s)}{ds^3} - 3 \frac{d\bar{X}(s)}{ds} \frac{d^2\bar{X}(s)}{ds^2} + 2(\frac{d\bar{X}(s)}{ds})^3\right] \tag{5-21}$$

$\bar{X}(s)$ and $\bar{Y}(s)$ are the distribution functions which, in the mathematical sense, have the same properties as the residence time distribution function, $\bar{E}(s)$. If one replaces the $\bar{E}(s)$ in the right hand sides of Equations (5-11a), (5-11b), and (5-11c) by $\bar{Y}(s)$ or $\bar{X}(s)$, the following equations will be obtained:

$$\mu_{\theta Y} = - \lim_{s \to 0} \frac{d\bar{Y}(s)}{ds}$$

$$\mu_{\theta X} = - \lim_{s \to 0} \frac{d\bar{X}(s)}{ds}$$

$$\sigma^2_{\theta Y} = \lim_{s \to 0} \left[\frac{d^2\bar{Y}(s)}{ds^2} - (\frac{d\bar{Y}(s)}{ds})^2\right]$$

$$\sigma_{\theta X}^2 = \lim_{s \to 0} \left[\frac{d^2 \overline{X}(s)}{ds^2} - \left(\frac{d\overline{X}(s)}{ds} \right)^2 \right]$$

(5-22)

$$\tau_{\theta Y}^3 = -\lim_{s \to 0} \left[\frac{d^3 \overline{Y}(s)}{ds^3} - 3 \frac{d\overline{Y}(s)}{ds} \frac{d^2 \overline{Y}(s)}{ds^2} + 2 \left(\frac{d\overline{Y}(s)}{ds} \right)^3 \right]$$

$$\tau_{\theta X}^3 = -\lim_{s \to 0} \left[\frac{d^3 \overline{X}(s)}{ds^3} - 3 \frac{d\overline{X}(s)}{ds} \frac{d^2 \overline{X}(s)}{ds^2} + 2 \left(\frac{d\overline{X}(s)}{ds} \right)^3 \right]$$

Substituting Equation (5-22) into Equations (5-19), (5-20), and (5-21) yields

$$-\lim_{s \to 0} \frac{d\overline{H}(s)}{ds} = \mu_{\theta Y} - \mu_{\theta X} = \Delta \mu_{\theta YX}$$

(5-23)

$$\lim_{s \to 0} \left[\frac{d^2 \overline{H}(s)}{ds^2} - \left(\frac{d\overline{H}(s)}{ds} \right)^2 \right] = \sigma_{\theta Y}^2 - \sigma_{\theta X}^2 = \Delta \sigma_{\theta YX}^2$$

(5-24)

and

$$-\lim_{s \to 0} \left[\frac{d^3 \overline{H}(s)}{ds^3} - 3 \frac{d\overline{H}(s)}{ds} \frac{d^2 \overline{H}(s)}{ds^2} + 2 \left(\frac{d\overline{H}(s)}{ds} \right)^3 \right] = \tau_{\theta Y}^3 - \tau_{\theta X}^3 = \Delta \tau_{\theta YX}^3$$

(5-25)

Recall that $\underline{\overline{E}}(s) = \overline{H}(s)$. From Equation (5-11a), (5-11b), and (5-11c), it can then be established that

$$-\lim_{s \to 0} \frac{d\overline{E}(s)}{ds} = \Delta \mu_{\theta YX} = \mu_\theta$$

(5-26)

$$\lim_{s \to 0} \left[\frac{d^2 \overline{E}(s)}{ds^2} - \left(\frac{d\overline{E}(s)}{ds} \right)^2 \right] = \Delta \sigma_{\theta YX}^2 = \sigma_\theta^2$$

(5-27)

and

$$-\lim_{s \to 0} \left[\frac{d^3 \underline{\overline{E}}(s)}{ds^3} - 3 \frac{d\overline{E}(s)}{ds} \frac{d^2 \overline{E}(s)}{ds^2} + 2 \left(\frac{d\overline{E}(s)}{ds} \right)^3 \right] = \Delta \tau_{\theta YX}^3 = \tau_\theta^3$$

(5-28)

From the pulse testing data, $\bar{Y}(\theta)$ and $\bar{X}(\theta)$, one can calculate the variance, $\triangle\sigma^2_{\theta YX}$ and the skewness, $\triangle\tau^3_{\theta YX}$. For a two-parameter model, one can make use of Equations (5-27) and (5-28) to calculate the model parameters. One can see that, in general, n+1 moments are required for a n-parameter model.

Discussion of the moments method of analysis

In general, the nth moment of the transfer function can be obtained by taking the limit of the nth derivative of the Laplace transform and letting the transform variable tend toward zero. This yields

$$\lim_{s \to 0} \bar{Y}^n(s) = (-1)^n \int_0^\infty t^n f(t)\, dt$$

It has been observed that the tails of $Y(\theta)$ and $X(\theta)$ curves may be unreliable due to the difficulties of accurate measurements of tracer concentration at low concentrations. Therefore, it becomes obvious that the moments method has its disadvantages (16, 17), especially when higher moments are required. Small uncertainties in the values on the tail of the input and output concentration time curves introduce appreciable truncation errors in the analysis of data.

Although the moments method of analysis has significant drawbacks, it is still of value due to a saving in computer time in obtaining the first and the second moments which can be used to describe the extent of mixing.

CHAPTER VI

MODELS OF DISTILLATION TRAYS

The models used in fitting a mixing system are of two kinds: the purely mathematical model and the physical model.

As mentioned by Adler (18), the use of a model has the following advantages over the use of experimental data without a model.

(1) Scale up and extrapolation can be more accurately carried out. The model helps predict the effects of unavoidable differences in fluid mixing, which occur when moving from laboratory to pilot plant to a commercial unit.

(2) Experimental data can be more fully utilized.

(3) Dynamic as well as static analysis and prediction are possible, permitting early opportunities for optimization and control studies.

(4) The amount of pilot plant time and data needed is often reduced.

The pool model of a distillation tray, originally proposed by Kirchbaum (19) and later by Nord (20), Gatreaux and O'Connell (21), Mickley, et al. (22), and Leonard (11), postulates that the plate may be pictured as a series of completely mixed pools along the length of the tray. While it assumes complete mixing within each pool, there is no mixing between pools. A plate with a single pool corresponds to a perfectly mixed plate and one with an infinite number of pools to a plug flow plate.

The recycle model of Oliver and Watson (23) and Warzel (24) assumes that the liquid mixing is affected by a recycle of liquid which moves from the tray exit to tray inlet. The parameter which characterizes mixing is the concentration jump at the inlet weir.

The splashing model was proposed by Johnson and Maranjozis (25). In the

model, splashing of the liquid is considered to be the major mixing mechanism.

The axial dispersed plug flow model has been applied to distillation plates by Anderson (26), Gerster, et.al. (27), Welch (28), Iyer and Multi (29). This model assumes that the rate of mixing or dispersion of a component is proportional to the concentration gradient of that component.

Foss (30) has shown how the residence time distribution function can be used to include liquid mixing effects in the calculation of plate efficiency.

Mutzenberg (31) has used the impulse test to measure the residence time distribution of a flow pattern on a sieve tray. He has pointed out that the total tray efficiency on a sieve plate based on the vapor phase is a function of the local tray efficiency, fluid velocity, slope of the equilibrium curve, and number of pools connected in series.

Leonard (11) concluded that the macroscopic splashing model of Johnson and Maranjosis (25) is unsuitable for predicting dispersion or tray efficiency.

Olson and Heideger (32) demonstrated that eddy diffusion does not adequately describe the mixing on a sieve tray. He concluded that the mixing is apparently of such large scale as to cause interactions between local regions on the tray.

Strand (33) measured the efficiency of desorption of acetone, methyl isobutyl ketone and isopropyl alcohol from water by air on bubble cap trays. He derived an equation for evaluating the tray efficiency. By using an axial dispersed plug flow model around which a fraction of the entering liquid is effectively bypassed, a better agreement between experimental and predicted efficiencies was obtained as compared with the result obtained from the A. I. Ch. E. method (34).

The above survey indicates that the mixing on a distillation tray may

be represented by either the axial dispersed model with bypassing or the pool model in series with bypassing.

Cha (35) has discussed the Γ-distribution model at great length. The Γ-distribution model is a mathematical model which is more flexible than the pools in-series model. The reason is discussed in the next section.

Johnson (1) was the first who used the Γ-distribution model to describe a distillation tray. Modification by addition of a bypassing stream to the Γ-distribution was proved to be satisfactory. In this work, a similar model, based on previous work and the physical reality of the specific nonideal sieve tray is proposed. An alternative model with a different path for the bypassing stream is suggested, which may prove to be useful in understanding the bypassing on the distillation tray.

The relationship between the Γ-distribution model and the pools in-series model

The pools-in-series model, or the completely mixed tanks-in-series model is an alternative approach to the dispersion model for dealing with small deviations from plug flow.

Consider a vessel consisting of j pools in series. Then the exit age distribution can be obtained by a material balance as (19)

$$\underline{E}(\theta) = \frac{j^j \theta^{j-1}}{(j-1)!} e^{-j\theta} \qquad (6-1)$$

According to Cha (35), the mathematical representation of the Γ-distribution model is

$$E(t) = \frac{1}{\nu^p \Gamma_{(p)}} (t-D)^{P-1} \exp(-\frac{t-D}{\nu}) \qquad (6-2a)$$

where

$$\Gamma(P) = \int_0^{\infty} X^{P-1} e^{-X} dX$$

ν, p and D are the parameters of the model. D corresponds to the dead time or delay time of the system. Cha (35) also shown that

$$\mu_t = \nu P + D$$

and for a closed system the mean of $E(t)$, denoted by μ_t, can be represented by

$$\mu_t = \bar{t} = \frac{V}{v}$$

Therefore, one can write

$$\nu = \frac{\bar{t} - D}{P}$$

This means that only two parameters among ν, P, and D are independent. Equation (6-2) can now be written as

$$E(t) = \frac{P^P}{(\bar{t} - D)^P \Gamma(P)} (t - D)^{P-1} \exp\left[- P \left(\frac{t - D}{\bar{t} - D}\right)\right] \tag{6-2b}$$

letting $\theta = \frac{t}{\bar{t}}$ and noting that $\underline{E}(\theta) = \bar{t} E(t)$, one obtains

$$\underline{E}(\theta) = \frac{P^P}{(1 - \tau_d)^P \Gamma(P)} (\theta - \tau_d)^{P-1} \exp\left[- P \left(\frac{\theta - \tau_d}{1 - \tau_d}\right)\right] \tag{6-3}$$

where

$$\tau_d = \frac{D}{\bar{t}}$$

If one considers τ_d as the dimensionless dead time, by letting $\tau_d = 0$ Equation (6-3) reduces to

$$\underline{E}(\theta) = \frac{p^P \theta^{P-1}}{\Gamma(p)} e^{-p\theta} \tag{6-4}$$

Therefore, comparing this with Equation (6-1), one can see that the age distribution function of the tanks-in-series model is identical to the Γ-distribution model, if the two parameters in the Γ-distribution model are restricted by equating τ_d to zero, and making p take a positive integer.

The Γ-distribution model with by-passing across the Γ-mixing system is shown in Fig. 7. This mixed model can be derived as follows:

Let

$$\beta = \frac{V_1}{V_T} \quad , \qquad\qquad 1 - \tau_d = \frac{V_1}{V_T}$$

$$V_1 + V_2 + V_3 = V_T \quad , \qquad\qquad \frac{V_1}{V_T} + \frac{V_2}{V_T} + \frac{V_3}{V_T} = 1 \tag{6-5}$$

and thus

$$\frac{V_2}{V_T} = f_2 \tau_d \quad , \qquad \frac{V_3}{V_T} = f_3 \tau_d \quad , \qquad \text{with } f_2 + f_3 = 1 \tag{6-6}$$
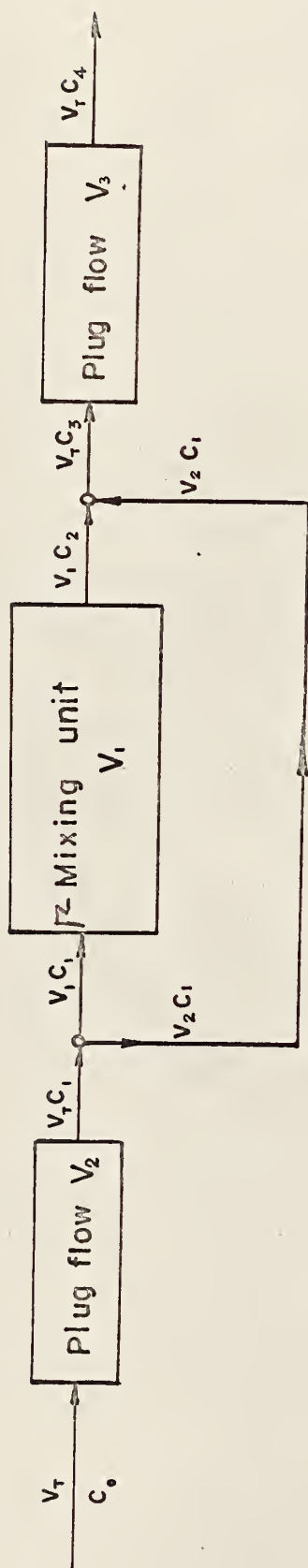
f_2 and f_3 are constant.

Also let

$$\overline{t} = \nu p = \frac{V_1}{v_1} = \frac{V_1}{V_T} \frac{V_T}{v_1} \frac{V_T}{V_T} = \frac{\overline{t}(1 - \tau_d)}{\beta} \tag{6-7}$$

and thus

$$\nu = \frac{\overline{t}(1 - \tau_d)}{\beta p} \tag{6-8}$$

$\overline{t}$ is the mean residence time based on the entire system.

v_1 = Volumetric flow rate through Γ-mixing unit

v_2 = Volumetric flow rate of by-passing stream

v_T = Total volumetric flow rate

V_1 = Volume of Γ-mixing unit

V_2 = Volume of the first plug flow section

V_3 = Volume of the second plug flow section

V_T = Total volume of system

c_i = Tracer concentration a function of time

Fig. 7. The Γ-distribution model with by passing across the Γ-mixing unit.

The Γ-mixing system without dead time can be obtained by setting $D = 0$ in Equation (6-2a) as

$$E(t)_\Gamma = \frac{1}{\nu^P \Gamma_{(p)}} t^{P-1} \exp(-\frac{t}{\nu}) \qquad (6\text{-}9a)$$

Substituting Equation (6-8) into Equation (6-9a) yields

$$E(t)_\Gamma = \frac{1}{\left[\dfrac{\bar{t}(1 - \tau_d)}{\beta P}\right]^P \Gamma_{(p)}} t^{P-1} \exp\left[\frac{-t}{\dfrac{\bar{t}(1 - \tau_d)}{\beta P}}\right] \qquad (6\text{-}9b)$$

Recalling that $\underline{E}(\theta) = \bar{t}E(t)$, one has

$$\underline{E}(\theta)_\Gamma = \frac{\beta^P P^P}{(1 - \tau_d)^P \Gamma_{(p)}} \theta^{P-1} \exp(-\frac{\beta P}{1 - \tau_d} \theta) \qquad (6\text{-}9c)$$

Taking Laplace transform of Equation (6-9c) yields

$$\underline{\bar{E}}(s)_\Gamma = \frac{\beta^P P^P}{(1 - \tau_d)^P}\left[\frac{1}{s + \dfrac{\beta P}{1 - \tau_d}}\right]^P = \left[\frac{\beta P}{(1 - \tau_d)s + \beta p}\right]^P \qquad (6\text{-}9d)$$

From the relation, $\underline{\bar{E}}(s) = \underline{\bar{H}}(s)$, one can write

$$\underline{\bar{E}}(s)_\Gamma = \frac{\bar{c}_2}{\bar{c}_1} \qquad \text{or} \qquad \bar{c}_2 = \bar{c}_1\left[\frac{p\beta}{(1 - \tau_d)s + p\beta}\right]^P \qquad (6\text{-}10)$$

A material balance over the differential volume in the first plug flow section gives

$$-v_T\frac{dC}{dv} = \frac{dC}{dt}$$

Rewriting in terms of reduced time

$$- v_T \frac{dC}{dv} = \frac{dC}{dt} \frac{\bar{t}}{t} \quad , \qquad \bar{t} = \frac{V_T}{v_T}$$

$$\text{(6-11a)}$$

$$- V_T \frac{dC}{dv} = \frac{dC}{d\theta}$$

Taking the Laplace transform and noting that $C(0) = 0$ yields

$$- V_T \frac{d\bar{C}}{dv} = s\bar{C} \qquad \text{(6-11b)}$$

Integrating over the boundary conditions, $C_i = C_0$ at $V = 0$; $C_1 = C_1$ at $V = V_2$, yields

$$\int_{C_0}^{C_1} \frac{d\bar{C}}{\bar{C}} = - \frac{s}{V_T} \int_0^{V_2} dV$$

$$\ln \frac{\bar{C}_1}{\bar{C}_0} = - \frac{s}{V_T} V_2 = - s \left[f_2 \tau_d \right]$$

Thus

$$\bar{C}_1 = \bar{C}_0 \exp\left[- f_2 s \tau_d \right] \qquad \text{(6-12)}$$

Material balance over the second plug section, using the same argument, gives similarly

$$\int_{C_3}^{C_4} \frac{d\bar{C}}{\bar{C}} = - \frac{s}{V_T} \int_0^{V_2} dV$$

Thus one obtains

$$\bar{C}_4 = \bar{C}_3 \exp\left[- f_3 s \tau_d \right] \qquad \text{(6-13)}$$

Material balance over the second pot gives

$$v_1 \bar{c}_2 + v_2 \bar{c}_1 = v_T \bar{c}_3$$

$$\bar{c}_3 = \frac{v_1}{v_T} \bar{c}_2 + \frac{v_2}{v_T} \bar{c}_1$$

$$= \beta \bar{c}_2 + (1 - \beta) \bar{c}_1 \tag{6-14}$$

Substituting Equations (6-10), (6-12), and (6-14) into Equation (6-13) leads to

$$\bar{E}(s) = \bar{H}(s) = \frac{\bar{c}_4}{\bar{c}_0} = \left[\beta \left\{ \frac{p\beta}{(1 - \tau_d)s + p\beta} \right\}^p + (1 - \beta) \right] \exp\left[-s\tau_d \right] \tag{6-15}$$
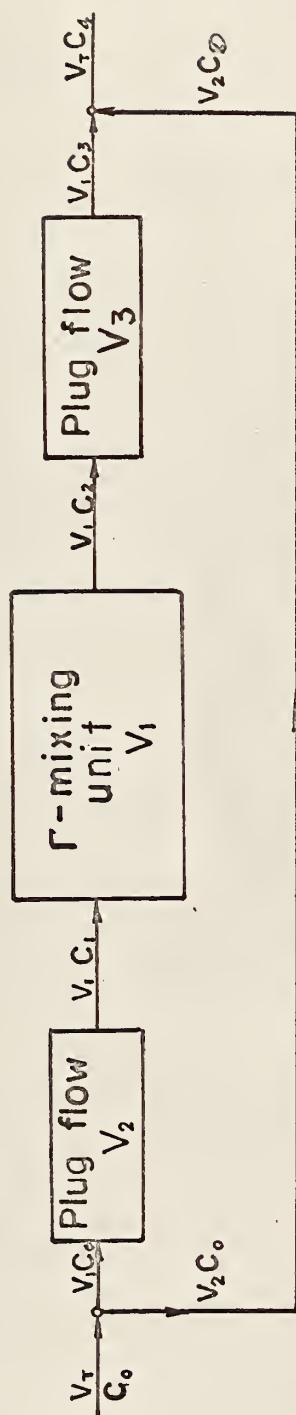
Taking the inverse transform yields

$$E(\theta) = \frac{\beta^{p+1} p^p}{(1 - \tau_d)^p \ (p)} \left[\theta - \tau_d \right]^{p-1} \exp\left[-\frac{p\beta}{1 - \tau_d} \theta \right] + (1 - \beta)\delta\left[\theta - \tau_d \right] ;$$

$$\theta > \tau_d \tag{6-16}$$

$$E(\theta) = 0 ; \qquad \theta < \tau_d$$

Note that the result is the same as putting the two equal sized plug flow sections together as expected (1).

The Γ-distribution model with by-passing from inlet to outlet (Fig. 8) can be derived in the same way as the first model. Let

$$\beta = \frac{v_1}{v_T} , \qquad\qquad 1 - \tau_d = \frac{v_1}{v_T}$$

$$v_1 + v_2 + v_3 = v_T , \qquad \frac{v_1}{v_T} + \frac{v_2}{v_T} + \frac{v_3}{v_T} = 1$$

$$\frac{v_2}{v_T} = f_2 \tau_d , \qquad \frac{v_3}{v_T} = f_3 \tau_d \qquad \text{with} \quad f_2 + f_3 = 1$$

v_1 = Volumetric flow rate through Γ-mixing unit
v_2 = Volumetric flow rate of by-passing stream

v_t = Total volumetric flow rate

V_1 = Volume of the Γ-mixing unit

V_2 = Volume of the first plug flow section

V_3 = Volume of the second plug flow section

V_T = Total volume of system
c = Tracer concentration a function of time

Fig. 8. The Γ-distribution model with by passing from inlet to outlet.

f_2 and f_3 are constant. Again, letting

$$\bar{t} = \nu p = \frac{V_1}{v_1} = \frac{\bar{t}(1 - \tau_d)}{\beta}$$

one has

$$\nu = \frac{\bar{t}(1 - \tau_d)}{\beta p}$$

$\bar{t}$ is the mean residence time based on the entire system.

The Laplace transform of the Γ-mixing unit without dead time is represented by

$$\bar{E}(s)_\Gamma = \frac{p^p \beta^p}{(1 - \tau_d)^p} \left[\frac{1}{s + \frac{\beta p}{1 - \tau_d}} \right]^p = \left[\frac{p \beta}{(1 - \tau_d)s + p\beta} \right]^p$$

Since

$$\bar{E}(s)_\Gamma = \frac{\bar{c}_2}{\bar{c}_1}$$

one has

$$\bar{c}_2 = \bar{c}_1 \left[\frac{p\beta}{(1 - \tau_d)s + p\beta} \right]^p \tag{6-17}$$

A material balance over the first plug flow section yields, in the Laplace transformed domain,

$$\bar{c}_1 = \bar{c}_0 \exp\left[-\frac{f_2}{\beta} s \tau_d \right] \tag{6-18}$$

Similarly for the second plug flow section

$$\bar{c}_3 = \bar{c}_2 \exp\left[-\frac{f_3}{\beta} s \tau_d \right] \tag{6-19}$$

Material balance over the second pot gives

$$v_1 \bar{c}_3 + v_2 \bar{c}_0 = v_T \bar{c}_4$$

$$\bar{c}_4 = \frac{v_1}{v_T} \bar{c}_3 + \frac{v_2}{v_T} \bar{c}_0 = \beta \bar{c}_3 + (1 - \beta) \bar{c}_0 \tag{6-20}$$

Substituting Equations (6-17), (6-18), and (6-19) into Equation (6-20) yields

$$\bar{c}_4 = \bar{c}_0 \; \beta \left(\frac{p \beta}{(1 - \tau_d)s + p\beta} \right)^p \exp\left[- \frac{s \tau_d}{\beta} \right] + (1 - \beta) \tag{6-21}$$

Therefore, the exit age distribution function is

$$\bar{E}(s) = \bar{H}(s) = \frac{\bar{c}_4}{\bar{c}_0}$$

$$= \beta \left(\frac{p \beta}{(1 - \tau_d)s + p\beta} \right)^p \exp\left[- \frac{s \tau_d}{\beta} \right] + (1 - \beta) \tag{6-22}$$

Taking the inverse transform

$$E(\theta) = \frac{\beta^{p+1} \, p^p}{(1 - \tau_d)^p \, \Gamma(p)} \left(\theta - \frac{\tau_d}{\beta} \right)^{p-1} \exp\left[- \frac{p\beta\theta}{(1 - \tau_d)} \right]$$

$$+ (1 - \beta) \, \delta(\theta) \quad ; \qquad\qquad \theta \geq \frac{d}{\beta}$$

$$\tag{6-23}$$

$$\underline{E}(\theta) = 0 \quad ; \qquad\qquad \theta < \frac{d}{\beta}$$

$\delta(\theta)$ stands for the delta function.

CHAPTER VII

EXPERIMENTAL

1. Equipment

The tray used in this work is a 12" x 48" rectangular sieve tray, consisting of five zones:

(1) Active or vapor-dispersion zone.

(2) Distributing zone.

(3) Disengaging zone.

(4) Downcomer zone.

(5) Periphery waste zone.

The area occupied by the five zones is shown in Fig. 9. The spacing of perforations, which were on an equilateral-triangular basis, range from 2.5 to 5 diameters. With spacing closer than 2.5 diameters, excessive coalescence of bubbles occurred. At spacings greater than five diameters, tray capacity was limited and inactive liquid zones developed between the perforations, which probably reduced transfer efficiency. The percentage of free area, which is defined as the ratio of the perforation area to the active area, was designed to be far less than the commercial range of 5 to 15%.

The gauges for measuring the liquid depth and the static pressure between the plates was specially designed as shown in Fig. 10.
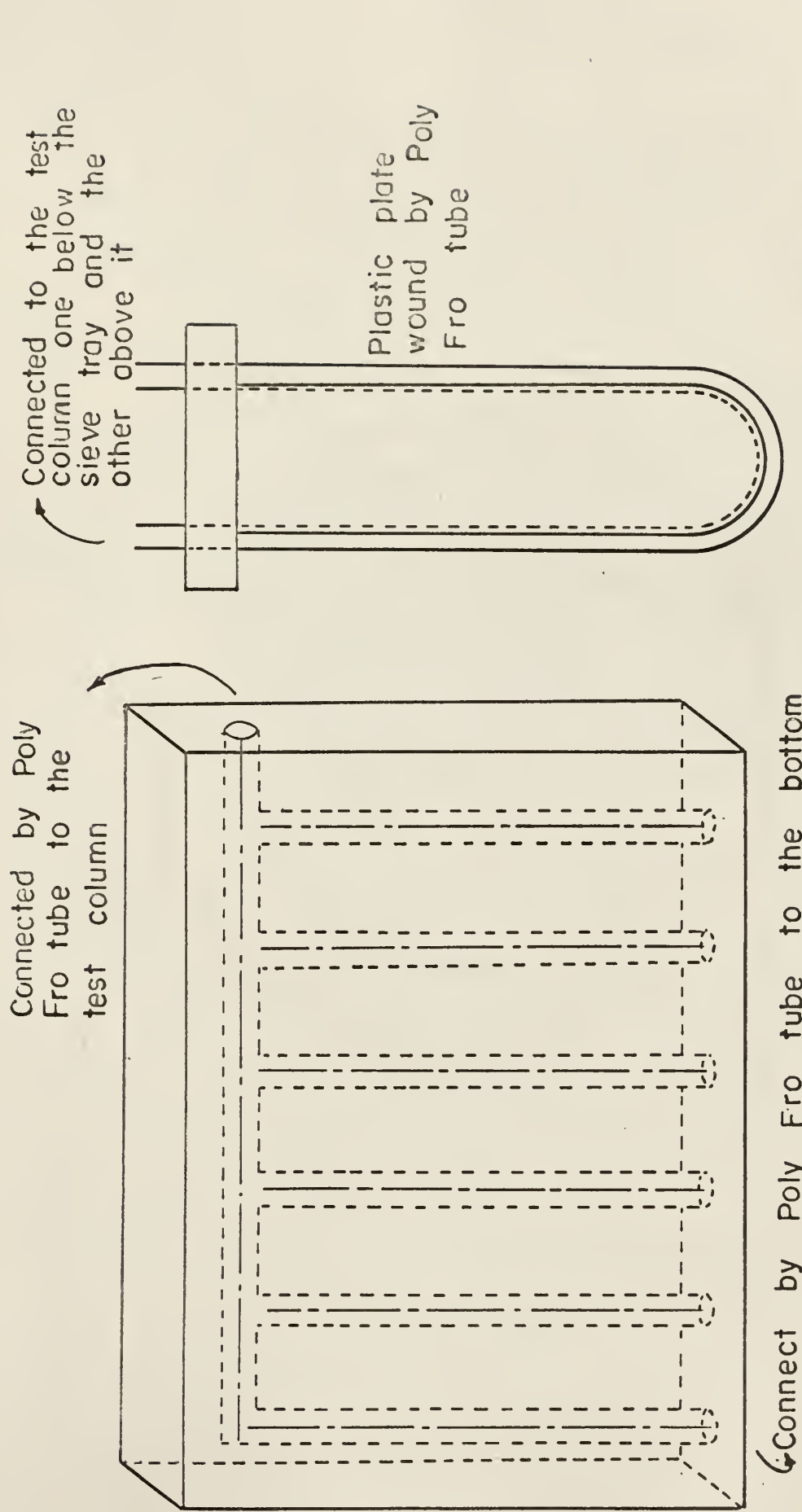
The accessories and the overall set up

The overall experimental set-up is shown in Fig. 11. The constant head tank shown in the upper left hand corner was a 150 gallon, stainless steel, cone-bottom vessel. The tank was supplied with tap water from the building main at a rate of 30 gallons per minute and provided a constant head of 20 feet.

Fig. 9. Test sieve tray layout.
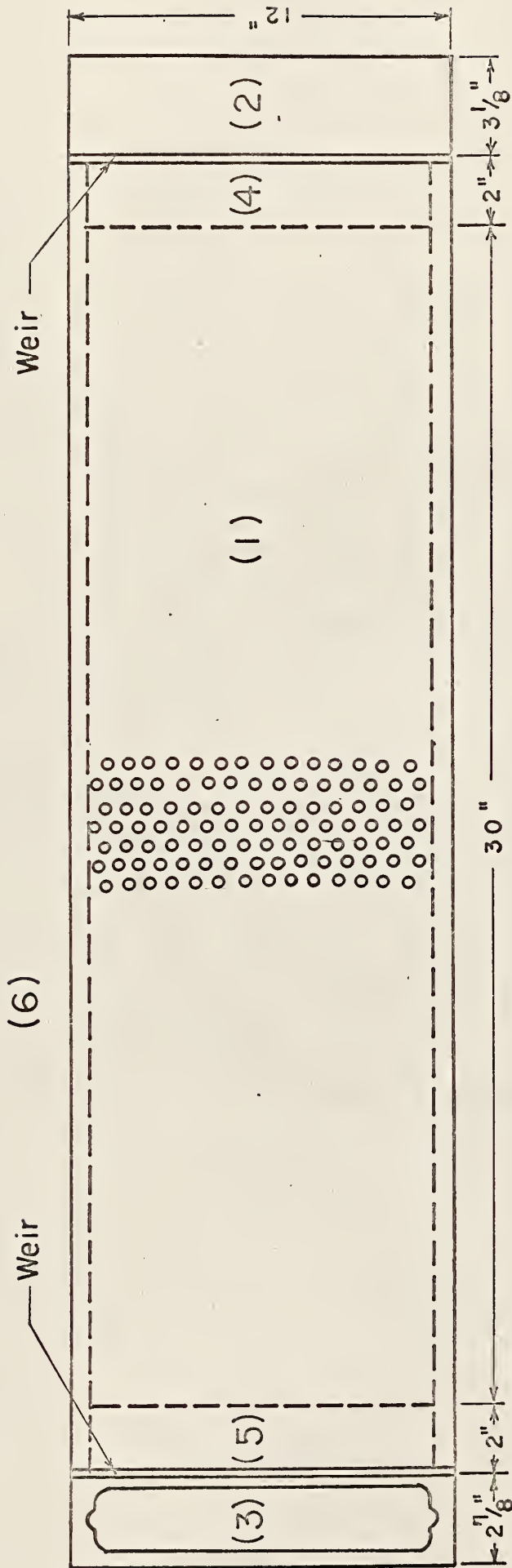
(1) Active area
(2) Downcomer area (Inlet)
(3) Downcomer area (Outlet)
(4) Disengaging zone
(5) Distributing zone
(6) Periphery waste zone

Connected to the test
column one below the
sieve tray and the
other above it

Plastic plate
wound by Poly
Fro tube

Connected by Poly
Fro tube to the
test column

Connect by Poly Fro tube to the bottom
of sieve tray. The water will flow down through holes of the tray where the
Poly Fro tube is connected and maintain the same level in the gauge as on the tray.

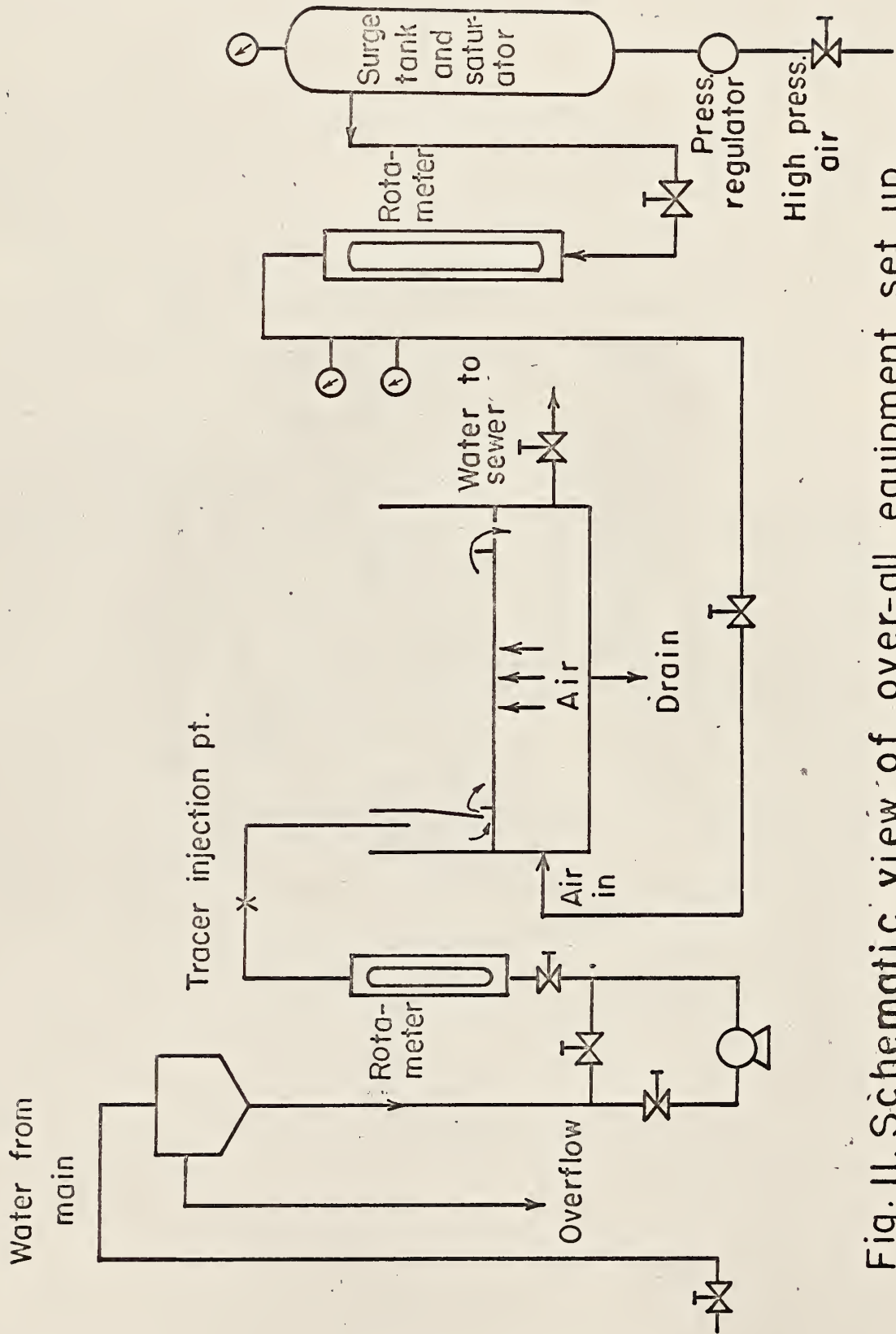Fig. 10. Liquid level measuring gauge and statistic pressure measuring
gauge.

Fig. II. Schematic view of over-all equipment set up.

Two Brooks Fullview rotameters were used to meter the water to the test trays. These rotameters had ranges of 0.5 to 5.4 g.p.m. and 2.0 to 23 g.p.m. The guaranteed accuracy of these meters was ± 2% of maximum scale reading from 10% to 100% of flow, but the check calibrations indicated that flow rates could be read accurately to within 1.5% of the scale reading. The calibration curves are given in the Appendix 1a and 1b.

One Brooks Fullview rotameter with a range of 5 - 50 s.c.f.m. was used to meter the air to the test tray. The calibration of the air rotameter was checked with a wet test meter. The temperature and pressure calibration correction curves are given in Appendix 2a, 2b.

In order to get a uniform inlet concentration of the tracer through the cross-section, a distributor was provided so that the water was divided into five streams which were evenly distributed. The five streams flowed into the downcomer which was packed with spherical glass particles. The glass particles were used to obtain uniform flow and to reduce bubbling of the entering fluid (see Fig. 12).

High pressure air was fed into a 30 gallon surge tank where it was bubbled through water in order to saturate it. The combination of the pressure regulator and the surge tank served to damp out noticeable fluctuations in air pressure.

2. Instrument of measurement

The electrical conductivity method was employed in this work. Continuous recording of conductivity has been widely used by many previous researchers (39, 40, 41, 42). Prausnitz (43) used a conductivity probe to measure the turbulent mixing properties and Manning (44) improved the conductivity probe to measure the concentration fluctuations in a baffled stirred vessel.
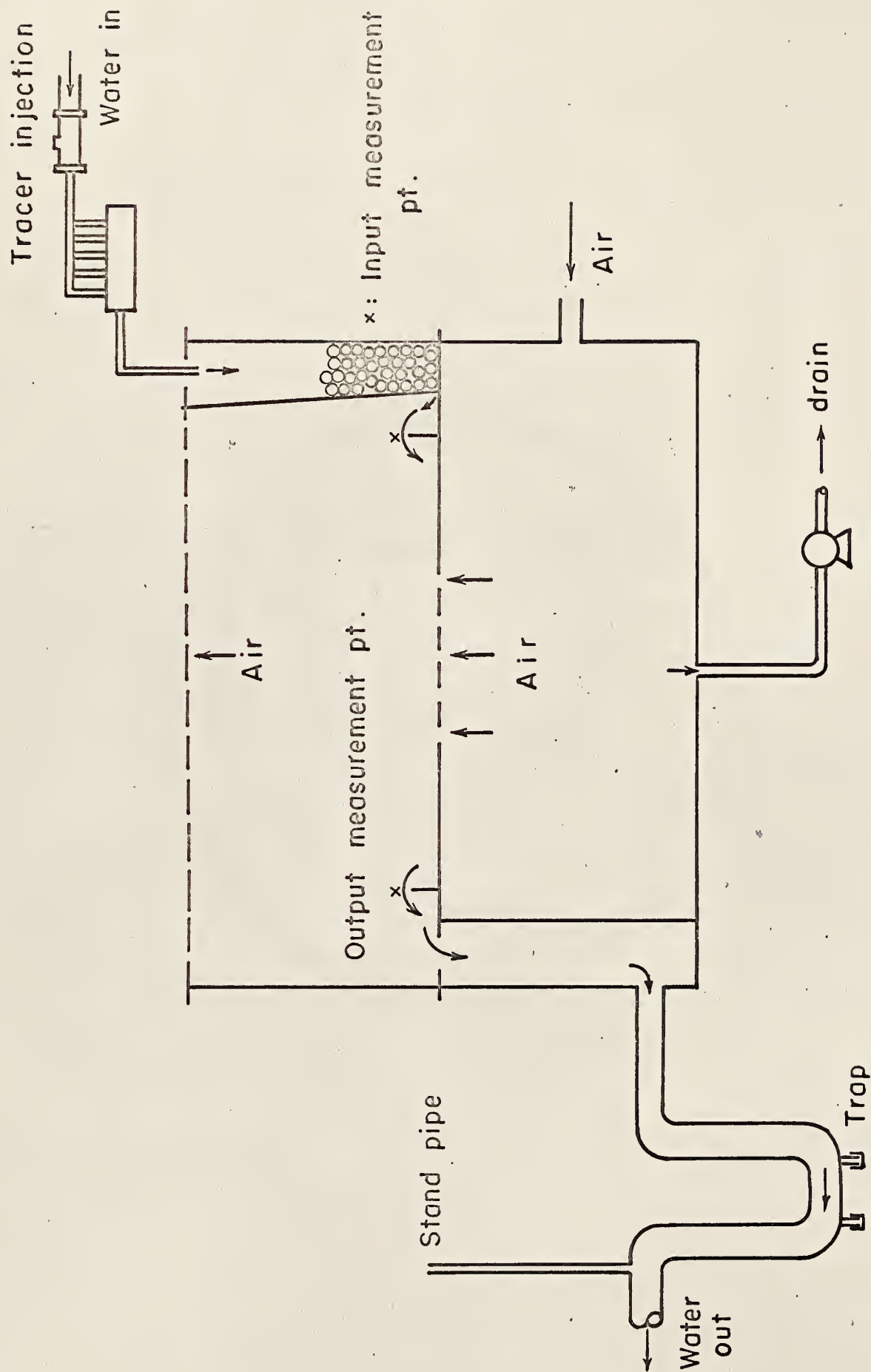
Fig. 12 Schematic view of rectangular test column.

Mutzenberg (31) used the conductivity instrument to measure the residence time distribution on a sieve tray.

The conductivity measurement

Electrolytic conductivity is a measure of the ability of a solution to carry an electric current. The specific conductance is defined as the reciprocal of the resistance in ohms of a 1 cm cube of the liquid at a specified temperature. The commonly used units of specific conductance are the reciprocal ohm-cm (or mho/cm), and one millionth of this, micro-mho/cm. High quality condensed steam and distilled or demineralized water have specific conductances at room temperature as low as, or lower than, 1 micro-mho/cm. This would be caused by about one-half ppm of a dissolved salt. (sodium chloride solution was used as a tracer in this work). Absolutely pure water has a conductivity of 0.055 micromhos/cm at 25°C.

The mechanism of electrolytic conduction differs from that of metals. In the latter, current is carried by free electrons; in the former, current is carried by ions only. Electrolytic conductivity is non-specific and all ions present in a solution contribute. This is in marked contrast to the general lack of influence of other ions on pH measurement which, over most of its useful range, is responsive to the H-ion concentration alone.

The conductivity probe

In this work small conductivity probes were desirable in order to minimize disturbance of the flow pattern by the probes. Two probes designed by the Industrial Instrument Inc. were used (Appendix 3). These two probes consisted of two small metal plates situated at the end of a 5 m.m. outside diameter, 12" long epoxy tube. The exposed ends of these two plates of

metal were platinized (Fig. 13).

The conductivity meter

The model RA4 Solu Meter used is a direct reading instrument providing a continuous indication of solution conductivity. A 0 to 10 DC signal proportional to the conductivity is provided to operate a remote potential recorder. A non-bridge type of measuring circuit is utilized. The conductivity ranges from 0 to 2500 micromhos/cm. The specifications of this conductivity meter are shown in Table 1. Fig. 14a shows the block diagram in the instrumental set up. Fig. 14b is a photograph of the instrumental set up.
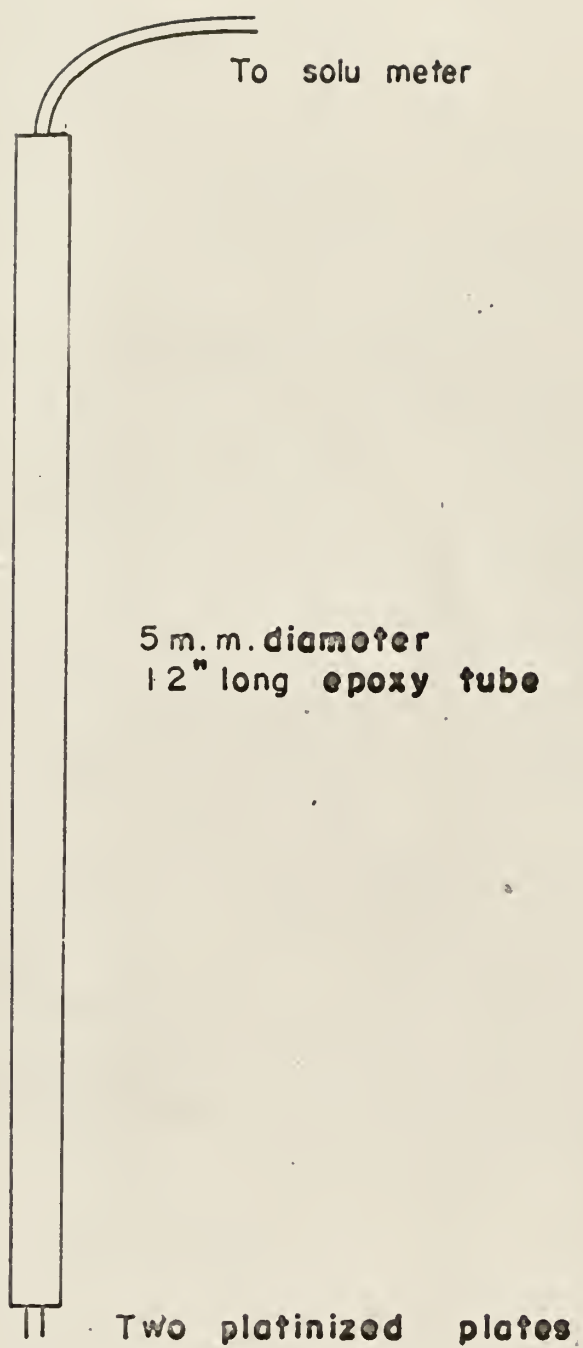
47

To solu meter

5 m.m. diameter
12" long epoxy tube

Two platinized plates

Fig. 13. The conductivity probe.

TABLE 1. SPECIFICATIONS OF TYPE RA4 SOLU METER

Ranges	Three standards 2000, 200 and 100 ohms measured resistance for full scale deflection.
Temperature compensation	Mannual or automatic
Cell voltage	3 volts maximum
Measurement	In undergrounded or grounded electrolytic solutions.
Output	0-10 mv DC across 100 ohms
Accuracy of output	$\pm 1\%$ of full scale, above 1/10 full scale
Power requirements	18 watts at 120 volts
Mounting	Panel or portable
Case	Aluminum gray finish
Dimensions	9" high (over handle) x 6-1/4" wide x 8" deep
Weight	8-1/2 pounds

Beckman offner type RC dyno-graph recorder	Solu meter	Conduc-tivity probe
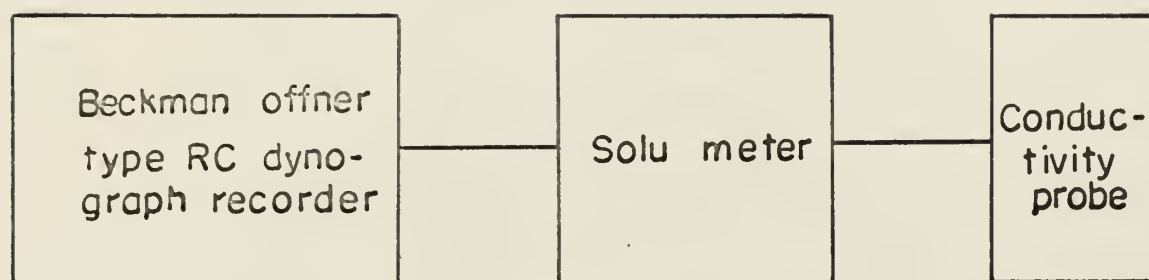
Type RA 4-WB-S17-T I

Ser. No. 74 4

Cell constant 0.500 /cm.

Fig. 14. Block diagram of the instrumental set up.

50

Fig. 14b. Photograph of the instrumental set up.

CHAPTER VIII

PHOTOGRAPHIC STUDY AND VISUAL OBSERVATION

The purposes of the photographic study and visual observation were as follows:

(1) To provide a physical picture of the flow pattern occuring on the sieve tray.

(2) To observe the effect of flow patterns (oscillating, normal flow patterns, etc.) on the degree of liquid mixing. The oscillating flow pattern of the first type may be especially important in this respect since it may decrease the backmixing and increase the Murphree vapor efficiency (51).

(3) To establish a plausible mechanism for a bypassing mechanism on the distillation tray.

Formation of the stratified elements

When the air flowed at a very low rate (say 2 g.p.m.), the frontal edge of the potassium permanganate solution injected as a tracer proceeded very uniformly near the inlet. (It is convenient to use $KMnO_4$ solution as a tracer for photographic study, since it has color). At a position about half way between the inlet and the bubble or active zone, fingerlike projections of the dye front occurred predominantly at or near the center. This fingerlike projections (probably stratified elements) appeared to be drawn forward through the action of the bubble fountain, producing a non-uniform dye concentration throughout the cross-section (Fig. 15). At a position half way between the inlet and the bubble zone, the concentration of the dye tracer appeared to be smaller in the vicinity of the walls, where the velocity of the stream flow was nearly equal to zero. The formation of the stratified

Stage one

Fig. 15 a.

Bubble zone
or
Fountain zone

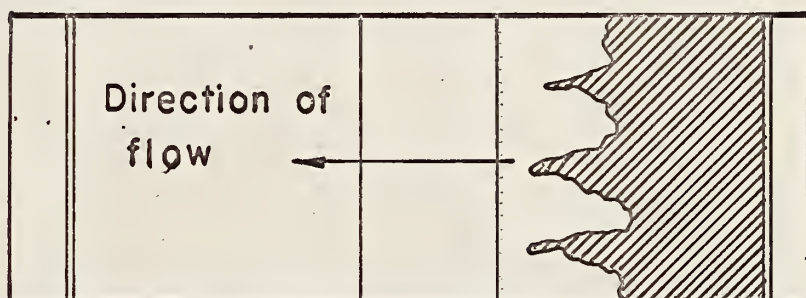Tracer flows in
uniformly

Stage two

Fig. 15 b.

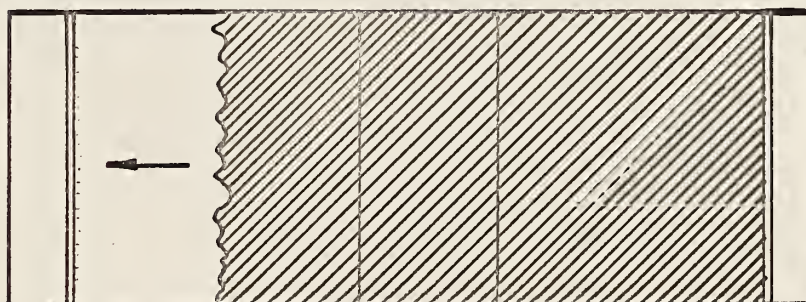Occurrence of non-uniform
distribution of tracer.

Stage three

Fig. 15 c.

Tracer flows out nearly uniformly

Fig. 15. Stages in the formation of stratified elements.

elements might be explained by an increase in the non-uniform velocity profile which in turn enhanced by the non-uniformity in tracer distribution which already existed at the inlet.

The frontal edge of the dye tracer at the bubble zone and at the outlet again appeared to be uniform, apparently due to the stirring and agitation of the air bubbles.

Figs. 16a, 16b, 16c, and 16d show the formation of stratified elements under various conditions.

Formation of cellular foam and bubble bursting

Here observations were confined to operations with a multiply perforated tray. The hole diameter was 3/16" and the spacing was 1-1/2". Fig. 17. is a photograph taken under the conditions with the air flow rate of 7.5 c.f.m., water flow rate of 7.5 g.p.m., weir height of 3 in. and 7 rows of holes. One can see the formation of bubbles, the growth of bubbles, and the bursting of bubbles.

When the air velocity was less than approximately 10 c.f.m., the frequency of the bubbling was low and hence sufficient time became available for the growth of the bubbles. When a bubble collided with others, two events might happen: one is the formation of a larger bubble and the other a breakdown into smaller bubbles. At the low air velocity, the formation of the larger bubble would be more probable, especially near the surface. Hence a collection of the larger bubbles flows upwards. When it reaches the surface, it becomes cellular foam (Fig. 18). Of course, the formation of the cellular foam not only depended on the air velocity, but also on the liquid properties, such as surface tension. At a very high air velocity(approximately over 20 c.f.m. in this system), the frequency of the bubbling was

Fig. 16a. Formation of stratified elements. The dye has proceeded to a position half way between the inlet and the bubble zone under the conditions G=10 c.f.m., L=15 g.p.m., WH=1.5 in., 1 row of holes. (Top view of the bubble zone and inlet, flow direction from right to left)
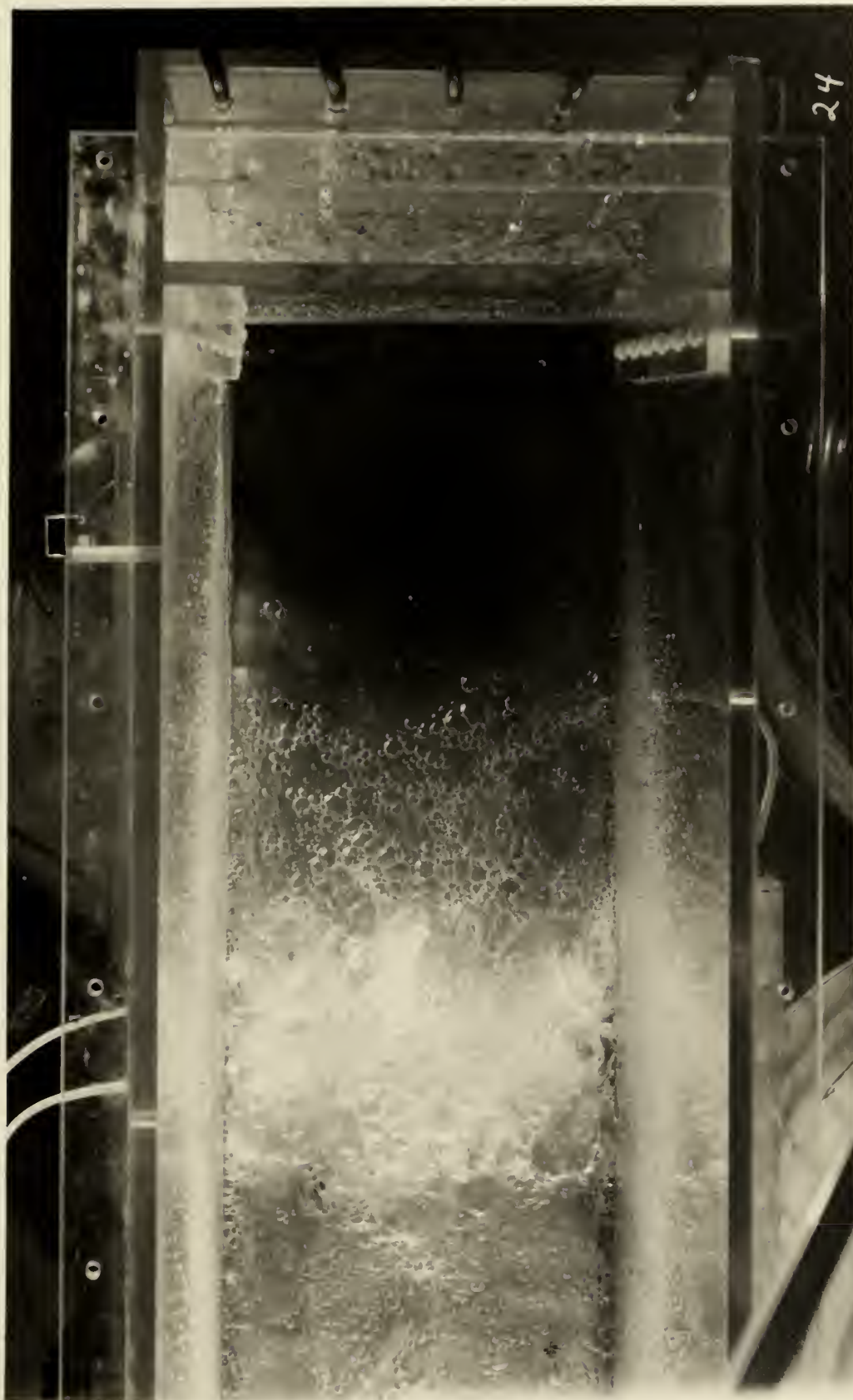
Fig. 16b. Formation of stratified elements. The dye has proceeded to a point near the bubble zone under the conditions G=10 c.f.m., L=5 g.p.m., WH=1.5 in., 1 row of holes. (Top view of the bubble zone and inlet, flow direction from right to left)

Fig. 16c. Formation of stratified elements. The frontal edge of the dye has just touched the bubble under the conditions G=10 c.f.m., L=10 g.p.m., WH=1.5 in., 1 row of holes. (Top view of bubble zone and outlet, flow direction from right to left)

Fig. 16d. Formation of stratified elements. The frontal edge of the dye is being agitated in the bubble zone under the conditions G=20 c.f.m., L=5 g.p.m., WH=1.5 in., 3 rows of holes. (Top view of the bubble zone and outlet, flow direction from right to left)

Fig. 17. Bubble formation and bursting. Under the conditions G=7.5 c.f.m., L=7.5 g.p.m., WH= 3 in., spacing=1-1/2 in. (Side view of the bubble zone facing from the direction perpendicular to the flow direction)
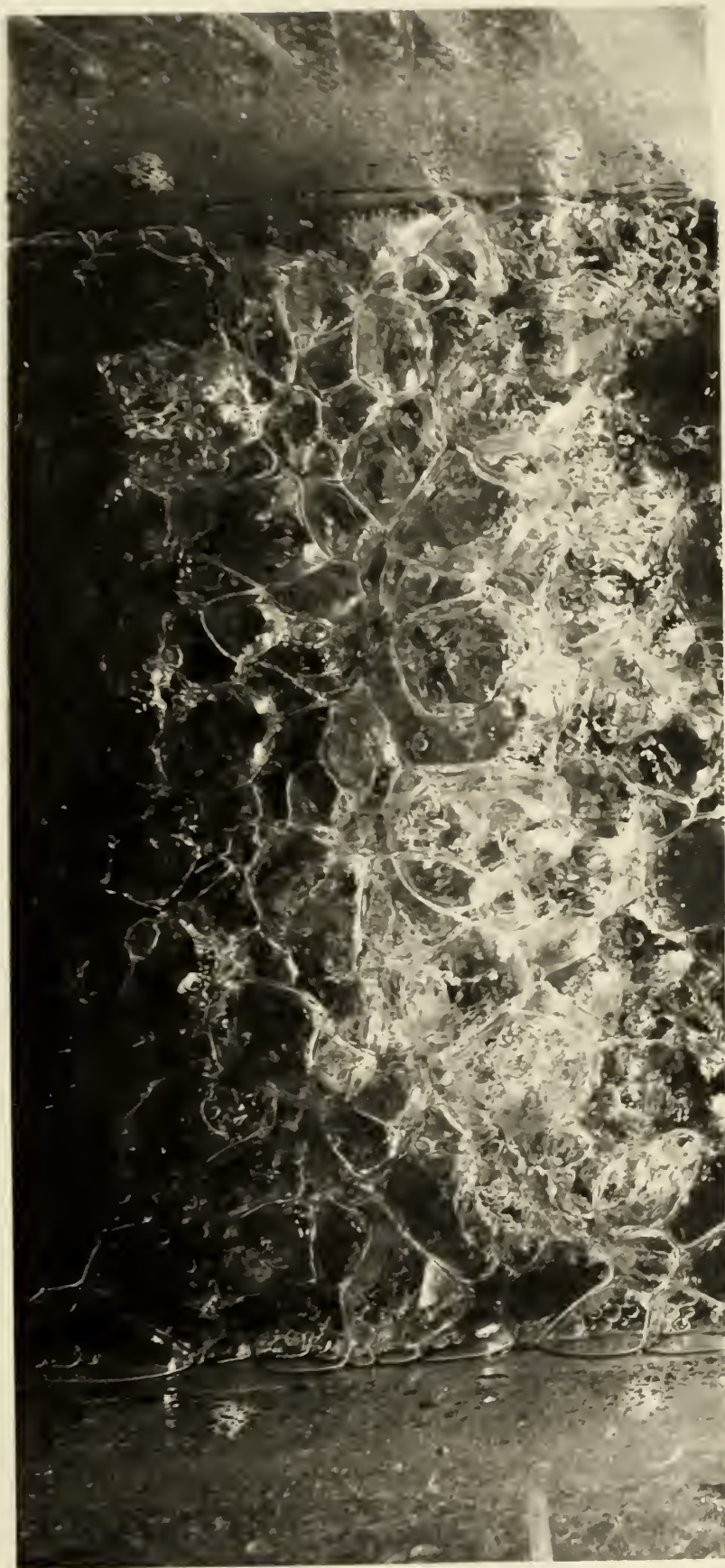
Fig. 18. Cellular foam formation. Under the conditions G=7.5 c.f.m., L=7.5 g.p.m. (Top view of bubble zone)

quite high. Sufficient time was probably not available for the growth of the bubbles at high air flow rates. The bubbles at a high air flow rates were easily broken, and a collection of smaller bubbles was formed at the top of the bubble zone, which appeared as froth.

Studies of the relations between the bubble formation and mass transfer can be found in the published literature (46,47,48).

Formation of the fountain and bypassing effect

The behavior of the fountain or bubble zone may be qualitatively explained as follows. In a circular jet, the volume of flow at a given distance from the orifice is independent of the momentum or the excess of pressure under which the jet leaves the orifice. A jet which leaves under a large pressure difference remains narrower than one leaving with a small pressure difference. The latter carries with it comparatively more stationary fluid than the former.

The stationary fluid, after the injection of air, no longer remains stationary. The horizontal velocity (or velocity in the radial direction perpendicular to the flow through the jet) of water is increased at a distance near the bottom of the wall; while a part of the stationary fluid, far from the wall acquires both horizontal and vertical (or axial direction, the same direction as flow through a jet) velocities. If the stationary fluid (water) has its boundary exposed to the air, part of the fluid (water) will possibly be carried to the top of the jet. Figure 19a shows the change in velocity profile with respect to distance and the stream line pattern of a circular jet.

The behavior of the flow pattern on the sieve tray may be explained by means of an analogy to a circular jet. The injected fluid was air and the
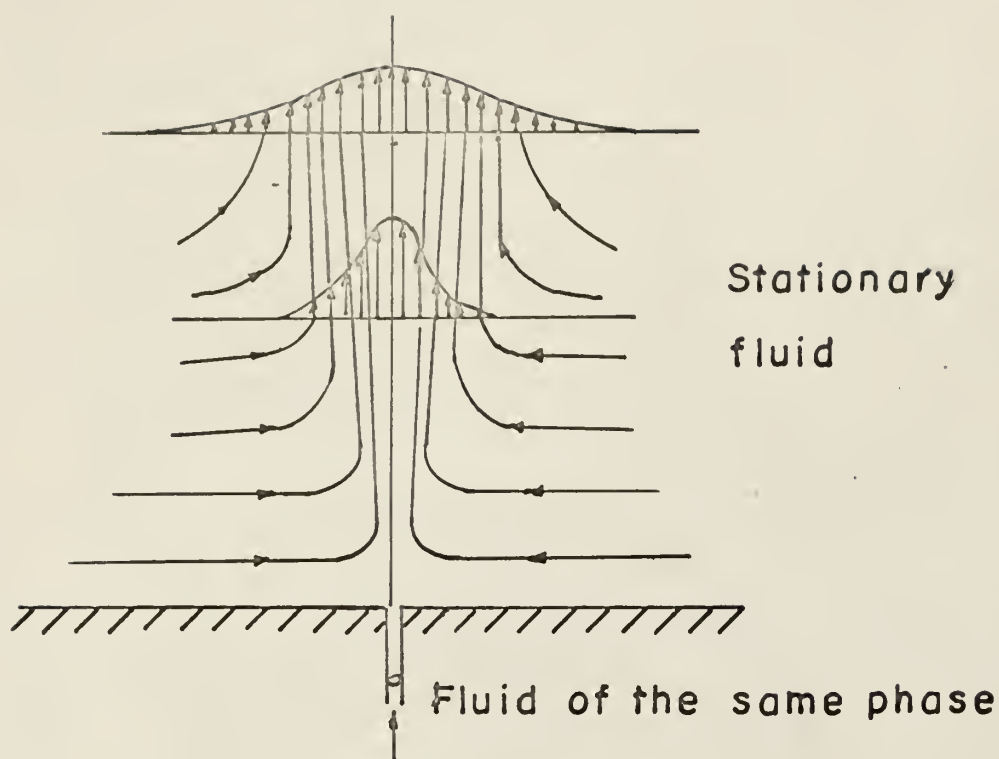
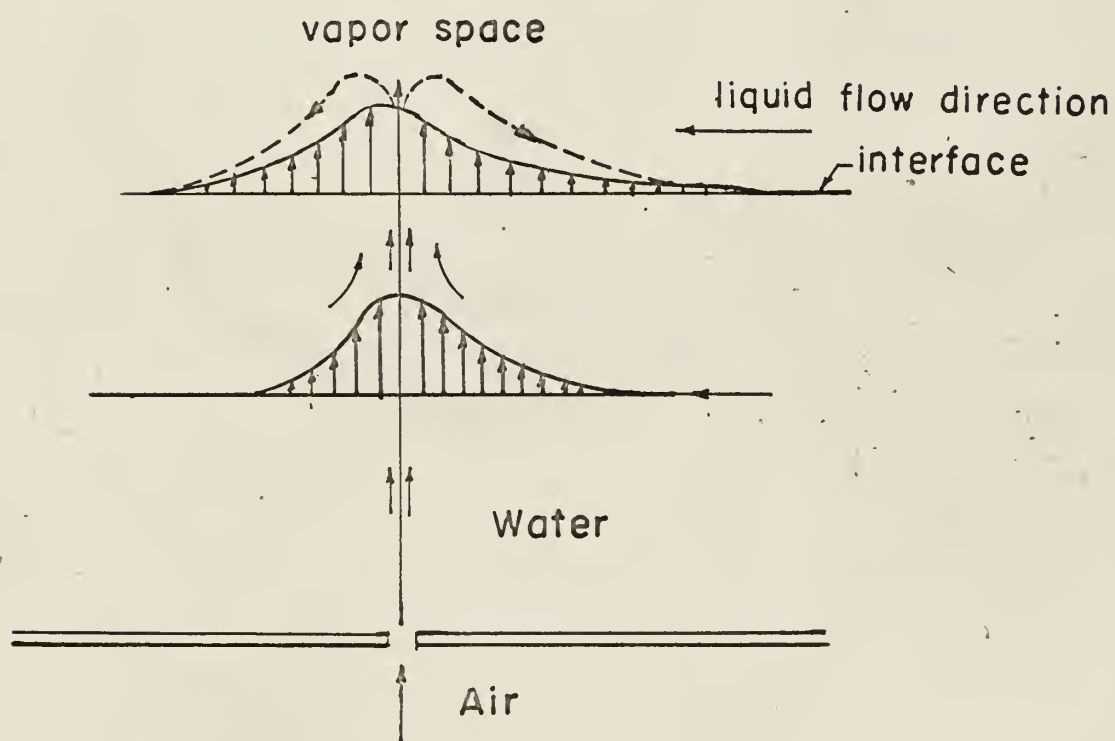Fig. 19a Stream line pattern for a circular lamilar jet (45).

Fig. 19b. Hypothetical flow pattern for air passing through a distillation tray with one row of holes.

liquid on the tray was actually not stationary. However, the holes of the tray may be regarded as a group of jets. Figure 19b shows the hypothetical flow pattern for air passing through a distillation tray with one row of holes perpendicular to the direction of flow. When the upwards liquid flow reaches the interface (interface between the vapor space and liquid), it is then divided into two streams, one stream flowing to the direction of the original liquid flow, and the other flowing against the direction of the liquid flow as shown in Fig. 19b. This gives rise to the formation of fountain. The phenomenon of the fountains will be discussed later in connection with the swinging flow pattern or oscillating flow pattern of the second type.

The mechanism for the occurrence of bypassing streams on a distillation tray still remains unknown. Mutzenberg (31) carried out an interesting investigation in which he compared the tray efficiencies evaluated under different conditions. He found that the tray efficiency was increased by 20% when baffle plates were inserted into the bubbling zone at different depths. This may enable one to suspect that bypassing may occur through the froth and can be reduced by inserting the plates. Another explanation is that the residence time of the fluid element is increased when several plates are inserted into the bubble zone. If one fit the data both with and without the plates to the Γ-distribution model with bypassing across the Γ-mixing unit, the result might show a change in the bypassing parameter, and hence indicate which is the more plausible mechanism.

Occurrence of oscillating flow pattern

The four variables investigated in this work were weir height, liquid flow rate, gas flow rate, and the percentage free area for gas flow.

The oscillating flow patterns observed could be classified into two types, one that oscillates perpendicular to the direction of liquid flow (the first type) and the other parallel to the direction of liquid flow (the second type).

In runs where the weir height was 1", normal flow patterns were obtained regardless of the changes made in the other variables within the range of interest (gas flow rate of approximately 5 to 20 c.f.m., liquid rate of approximately 5 to 15 g.p.m.). The term, normal flow pattern, is used here to distinguish it from an oscillating flow patterns.

However, at a weir height of 1.5 in. and a liquid rate of 10 g.p.m. with a gas rate of 10 c.f.m. and 3 rows of holes, an oscillating phenomenon was observed. Careful observation showed that the flow pattern fluctuated regularly. The peaks rose up the side walls leaving a central valley and then damped down. As this happened a peak was formed in the approximately central region. The process was repeated regularly. When the peaks on both sides were decreasing in height, water forced down through the holes near the sides: while a peak in the center was diminishing, water came through holes near the sides. The amplitude of the oscillation was larger at higher air flow rates and liquid flow rates. Figure 20 illustrates the stages of the first type of oscillating flow pattern. While the oscillating flow pattern shown in Fig. 21a,b was slightly different from that depicted in Fig. 20, they essentially show the oscillating flow pattern of the first type. The front view of the normal flow pattern is given in Figure 20c for comparison. Figures 21a and 21b were taken under the same conditions. Figures 22a,b,c, and d show the side view of the oscillating flow pattern of the first type.

Figures 23a and b show the side view of the swinging flow pattern, that

64

Stage I

Peak

Valley

Air

Water

Air
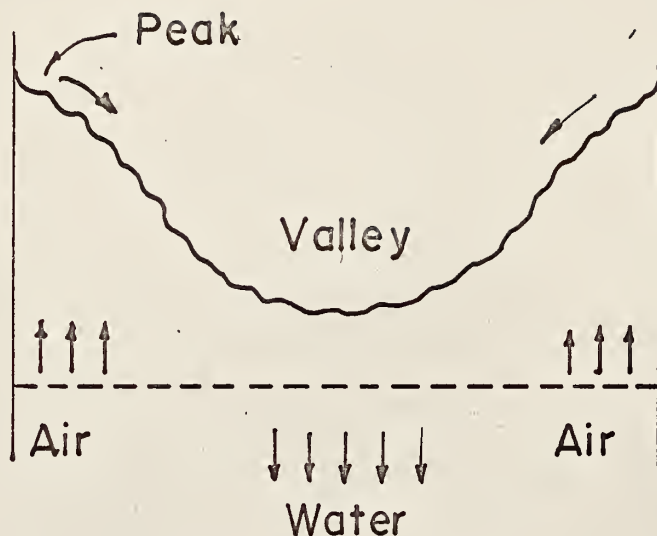
Water tends to
flow down, when
the peak reaches
its maximum
height.

Stage 2

Peak
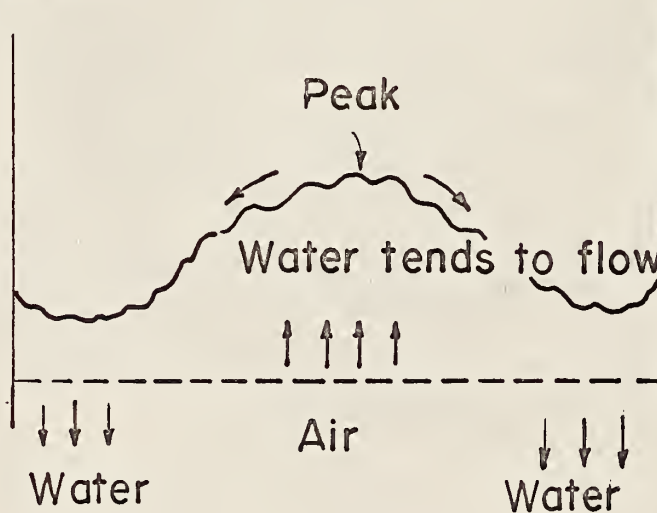
Water tends to flow down

Air

Water

Water

Air has been
flowing into
the center
region

Fig. 20. Stages in the formation of
ocillating flow pattern.
(front view, facing in the direction
from downstream to upstream).

Fig. 21a. Oscillating flow pattern of the first type. Peaks form at the left side of the wall and near the center of the cross-section under the conditions G=10 c.f.m., L=10 g.p.m., WH=1.5 in., 3 rows of holes. (Front view, facing from downstream to upstream)

Fig. 21b. Oscillating flow pattern of the first type. Peaks form at the right side of the wall and near the center of the cross-section under the conditions G=10 c.f.m., L=10 g.p.m., WH= 1.5 in., 3 rows of holes. (Front view, facing from downstream to upstream)

Fig. 21c. Normal flow pattern. (Front view, facing from downstream to upstream)

Fig. 22a. Normal flow pattern. Under the conditions G=20 c.f.m., L=2 g.p.m., WH=1.5 in., 7 rows of holes. (Side view, the flow direction is from right to left)
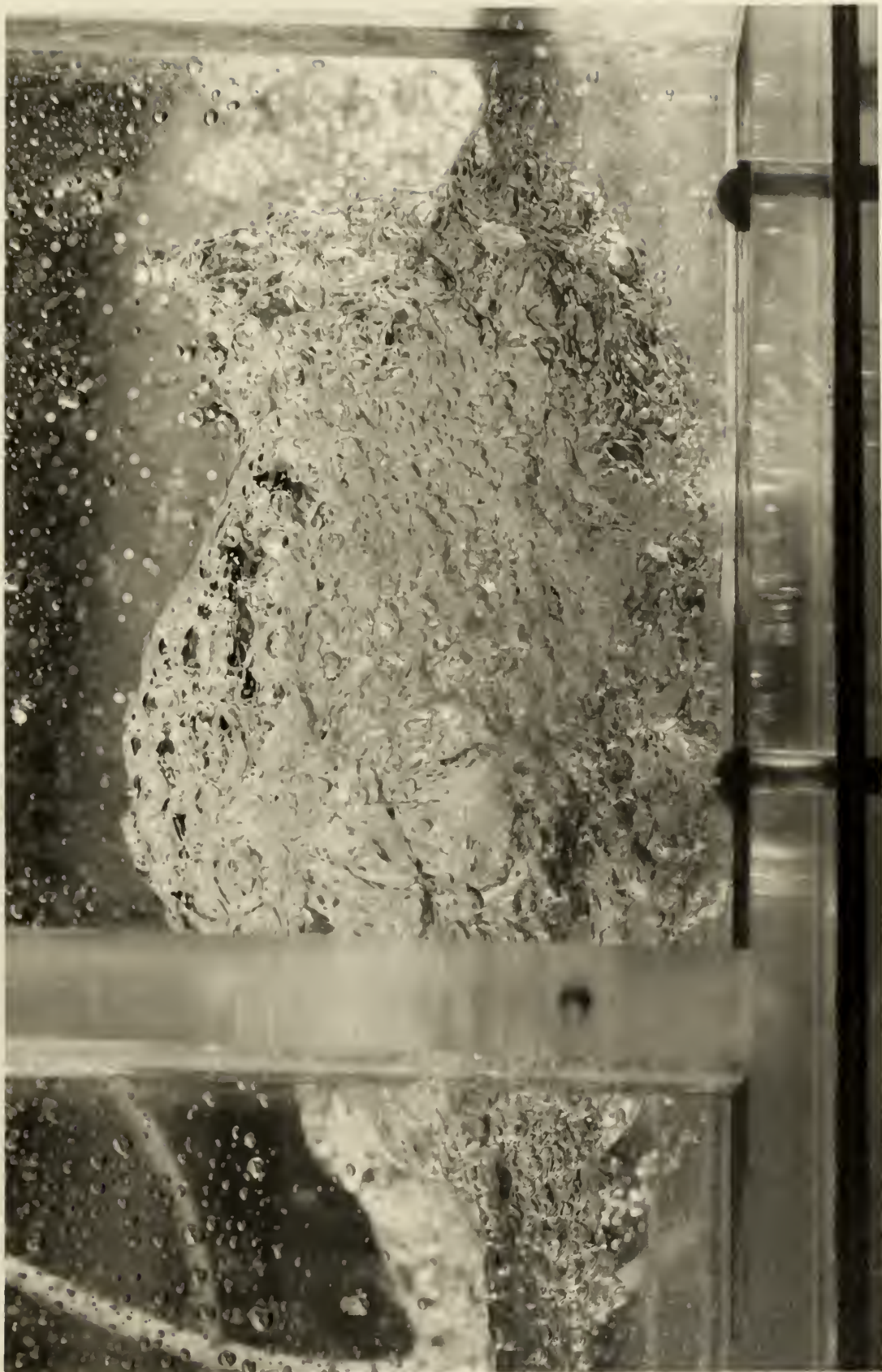
Fig. 22b. Oscillating flow pattern of the first type. Under the conditions G=20 c.f.m., L=15 g.p.m., WH=1.5 in., 7 rows of holes. (Side view, the flow direction from right to left)

Fig. 22c. Oscillating flow pattern of the first type. Under the conditions G=20 c.f.m., L=10 g.p.m., WH=1.5 in., 7 rows of holes. (Side view, the flow direction from right to left)

71

Fig. 22d. Oscillating flow pattern of the first type. Under the conditions G=20 c.f.m., L=5 g.p.m., WH=1.5 in., 7 rows of holes. (Side view, the flow direction is from right to left)

Fig. 23a. Swinging flow pattern or oscillating flow pattern of the second type. Swinging towards the outlet direction under the conditions G=20 c.f.m., L=2 g.p.m., WH=1.5 in., 1 row of holes. (Side view, the flow direction is from right to left)

Fig. 23b. Swinging flow pattern or oscillating flow pattern of the second type. Swinging towards the inlet under the conditions G=20 c.f.m., L=2 g.p.m., WH=1.5 in., 1 row of holes. (Side view, the flow direction is from right to left)

is, the second type of oscillating flow patterns. The swinging flow pattern occurred at very low liquid flow rate (2 g.p.m. or less). The direction of the oscillation was different from the first type oscillating flow pattern. It oscillated parallel to the direction of the liquid flow. The swinging type oscillation phenomenon could be eliminated by simply increasing the liquid flow rate. The side view of the normal flow pattern is given in Fig. 23c for comparison.
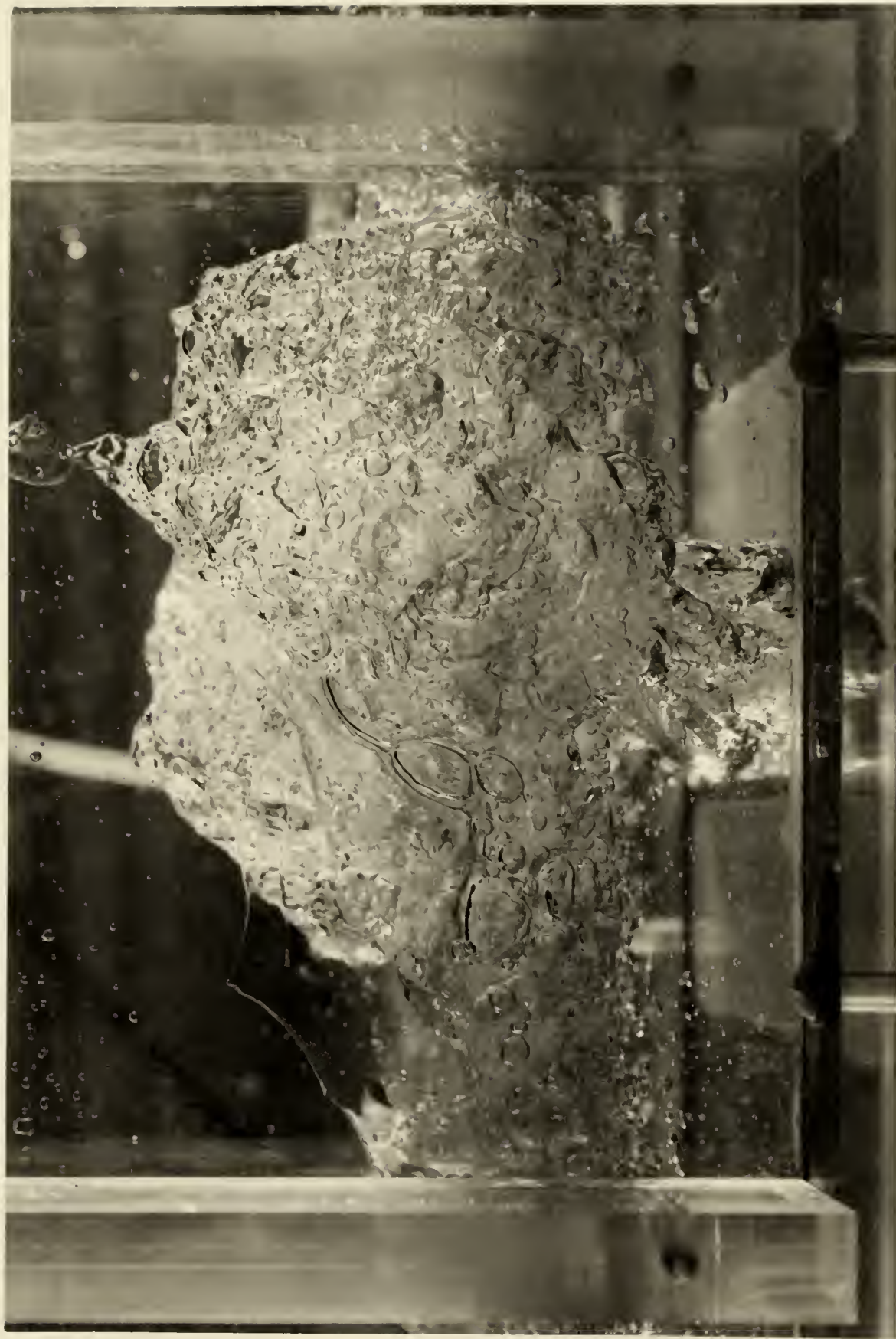
Fig. 23c. Normal flow pattern. Under the conditions G=20 c.f.m., L=10 g.p.m., WH=1.5 in., 1 row of holes. (Side view, the flow direction is from right to left)

Explanation for the occurrence of the oscillating flow patterns

A possible explanation for the occurrence of the oscillating flow pattern of the first type is given below:

Due to the non-uniform velocity profile (the water flowing near the center region of a tray being faster than that near the wall), a static pressure difference may exist between the central region and the region near the wall. When the upwards flow of air is just at its critical pressure to overcome the overall liquid head, it tends to pass through the holes where the pressure head is low. Supposing that the low pressure head first occurs in the central region where the water flow velocity is higher than that at both sides as mentioned above, the air stream will cause the liquid level to peak in the center region. As the peak reaches its maximum height, the region of the low pressure head moves toward one or both sides near the wall. Now the air tends to flow through the region near the wall and this in turn causes a peak or peaks to be formed in the corresponding region as illustrated in Fig. 20. The repeated processes cause the oscillation phenomenon.

The second type of oscillating flow pattern might be explained as below:

High velocity air (air flow rate of approximately ten c.f.m. for from one to three rows of holes in the sieve tray under consideration) can readily overcome the liquid depth. The flow of liquid under such a high air flow rate tends to be blocked by the bubble zone. This in turn tends to cause the liquid to accumulate temporarily behind the bubble zone until its level reaches a certain depth to overcome the "blocking" action by the bubble zone. The repetition of this process gives rise to the oscillation phenomenon of the second type.

CHAPTER IX

QUANTITATIVE ANALYSIS

The response of the measuring instrument must be understood before the details of the quantitative analysis of the experimental data can be carried out.

Range of the conductivity

The range of the conductivity of common solutions is shown in Fig. 24. The minimum concentration detected in this work is the concentration of tap water. The salt solution being measured here was a function of the water flow rate, and the concentration and amount of the salt solution which was injected. If the range were so chosen that it was much over the required range, the output signal of the Solu Meter would be very weak so that the recorder would fail to strengthen it. On the other hand, if the range was too small the variation of the tap water salt concentration would have introduced appreciable error into the recorded curves. For this reason, the daily variation of the tap water salt conductivity was measured continuously for one month. There was no significant change.

Problems of the linearity of the relation between concentration and conductivity and temperature effect on the conductivity change have been partially discussed in Chapter 7. These two problems are discussed further below.

Relationship between conductivity and concentration

The relationship between conductivity and concentration is, in general, non-linear. However, at very low concentration it is approximately linear.

Specific
resistance

100MEG 10MEG 1000K 100K 10K 1000 100 10 1 Ohm-cm

.01   .1   1   10   100   1000   10K   100K   1000K Microhms/cm

Specific
conductance

Ultra
pure water

Good quality
distilled water

.05%NaCl

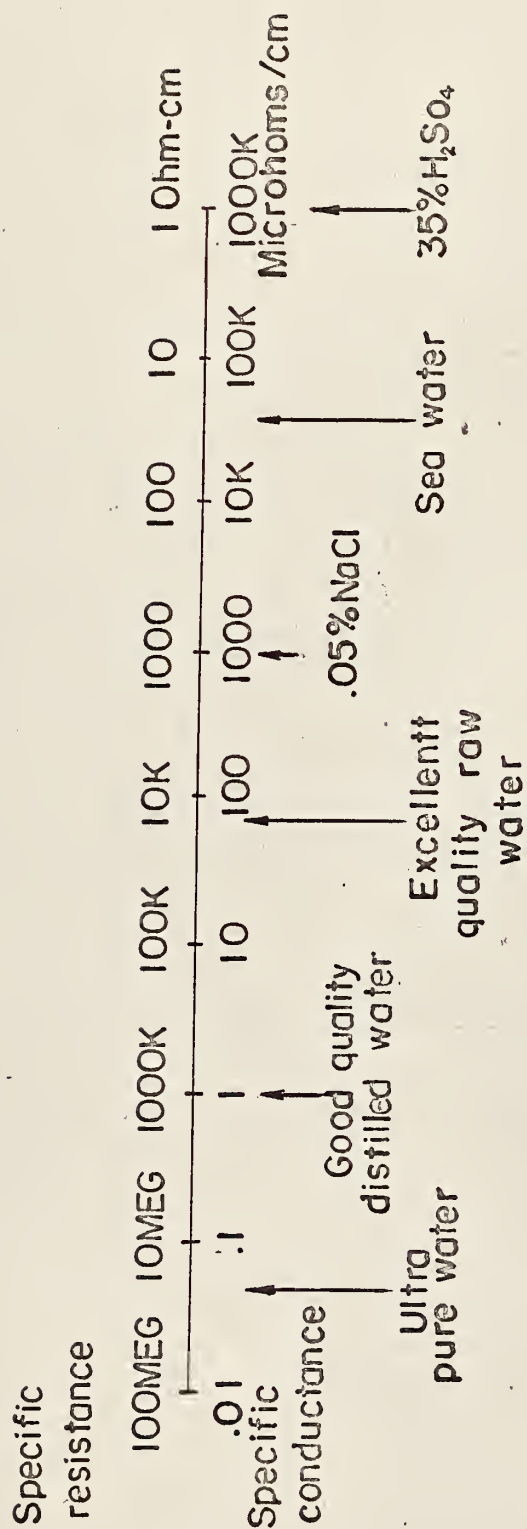Excellent
quality raw
water

Sea water

35%H₂SO₄

Fig. 24. Spectrum of the conductivity of common solutions.

(from catalog 27 of Industrial Instrument Inc.)

78

Prausnitz (43) has presented the following equation for his specific instrument:

$$N = \frac{8.73 - 0.136t}{R^{0.93}} \qquad (9\text{-}1)$$

where

N = normality of the hydrochloric acid,

R = resistance, ohm,

t = temperature, °C.

In this experiment the absolute concentration was not required. Two concentration-time responses, one at the inlet and the other at the outlet, were needed. The important requirements were that

(1) The recorded millivolts be proportional to the conductivity. It was necessary that the conductivity be proportional to the concentration within the range of interest.

(2) The two probes have the same efficiencies.

The first requirement was of the utmost importance, while the second was not absolutely necessary since a correcting program could adjust the data. Therefore it was necessary to make two equipment tests, one before and the other after each experimental run. This primary test was carried out as follows:

(1) Prepare 1000 c.c. of the tap water in a container and immerse the probes into the water. Adjust the recorder pens to get the base zero line (The tap water is collected directly from the system).

(2) Drop one c.c. of the salt solution into the container and stir it thoroughly.

(3) Observe the recorded curve until it reaches the plateau. Then

record the change in the millivolt reading.

(4) Drop another c.c. of the same salt solution and record the change in the millivolt reading.

(5) Repeat the procedure until the range of interest has been exceeded.

The results first obtained for one of the probes were not satisfactory, but after careful adjustment of the manual temperature compensation, two linear curves were obtained. The test was repeated after each run to make sure that the temperature change during the period of operation did not change the recording. Two typical curves are given in Figs. 25 and 26.

Since the amount of salt solution introduced was not over 10 c.c., the concentration increase could be treated as an arithmetical progression.

Experimental data

Table 2 shows a sample of the data sheets used in recording the experimental data. Two sets of data were taken in order to analyze the effect of the stratified elements on the degree of mixing. One set of data was obtained using one row of holes (15 holes) in the bubble zone while the other set was collected using three rows of holes (43 holes). Figs. 27a and 27b show records of the input and output pulses obtained in two duplicates of run 11. Both the input and the output concentration-time curves appear to be very similar. This gives some assurance that the recording devices were functioning normally.

Figures 28a, 28b, and 28c show records of the input and output pulses for three runs (runs 12, 19, and 20) at different water flow rates but at a constant air flow rate of 8 c.f.m. Appearance of peaks on the response curves for these runs are appreciably different. Run 12 was carried out at a water rate of 10 g.p.m. and an air rate of 8 c.f.m. Run 19 was carried out at a

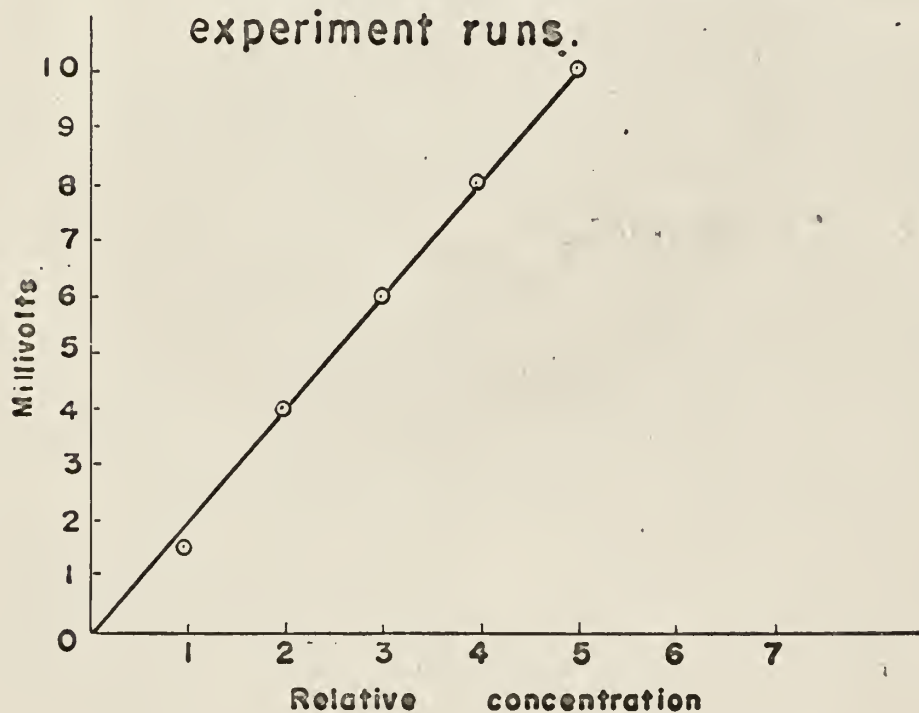Fig. 25 a. Primary test for the linearity of the inlet probe before experiment runs.

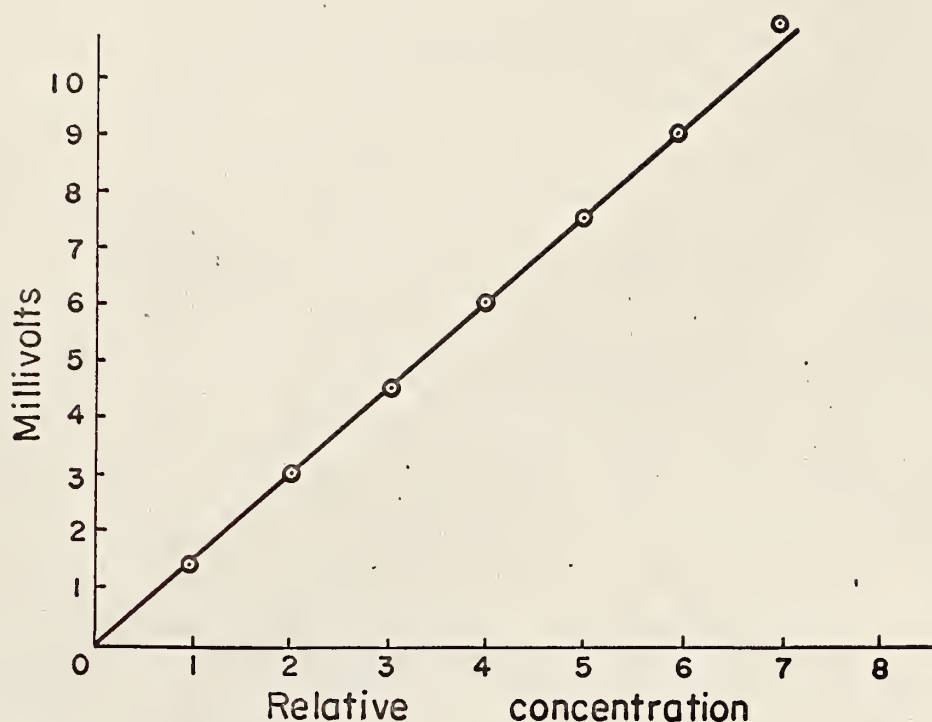Fig. 25b. Primary test for the linearity of the outlet probe before experimental runs.

Fig.26a. Primary test for the linearity of the
inlet probe after experimental runs.
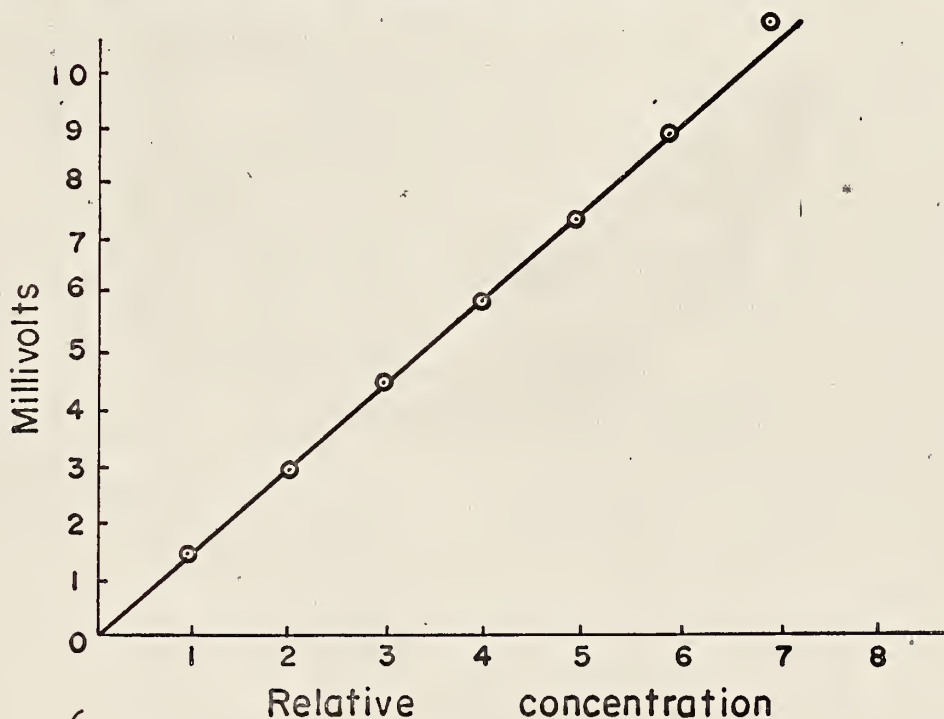
Fig.26b. Primary test for the linearity of the
outlet probe after experimental runs.

TABLE 2

Data Sheet

Run Number _____ 11 _____   Date __May 19, 1966_

Tray Variables   Water Flow Rate __10 g.p.m.___

Number of Holes __15 (1 row)__   Air Flow Rate _____8 c.f.m.___

Weir Height _____1.5 in_____   Water Temperature __15.5°C___

Liquid Depth (Average) _2.1292 in_   Room Temperature ___25.5°C___

Pressure Drop _9.1 cm H_2O__   Total Pressure Drop _9.1 cm H_2O

Position of the Probes Located

Inlet ___Center_____

Outlet _2.4 in from left__

Local Liquid Depth   Instrument Settings

1. ___5.25 cm_____   Scale __.1x to .1x___

2. ___5.31_____   Time Constant ___0.5 sec____

3. ___5.45_____   Preamplifier ___.5/.5_____

4. ___5.37_____   Chart Speed __5 mm/sec_____

5. ___5.50_____   Preamplifier Gain _____

6. ___5.57_____

Comments

Tracer Volume _10 c.c. saturated salt solution_

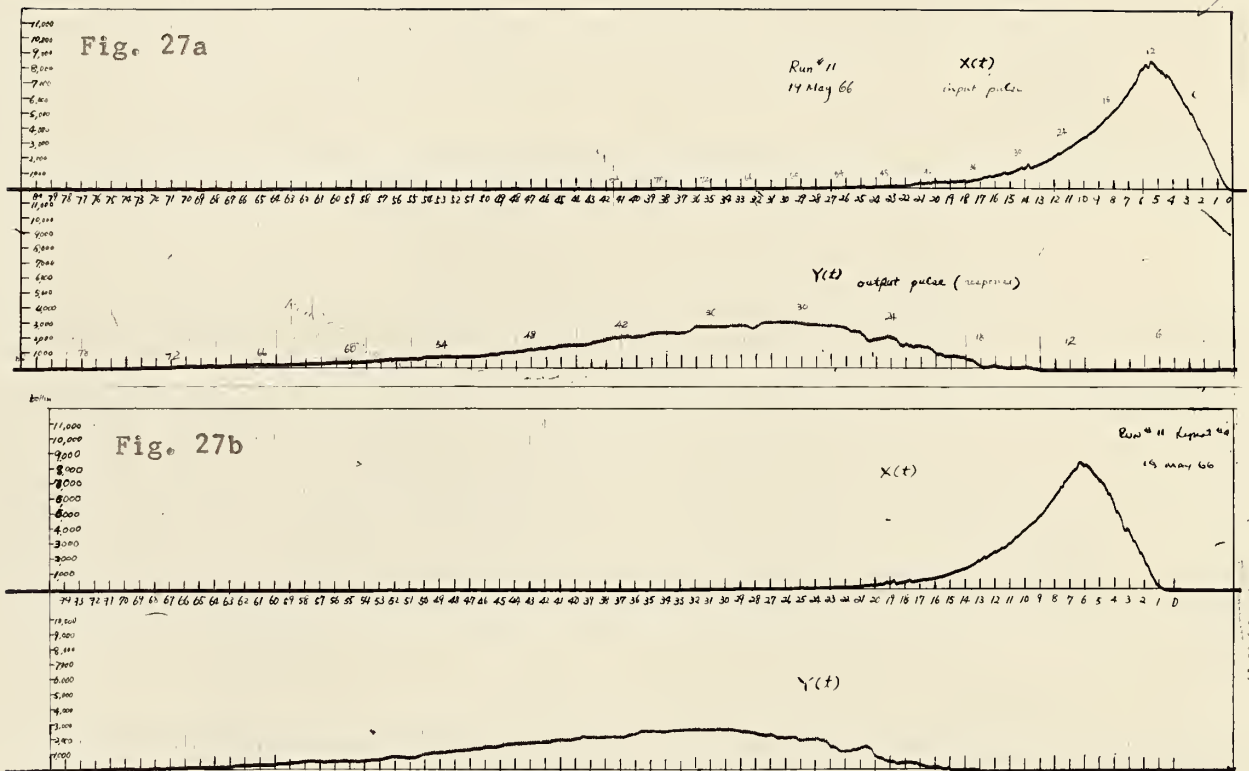Fig. 27a. The input and output curves of Run 11.

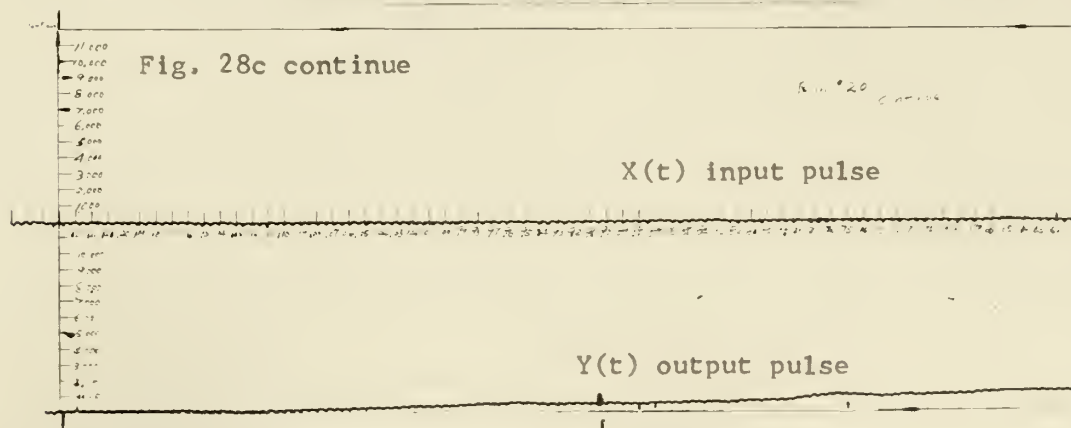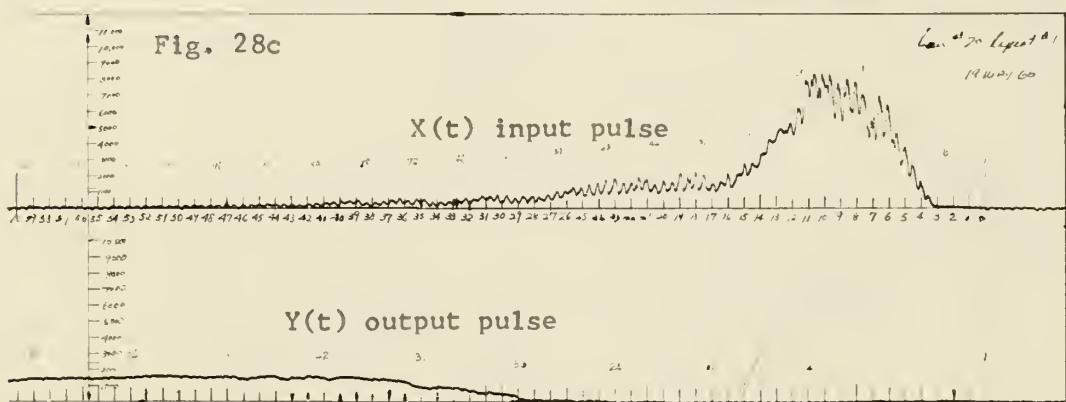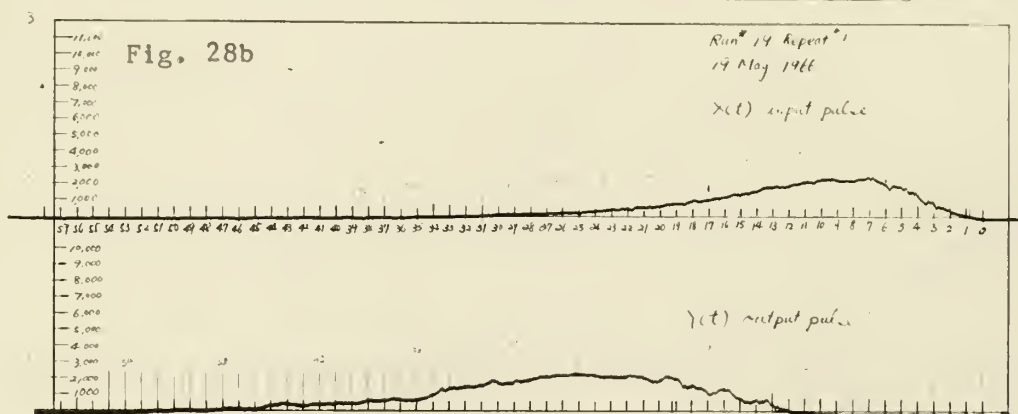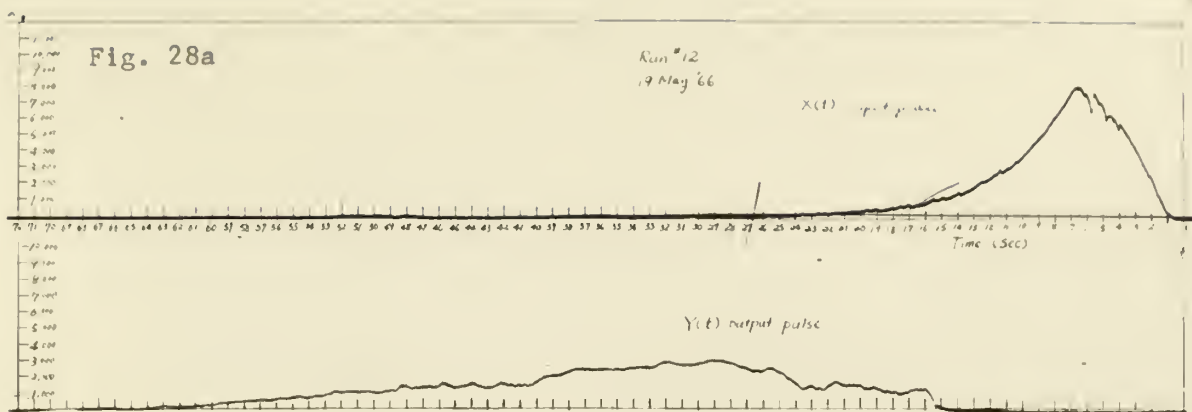27b. The input and output curves of a duplicate run for Run 11.

Fig. 28a, The input and output curves of Run 12,
28b, The input and output curves of Run 19,
28c, The input and output curves of Run 20,

very high flow rate of water (16 g.p.m.), therefore, the broadening of the response curve as compared with the inlet signal was almost indistinguishable. Run 20, carried out at a very low water flow rate (4 g.p.m.), gave a broader peak with a very long tail. The fluctuations in the curves in Run 20 were probably due to the oscillating flow patterns of the second type (swinging back and forth in the direction of flow) described in the preceding chapter.

As previously mentioned, the small uncertainty as to the end of the response curve causes a significant error in the calculation of the variance of the response curve. This was tested by sightly changing the cut-off point of the tail, which caused a change in the total area of less than 1%. However, it changed the variance about 10%.

In addition, appreciable differences between the total areas of the input signal and output signal were found in some of the experimental runs. This was probably partially due to uneven distribution of the inlet tracer and also to the stratification effect. Therefore, a systematic adjustment of the data was required.

Roose (49) proposed the method which changes the ordinates of $Y(\theta)$ with the empirical correction formula,

$$Y(\theta)_c = P Y(\theta) \left[1 - Q \theta \right] , \qquad (9\text{-}2)$$

where $Y(\theta)_c$ represents the adjusted response data, $Y(\theta)$ the raw normalized response data, P and Q are the correction factors. If the data are good, the values of P and Q should be close to one and zero respectively. For the pulse testing, it can be assumed that the input, $X(\theta)$, is fairly correct and that it is only necessary to correct the output data. P and Q can be computed by noting two properties of the pulse testing data.

The first property is

$$\int_0^\infty X(\theta)\, d\theta = \int_0^\infty Y(\theta)\, d\theta = 1 \qquad (9\text{-}3)$$

The second property, which has been stated, is that the mean, $\mu_{\theta Y}$, of $Y(\theta)$ minus the mean, $\mu_{\theta X}$, of $X(\theta)$ is equal to the mean, μ_θ, of $\underline{E}(\theta)$, that is,

$$\mu_{\theta Y} - \mu_{\theta X} = \vartriangle \mu_{\theta Y X} = \mu_\theta \qquad (9\text{-}4)$$

Zwietering (11) has shown that for a closed system the mean of $\underline{E}(\theta)$ is equal to unity. Therefore

$$\mu_{\theta Y} - \mu_{\theta X} = \vartriangle \mu_{\theta Y X} = 1 \qquad (9\text{-}5)$$

From equations (9-2) and (9-3) we have

$$\int_0^\infty Y(\theta)_c\, d\theta = P \int_0^\infty Y(\theta)\, d\theta - PQ \int_0^\infty \theta\, Y(\theta)\, d\theta = 1 \qquad (9\text{-}6)$$

From equations (9-2), (9-5) and (9-6)

$$\int_0^\infty \theta\, Y(\theta)_c\, d\theta - \int_0^\infty \theta\, X(\theta)\, d\theta$$

$$= P \int_0^\infty \theta\, Y(\theta)\, d\theta - PQ \int_0^\infty \theta^2\, Y(\theta)\, d\theta - \int_0^\infty \theta\, X(\theta)\, d\theta = 1$$

By letting

$$A = \int_0^\infty \theta\, Y(\theta)\, d\theta \ ,$$

$$B = \int_0^\infty \theta\, X(\theta)\, d\theta \ , \qquad (9\text{-}8)$$

and

$$M = \int_0^\infty \theta^2 Y(\theta)\, d\theta \quad,$$

the solution of equations (9-6) and (9-7) for P and Q can be obtained as

$$P = \frac{A(1 + B) - M}{A^2 - M} \quad,$$

$$Q = \frac{1 + B - A}{A(1 + B) - M}$$

(9-9)

Tables 3 and 4 contain the conditions of the experimental runs, Table 5 and 6 list values of the correction factors P and Q.

Analysis of the data and results

The following procedures were used to obtain the mean and variance from the input pulse of $X(t)$, and output pulse of $Y(t)$.

(1) Read the input and output pulses.

Since the recorded pulses were sufficiently smooth, the time increment for $X(t)$ of 0.5 sec. and that for $Y(t)$ of 1.0 sec. were used. The average points counted for $X(t)$ and $Y(t)$ were nearly the same. It was about 80 points respectively. Much smaller increments were necessary if the pulse was not sufficiently smooth.

(2) Punch the data read from the $X(t)$ and $Y(t)$ curves on the IBM cards.

(3) Calculate P and Q and obtain a set of corrected data from the data correction program.

(4) Use the corrected data to calculate the $\Delta\mu_{\theta YX}$, and $\Delta\sigma^2_{\theta YX}$ according to the following equations:

The first moment, or the mean, of a distribution, $f(t)$, is defined as (8)

TABLE 3. CONDITIONS OF THE EXPERIMENTAL RUNS FROM RUN 1 TO RUN 8.

Run No.	Liquid flow rate (g.p.m.)	Air flow rate (c.f.m.)	Weir height (in.)	No. of holes	Probe positions outlet (in.)	Probe positions inlet (in.)
1	10	20	1.5	43	2.4	center
2	10	20	1.5	43	4.8	center
3	10	20	1.5	43	7.2	center
4	10	20	1.5	43	9.6	center
5	10	20	1.5	43	center	2.4
6	10	20	1.5	43	center	4.8
7	10	20	1.5	43	center	7.2
8	10	20	1.5	43	center	9.6

* Probe positions are defined in such a manner that facing the direction from down-stream to upstream, the position of the left hand side wall is equal to 0 and the position of the right hand side wall is equal to 12 in.

TABLE 4. CONDITIONS OF THE EXPERIMENTAL RUNS FROM RUN 11 TO RUN 18.

Run No.	Liquid flow rate (g.p.m.)	Air flow rate (c.f.m.)	Weir height (in.)	No. of holes	Probe positions outlet (in.)	Probe positions inlet (in.)
11	10	8	1.5	15	2.4	center
12	10	8	1.5	15	4.8	center
13	10	8	1.5	15	7.2	center
14	10	8	1.5	15	9.6	center
15	10	8	1.5	15	center	2.4
16	10	8	1.5	15	center	4.8
17	10	8	1.5	15	center	7.2
18	10	8	1.5	15	center	9.6

TABLE 5.   CORRECTION FACTORS P AND Q FROM RUN 1 TO RUN 8.

Run Number	P	Q
1	2.03129	0.320165
2	2.45992	0.337048
3	1.74853	0.257272
4	1.93885	0.287961
5	2.07940	0.296839
6	2.06114	0.284637
7	1.97809	0.284637
8	2.09876	0.282301
average	2.056	0.294

TABLE 6.   CORRECTION FACTORS P AND Q FROM RUN 11 TO RUN 18.

Run Number	P	Q
11	3.53030	0.382755
12	3.19750	0.380024
13	2.85484	0.377417
14	2.34872	0.358905
15	2.21319	0.326604
16	2.93831	0.363699
17	2.91013	0.369718
18	2.78836	0.368090
average	2.847	0.366

$$\mu_t = \frac{\int_0^\infty t\, f(t)\, dt}{\int_0^\infty f(t)\, dt} \qquad (9\text{-}10)$$

The second moment about the mean, or the variance, is defined as (8)

$$\sigma_t^2 = \frac{\int_0^\infty (t - \mu_t)^2\, f(t)\, dt}{\int_0^\infty f(t)\, dt} \qquad (9\text{-}11)$$

If $f(t)$ is read at N equidistant points, equations (9-10) and (9-11) may be expressed for the purposes of numerical computation as

$$\mu_t = \frac{\sum_{i=1}^N t_i\, f(t_i)}{\sum_{i=1}^N f(t_i)} \qquad (9\text{-}12)$$

$$\sigma_t^2 = \frac{\sum_{i=1}^N (t_i - \mu_t)^2\, f(t)}{\sum_{i=1}^N f(t_i)} \qquad (9\text{-}13)$$

A simple computer program was developed by Johnson (1) to compute the dimensionless quantities, $\Delta\mu_{\theta YX}$ and $\Delta\sigma_{\theta YX}^2$. This was done by first computing μ_t and σ_t^2 for both $X(t)$ and $Y(t)$ according to equations (8-12) and (8-13). The difference in the means was then calculated and made dimensionless by dividing it by $\bar{t}$, the mean residence time. The difference in the variances was calculated and then normalized by dividing it by $\bar{t}^2$. The results can be found in Tables 7, and 8.

TABLE 7. EXPERIMENTAL VALUES OF $\Delta\mu_{\theta YX}$ AND $\Delta\sigma^2_{\theta YX}$ FROM ADJUSTED DATA FOR RUN 1 TO RUN 8.

Run Number	$\Delta\mu_{\theta YX} = \mu_\theta$	$\Delta\sigma^2_{\theta YX} = \sigma^2_\theta$
1	1.0009	.0792
2	1.0009	.0669
3	1.0007	.2052
4	1.0007	.2075
5	1.0008	.1418
6	1.0008	.1608
7	1.0007	.1587
8	1.0008	.1233

TABLE 8. EXPERIMENTAL VALUES OF $\Delta\mu_{\theta YX}$ AND $\Delta\sigma^2_{\theta YX}$ FROM ADJUSTED DATA FOR RUN 11 TO RUN 18.

Run Number	$\Delta\mu_{\theta YX} = \mu_\theta$	$\Delta\sigma^2_{\theta YX} = \sigma^2_\theta$
11	1.0278	-.1843
12	1.0277	-.0600
13	1.0276	-.0348
14	1.0275	-.0646
15	1.0274	.0906
16	1.0276	-.0043
17	1.0276	-.528
18	1.0276	.0161

The third moment about the mean, or the skewness, if required, can be calculated from its definition,

$$\tau_t^3 = \frac{\int_0^\infty (t - \mu_t)^3 f(t)\,dt}{\int_0^\infty f(t)\,dt} \qquad (9\text{-}14)$$

If $f(t)$ is read at N equidistance points, equation (8-14) may be expressed for the purposes of numerical computation as

$$\tau_t^3 = \frac{\sum_{i=1}^N (t_i - \mu_t)^3 f(t_i)}{\sum_{i=1}^N f(t_i)} \qquad (9\text{-}15)$$

This can be done by first computing τ_t^3 for both $X(t)$ and $Y(t)$ according to equation (9-15). The difference in the skewness can then be calculated and made dimensionless by dividing it by $\bar{t}^3$.

Evaluation of model parameters

There are three commonly used methods for evaluating model parameters: the moments method of analysis, the frequency response analysis, and the s-plane analysis. The advantages and disadvantages of the moments method have been discussed. Comparison of the frequency response analysis and the s-plane analysis has been given(14). The s-plane analysis is applicable only to non-oscillatory systems, such as the mixing process investigated in this work. The details of the s-plane analysis have been described by the previous worker (1). Model parameters were evaluated according to his procedure.

The Γ-distribution with by-passing across the Γ-mixing unit contains three parameters, τ_d, β, and p as mentioned in Chapter 5. The dimensionless dead time could be determined reasonably accurately from the recorded response curves. Dead time D was determined by taking the difference between time at the onset on the response of the output Y(t) and that of the input X(t). The dimensionless dead time, τ_d, was then calculated by dividing D by $\bar{t}$, the mean residence time. Tables 9 and 10 show τ_d, β, and p for the two sets of data.

Analysis of P and Q values

The area under the input distribution curve should theoretically be equal to the area under the output distribution curve for every experimental run. In the course of this investigation, it was found that in most of the runs, the areas under the output curves were larger than those under the input curves. The first set of data indicates that the average value of the area under output curves was 10% larger than the average value of the areas under the input curves, and 15% larger for the second set of data. For a closed system the mean, μ_θ, of an exit age distribution or the difference of the means, $\Delta\mu_{\theta YX}$, between the output distribution and input distribution should be equal to one. In order to satisfy these requirements, the data adjustment program was applied to the raw data as mentioned previously. As shown in Tables 5 and 6, the values of the correction factors, P and Q, are different from one and zero respectively. The average value of P is 2.056 for the first set of data and 2.847 for the second set of data (Tables 9 and 10). The average value of Q is 0.294 for the first set of data and 0.366 for the second set of data. The average values of P and Q for the first set are closer to one and zero respectively than those for the second set. This

TABLE 9. EXPERIMENTAL VALUES OF THE PARAMETERS, τ_d, β, AND p OF THE Γ-DISTRIBUTION MODEL WITH BY-PASSING ACROSS THE Γ-MIXING UNIT FROM RUN 1 TO RUN 8.

Run Number	β	p	τ_d Observed	Error Square x 10^6
1	.571	18.40	.678	.125
2	.853	5.521	.521	1.825
3	.797	2.630	.469	.0995
4	.755	3.265	.469	.619
5	.788	3.263	.521	.0999
6	.736	3.680	.521	.1401
7	.665	6.691	.521	.3792
8	.878	4.237	.417	.3442

TABLE 10. EXPERIMENTAL VALUES OF THE PARAMETERS, τ_d, β, AND p OF THE Γ-DISTRIBUTION MODEL WITH BY-PASSING ACROSS THE Γ-MIXING UNIT FROM RUN 11 TO RUN 18.

Run Number	β	p	τ_d Observed	Error Square x 10^6
11	.553	51.107	.735	416.850
12	.834	16.268	.630	50.750
13	.658	107.40	.735	20.395
14	.658	3424.02	.630	4.881
15	.680	7.17	.630	.192
16	.723	126.11	.682	43.48
17	.674	91.277	.682	43.48
18	.517	1685.96	.735	23.03

may be due partially to the smaller difference of areas between input and
output for the first set (10%) than for the second set (15%).

Two typical experimental runs, one from the first set and the other
from the second set will be considered. Fig. 25a is the input curve, X(t),
of Run 1 (first set) which is redrawn from the recorded curve. Fig. 25b is
the output curve of Run 1 redrawn from the recorded curve. The area under
the output curve is 4% larger than that under the input curve. In order to
satisfy the two requirements as mentioned, the correction factors, P and Q,
were computed. The points located on the figure are the points of the cor-
rected response, $Y(\theta)_c$, for P equals 2.03 and Q equals 0.32. Connection of
these points will give the adjusted output distribution curve. The adjusted
output curve has a higher peak than the recorded curve, while the tail of
the adjusted curve is lower than the recorded curve. The values of the
points on the tail of the adjusted output curve are very small and even
slightly negative. The unexpected negative values can be explained by Equa-
tion (9-2) in which if the correction factor Q is large such that $1-Q\theta$ is
negative, then $Y(\theta)_c$ can be negative.

Figure 26a is the input curve, X(t), of Run 16 (the second set). Fig.
26b is the output curve, Y(t), of Run 16. The area under the output curve
is 12.8% larger than that under the input curve. The correction factor, P,
equals 2.9 and Q equals 0.36. The adjusted curve again has a higher peak
and lower tail than those of the recorded curve. The magnitudes of the nega-
tive values of the tail of Run 16 are apparently larger than those of Run 1.
Those negative values of some points on the tail may contribute an appreciable
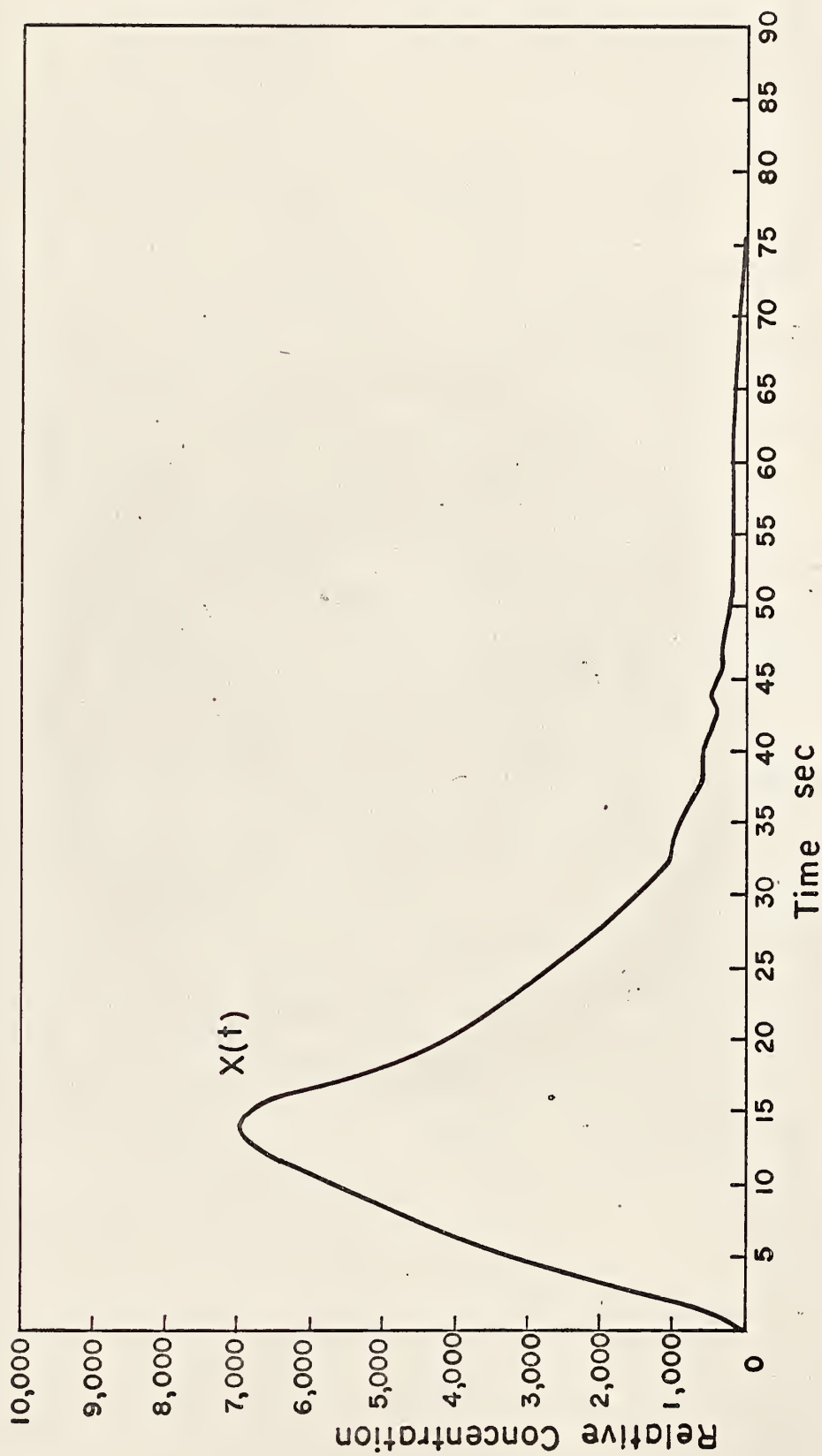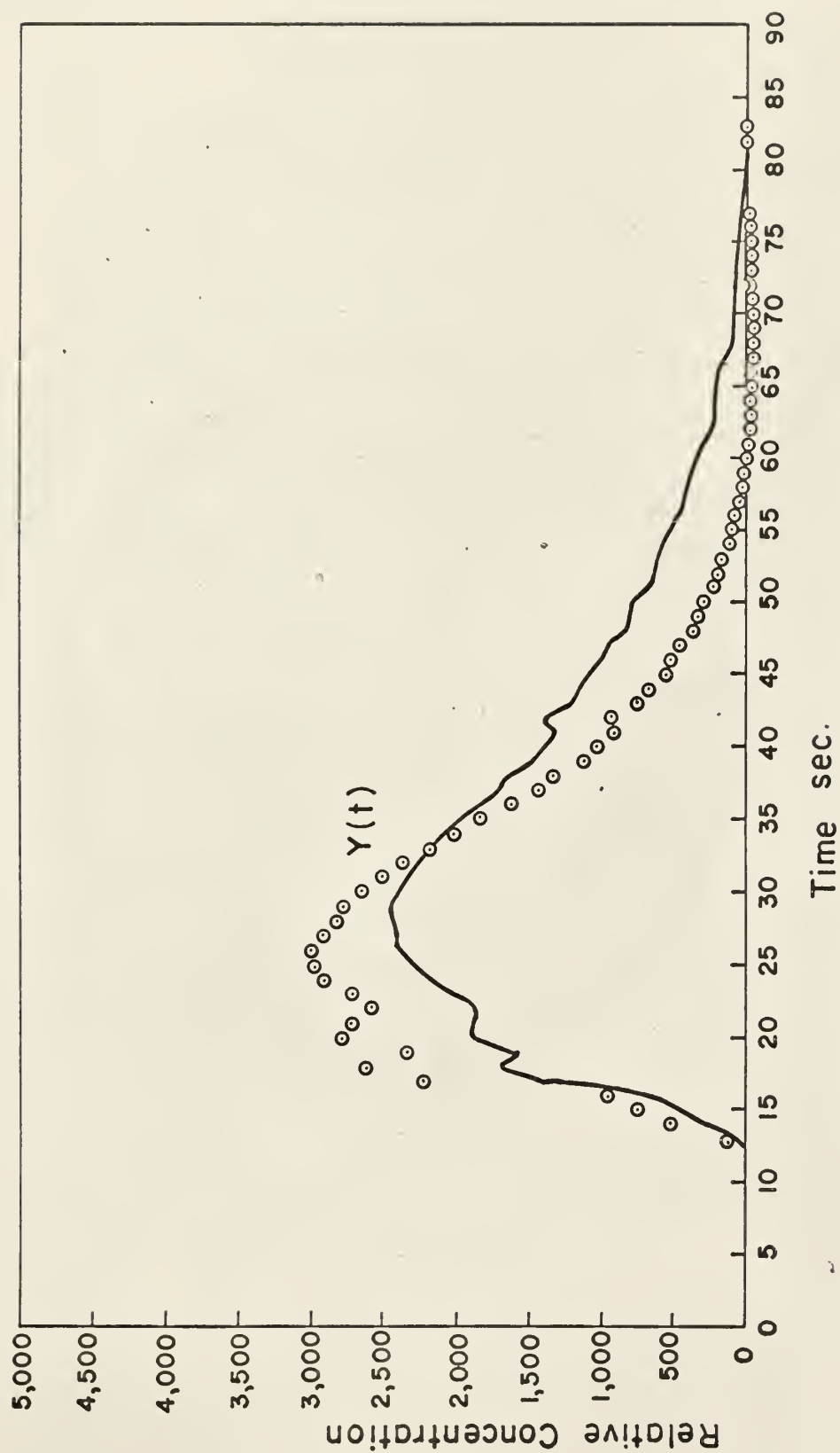negative values in the moments.

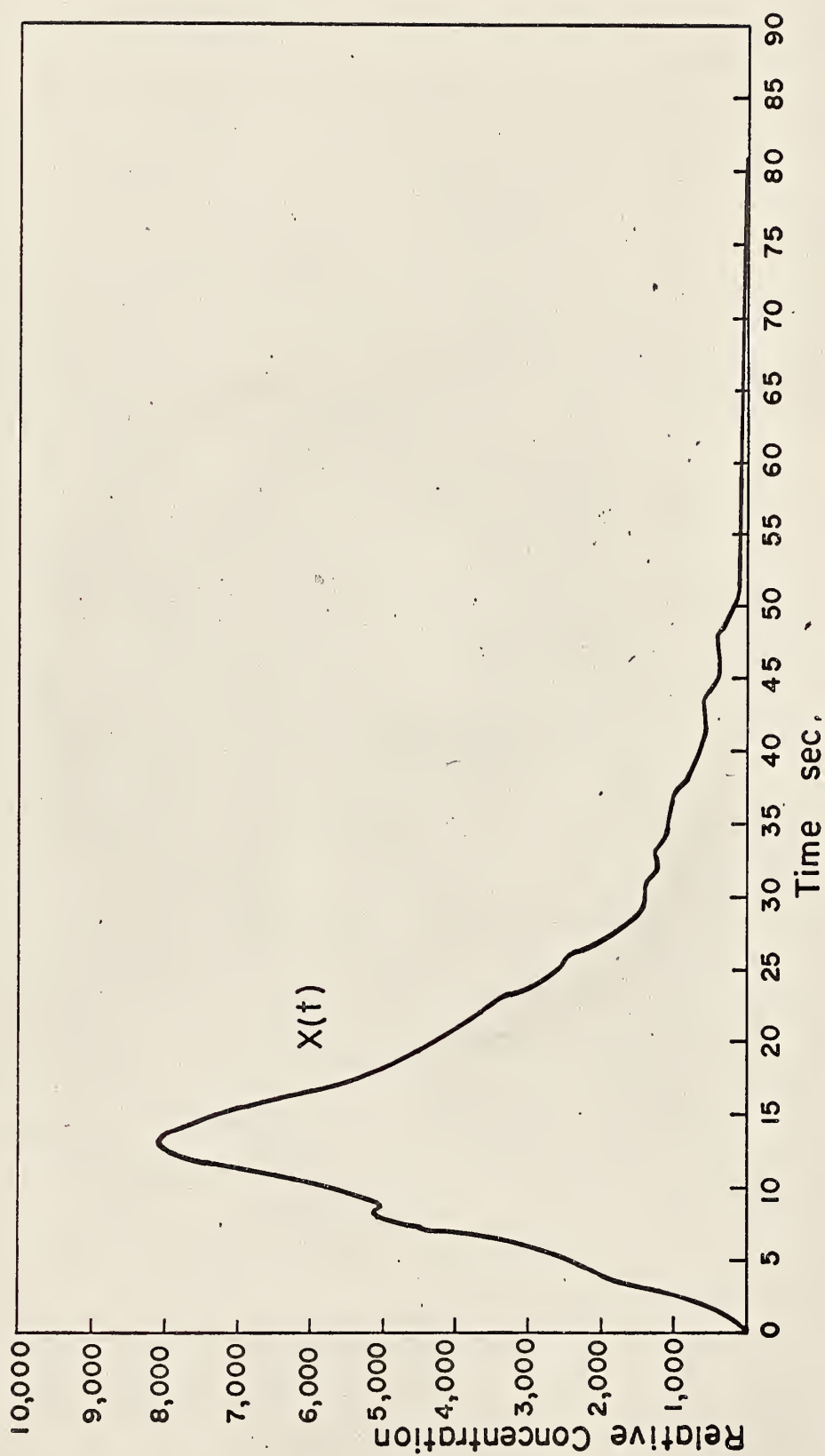Fig. 25 a. Input x(t) curve of Run I.

Fig. 25b. Output Y(t) curve of Run I.
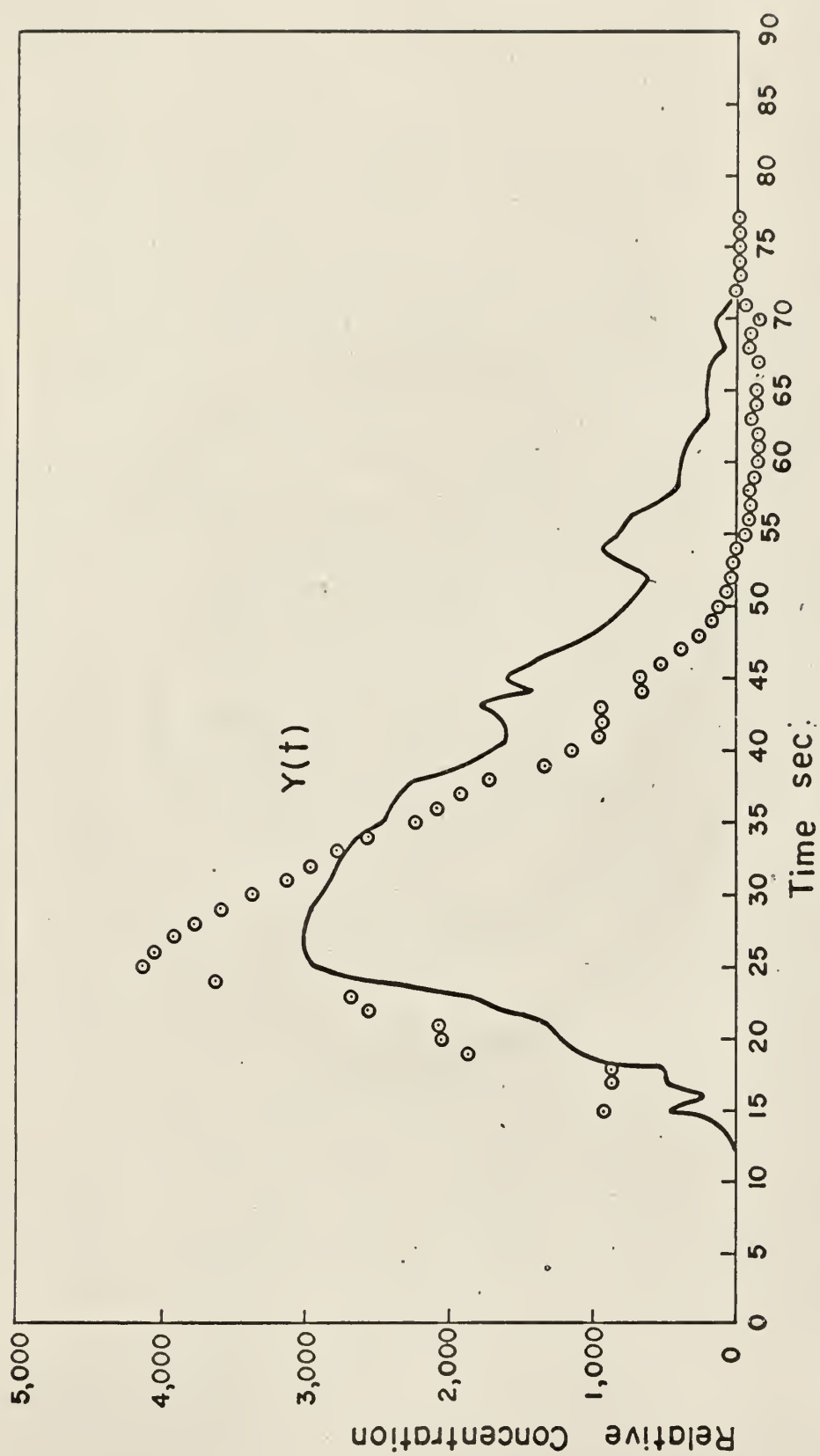
Fig. 26 a. Input x(t) of Run 16.

Fig. 26b. Output Y(t) curve of Run 16.

Analysis of the moments

The numerical values of the mean, $\Delta \mu_{\theta YX}$, which is equal theoretically to μ_θ for the corrected data, is very close to one as expected. The numerical values of $\Delta \sigma^2_{\theta YX}$ must equal σ^2_θ of the exit age distribution as it was described in Chapter 5, therefore, a positive value of $\Delta \sigma^2_{\theta YX}$ is always expected. A larger value of $\Delta \sigma^2_{\theta YX}$ represents a larger spread of the distribution curve and hence represents a larger extent of mixing. The first set of data shows that all the $\Delta \sigma^2_{\theta YX}$ are positive, while the second set of data is negative for most of the experimental runs. The negative values can be explained by the fact that the second moment about the mean of the output, $\sigma^2_{\theta Y}$, is smaller than those of the input $\sigma^2_{\theta X}$. The reason for the smaller $\sigma^2_{\theta Y}$ value may be due to the low degree of mixing, and also due to the negative values of some points which appeared on the tail in the adjusted output curves.

Let us analyze in more detail the numerical values of the second moments about the mean for each experimental run. For the first set of data, Run 1 through Run 4 were carried out separately by varying the position of the outlet probe over the cross-section at the downstream, while the inlet probe was fixed at the center of the cross-section at the upstream. Run 1 and Run 2 have values of $\Delta \sigma^2_{\theta YX}$ of 0.0792 and 0.0669 which are slightly different from each other. The values of $\Delta \sigma^2_{\theta YX}$ for Run 3 and Run 4 are very close, 0.2052 and 0.2075 respectively. However, comparing Runs 1 and 2 with Runs 3 and 4, the values of $\Delta \sigma^2_{\theta YX}$ are quite different. If the concentrations across the cross-section are very uniform, the $\Delta \sigma^2_{\theta YX}$ values for each run should be close or even equal to each other. Run 5 through Run 8 were also recorded separately by varying the position of the inlet probe across the cross section, while the outlet probe was fixed at the center. The values of $\Delta \sigma^2_{\theta YX}$ for Run 5 through

Run 8 are 0.1418, 0.1608, 0.1587, and 0.1233 respectively. Those values are all slightly different. Taking the average value of $\Delta\sigma^2_{\theta YX}$ for Run 1 through Run 4 and the average for Run 5 through Run 8, the first has the average value of 0.1397 and the second 0.1457. After taking the average value, the difference in the second moment about the mean for the average of Run 1 through Run 4 and for the Run 5 through Run 8 is 0.0062 which is so small that it is almost negligible. If one takes the overall average for the eight runs of the first set of data, the $\Delta\sigma^2_{\theta YX}$ value is equal to 0.1429.

The result may represent the true variance, $\Delta\sigma^2_{\theta YX}$, at this experimental condition (excluding the difference in positions), because it is a statistical average of the variances evaluated under different detecting positions. However, to eliminate the stratification effect on the evaluation of the true variance by this procedure may require excessive time. An improved tracer-monitoring technique specifically used for this non-ideal sieve tray is necessary. It will be discussed later.

Among the second set of experiments, Runs 11 through 14 were carried out separately by varying the position of the outlet probe over the cross section at the downstream, while the inlet probe was fixed at the center of the cross section at the upstream. The values of $\Delta\sigma^2_{\theta YX}$ for these runs are -0.1843, -0.0600, -0.0348, and -0.0646 respectively. The average value is -0.0859.

Runs 15 through 18 were recorded separately by varying the position of the inlet probe across the cross section at the upstream, while the outlet probe was fixed at the center of the downstream cross section. The values of $\Delta\sigma^2_{\theta YX}$ for these runs are 0.0906, -0.0043, -0.5280, and 0.0161 respectively. The average value of $\Delta\sigma^2_{\theta YX}$ is -0.1067.

The difference between the average variance for Run 11 through 14 and

that for the Runs 15 through 18 is -0.0208 which can no longer be negligible at the low degree of mixing which occurred in these runs.

Table 11 contains the values of the average, variance, and standard deviation for $\Delta\sigma^2_{\theta YX}$ and model parameters. The average of $\Delta\sigma^2_{\theta YX}$ for the first set is 0.1429 and for the second set is -0.0962. This shows that the mixing for the first set of runs was closer to backmix than that for the second set of runs. Recall that the first set of runs was carried out at a higher air flow rate than the second set of runs. The number of holes and the flow rate of air should contribute significantly to the extent of agitation and stirring and hence change the degree of liquid mixing. The negative value of $\Delta\sigma^2_{\theta YX}$ for the second set of runs may be due to the stratification which was pre- dominate at a low degree of mixing. As mentioned in the previous chapter, the stratification downstream was clearly observed when the extent of agita- tion in the bubbling zone was small.

The variance of $\Delta\sigma^2_{\theta YX}$ for the first set is 0.132 and the standard devia- tion is 0.3638; while for the second set, the variance is 5.122, the standard deviation is 2.263. It is obvious that the second set of data has a much larger variance (or standard deviation) than that of the first set of data. This may mean that the distribution of the tracer concentration for the second set is not as uniform as the first set of runs. The nonuniformity of tracer concentration is expected, because a thorough agitation or stirring probably can not be obtained by using only one row of holes for air passage.

From the above argument, one may conclude that the stratified elements observed half way between the inlet and bubble zone are not completely elimi- nated by the bubble zone; the effect of stratification on the degree of liquid mixing still exists. The effect can be decreased by increasing the degree of

TABLE 11. NUMERICAL VALUES OF THE AVERAGES, VARIANCES, AND

STANDARD DEVIATIONS OF $\Delta\sigma^2_{\theta YX}$, β, p AND τ_d.

	Variance $\Delta\sigma^2_{\theta YX}$		Bypassing parameter β		Parameter p		Dead time parameter τ_d	
	1st set	2nd set	1st set	2nd set	1st set	2nd set	1st set	2nd set
Average	0.1429	-0.0962	0.755	0.662	5.96	688.66	0.515	0.682
Variance	0.132	5.122	0.0175	0.0213	0.779	3.256	0.02175	0.00507
Standard Deviation	0.3638	2.263	0.1323	0.1462	0.8825	1.8045	0.1475	0.0712

agitation, for instance, increasing the percentage of free area.

Analysis of the model parameters

Two different distribution curves can have equal values of the variance. In order to characterize the shape of the distribution curve and also the physical significance of the distribution curve in this system, an exit age distribution function, namely the Γ-distribution model with by-passing across the Γ-mixing unit was used in this work as stated previously.

The parameter, β, in the Γ-mixing model with by-passing across the Γ-mixing unit, is defined as the ratio of the volumetric flow rate through the Γ-mixing unit to the total volumetric flow rate. The value of $1-\beta$ hence represents the ratio of the volumetric flow rate of the bypassing stream to the total volumetric flow rate. In other words, the value of $1-\beta$ represents the fraction of the entering fluid being bypassed. The average value of β for the first set of data is 0.755, i.e. 24.5% of the entering fluid being bypassed, while the average value of β for the second set of data is 0.662, i.e. 33.8% of the entering fluid being bypassed. The variance and standard deviation of β for the first set of data are 0.0175 and 0.1323, while those for the second set of data are 0.0213 and 0.1462 respectively, (see Table 11). It appears that the nonuniformity of the tracer concentration distribution or the stratification effect has only slight effect on the bypassing parameter.

The parameter, p, of the Γ-mixing unit has a physical meaning related to the number of pools connected in series. The parameter, p, can be any value equal to or greater than one, but not necessarily integer in this model. The physical significance constrains that p must be greater than one. The parameter p represents complete mixing or backmix when it is equal to one,

and plug flow when it is equal to infinity. The values of all the p's

obtained in this work are greater than one. This indicates that the use of

the Γ-distribution model with bypassing across the Γ-mixing unit can pro-

perly describe the system. The average values of p for the first set and

the second set are 5.96 and 688.66 respectively. The average value of p for

the first set of data is much smaller than that of the second set of data.

This again means that the mixing conditions for the first set of runs is

closer to the completely mixed state while that for the second set of runs is

closer to plug flow. Comparison of the p values of these two sets of runs

enables one to conclude that the p value will become close to unity as the

number of holes increases.

The value of the variance of p for the first set is 0.779 and that for

the second set is 3.256. The standard deviations for the first set and the

second set are, therefore, 0.8825 and 1.8045 respectively. This also means

that the stratification affects the model parameter, p. However, the effect

of stratification on the degree of liquid mixing and the values of model

parameter p may be decreased by increasing the number of holes.

τ_d represents the dimensionless dead time. τ_d was defined in the model

as the total volume of the plug flow unit divided by the volume of the system.

As has been described, the dead time D was experimentally determined by taking

the difference between times at the incipient responses or at the onsets of

the responses of the output $Y(t)$ and input $X(t)$. The dimensionless dead

time, τ_d, was then calculated by dividing D by $\bar{t}$, the mean residence time.

Theoretically for the plug flow model, the difference between time at the

onset on the responses of output $Y(t)$ and input $X(t)$ will be the time required

for each fluid element to travel from the inlet to the outlet. Therefore,

the dead time is equal to the mean residence time, and the dimensionless dead time will hence be equal to unity. As a backmix model, the dimensionless dead time approaches zero because there is no concentration gradient existing in the backmix system. The reasonable value for τ_d hence lies between one and zero. The average value of the first set of data is 0.515, and 0.682 for the second set of data (see Table 11). These values also show that τ_d of the first set is smaller than that of the second set. This appears to be reasonable because the first set of runs is closer to backmix than the second set of runs as mentioned previously. The variance of τ_d for the first set is 0.02175 and 0.00507 for the second set. The corresponding standard deviations of τ_d for the first set is 0.1475 and for the second set is 0.0712. The variances (or standard deviations) for the first set and the second set are all small. It appears that the effect of stratification on the model parameter τ_d is small.

Conclusions

1. The pulse testing technique using sodium chloride solution as a tracer material has been shown to be an effective experimental technique for gathering information on liquid mixing in a flow system. A tremendous amount of time and money can be saved by using the conductivity measurement instead of the measurement of radioactivity, which was used in the previous work. The response of the instrument required for the conductivity measurement can also be made sufficiently fast. The instrument used in this work has a time constant of about 0.25 sec. The advantages can be listed as follows:

    a. Salt tracer is much cheaper than radioactive isotopes.

    b. The source of salt tracer is almost unlimited.

    c. Biological effects are negligible.

    d. Waste disposal problems can be avoided.

2. The degree of liquid mixing and the parameters in the mixing model are affected by a stratification effect, when the experiment is carried out using only a pair of probes.

3. The extent of the stratification effect on the degree of liquid mixing and the model parameter, p, can be decreased by increasing the agitation and stirring of the system, for instance, an increase in number of openings or in the size of free area for vapor phase passage.

4. The Γ-distribution model with by-passing across the Γ-mixing unit adequately describes the liquid mixing on a distillation tray. The Γ-mixing model with by-passing from the inlet to the outlet is also expected to be adequate in describing liquid mixing on a full size sieve plate distillation column.

5. The moments method of analysis is a convenient way for evaluating the degree of liquid mixing.

6. The s-plane analysis is a suitable method for the evaluation of model parameters.

7. The tracer monitoring can be carried out by inserting several probes over the same cross section at the downstream or at the upstream. The concentration-time curve can be obtained by taking the average concentration from the curves (recorded from the responses of the probes) at the corresponding time.

Figures 27a,b,c, and d show the hypothetical response curves of the four probes located at equal distance over the cross section of the liquid stream. One can combine these four response curves to obtain a single response curve by simply taking the arithmetic average of the four responses at various

times. For instance, let one define $\bar{c}(t)$ as a single response, $c_1(t)$, $c_2(t)$, $c_3(t)$, and $c_4(t)$ are responses for Fig. 27a,b,c, and d respectively. One has, for the combined response,

$$\bar{c}(0) = \left[c_1(0) + c_2(0) + c_3(0) + c_4(0) \right] \times \frac{1}{4}$$

$$= \left[0 + 0 + 0 + 0 \right] \times \frac{1}{4}$$

$$= 0$$

$$\bar{c}(1) = \left[0 + 200 + 100 + 0 \right] \times \frac{1}{4}$$

$$= 755$$

$$\bar{c}(10) = \left[1980 + 2100 + 2080 \right] \times \frac{1}{4}$$
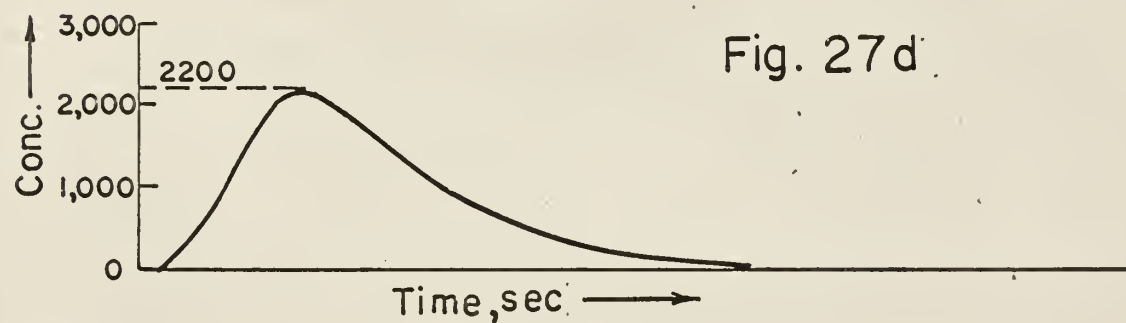
$$= 2090 \;.$$
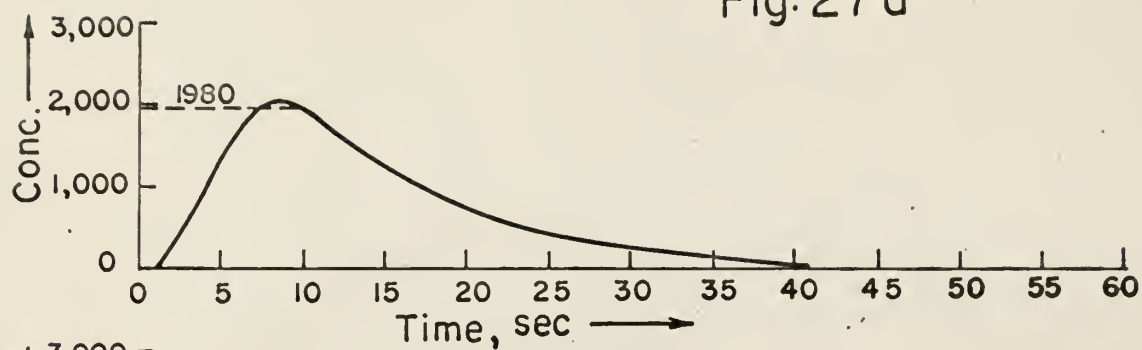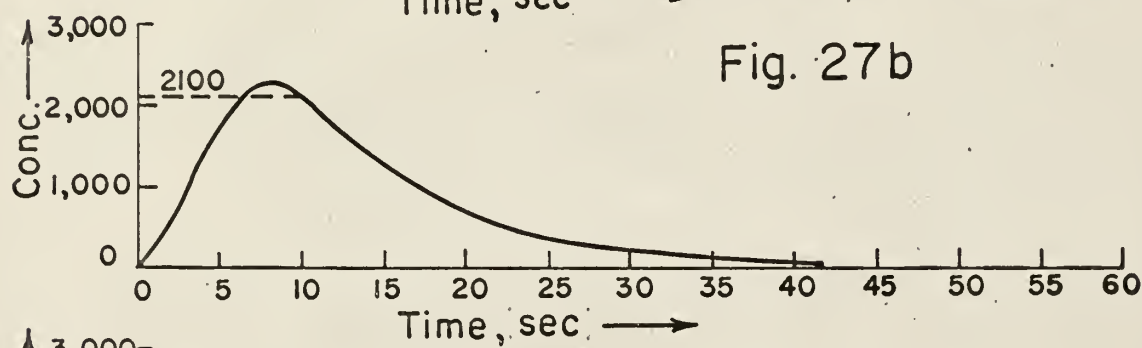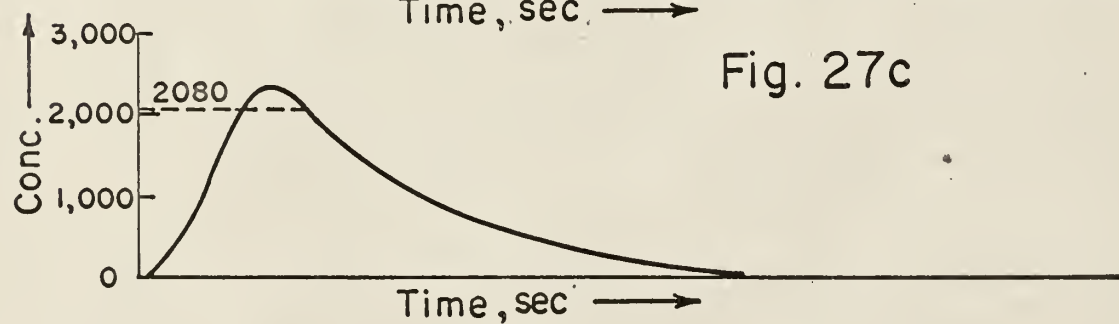
Fig. 27a, b, c, d. Hypotherical response curves

CHAPTER X

PROPOSAL FOR FUTURE STUDY

<u>Further study of liquid mixing on distillation trays</u>

A correlation chart or working equations for the reliable evaluation
of the degree of liquid mixing, which is an important factor of the overall
tray efficiency would be useful to designers. This chart, or equations,
should show the relationship between the model parameters and the four
variables, i.e. liquid rate, gas rate, weir height, and percentage of free
area. It would be convenient to prepare a correlation chart in such a way
that the relationship between the parameters and the dimensionless groups,
such as the Reynolds number and the Froude number, etc. are shown. In order
to prepare a good correlation chart, a large amount of additional data is
required. The data should include several different sources: data from the
previous study (1), data from the non-ideal sieve tray used in this work, and
data from a multistage distillation column. Comparison of the results of
these different sources of data can provide a more reliable industrial appli-
cation of the chart.

<u>Additional data for liquid mixing on non-ideal sieve tray</u>

1. Considerable attention should be given to setting up a good statis-
tical design for experimental runs before any data are taken. A factorial
design (see Appendis 3) is recommended here. This factorial design should
include four levels for each variable, i.e. $4^4=256$ runs, not including repli-
cate runs. We might start with a three level design for each variable which
requires $3^4=81$ runs as shown in the shaded area of Appendix 4.

2. The Γ-distribution model with by-passing across the Γ-mixing unit

has been proved to be adequate in describing the flow pattern. Another form of the Γ-mixing model with a different path for by-passing — the Γ-distribution model with bypassing from inlet to outlet can also be used to fit the experimental data. Comparison of the fit of the two models will clarigy further the mechanism of bypassing.

3. Another interesting investigation is to insert several baffle plates into the bubble zone at different depths without touching the bottom of the tray. Changes in the residence time and bypassing may thus be detected. Decreases in bypassing and mixing in the direction of flow are known to be favorable to the increase of Murphree liquid efficiency.

4. The actual cause of the oscillation phenomenon in the distillation tray still remains unknown. It should be investigated further.

5. The investigation may be repeated using a non-Newtonian fluid.

Additional data for liquid mixing on multi-stage distillation column

A three-stage distillation column is being built in the department of chemical engineering, Kansas State University. This will enable one to study liquid mixing on actual distillation trays by using the conductivity method. The study may include sieve trays, bubble cap trays and valve trays etc.

The study of concentration transients in response to flow rate changes

The study of concentration transients in response to flow rate changes can be carried out in a tube or a coil using experimental techniques described in this work. A tee-fitting at the outlet of the tube separates the flow into two lines, one of which is equipped with a solenoid valve and a globe valve, the other with a globe valve. Under steady state condition, the concentration will be constant at a fixed point if the effect of turbulent fluctuation can

be neglected. By varying the settings of the globe valves it is possible to introduce a step change in velocity which in turn leads to a change in concentration along the axial direction of the tube.

If an electrolyte is used as a tracer, one can measure the transient concentration response by using several well-designed conductivity probes located at different positions along the axial direction of the tube.

Assuming plug flow, no axial mixing, perfect radial mixing, constant physical properties, and constant overall mass transfer coefficient with length, one may first try to fit the following equation to the experimental data, i.e. (50)

$$\frac{\partial C}{\partial t} + \left[1 + r(t)\right]\frac{\partial C}{\partial x} = - P_o \left[1 + b\,r(t)\right] C$$

where

C = dimensionless concentration

t = dimensionless time

r(t) = function of flow disturbance

x = dimensionless distance along the tube

b = rate of change of overall mass transfer coefficient with fluid flow rate.

P_o = the measure of effectiveness of mass transfer, which equals zero if there is no mass transfer taking place from the wall (or packing) to the fluid.

If r(t) is a step change in flow, r(t) = a u(t), the above equation has an exact solution as follows (50)

$$C = \begin{cases} \exp(-P_o[x - a(1-b)t]) & , \quad t < \dfrac{x}{1+a} \\[2em] \exp(-P_o[-\dfrac{x(1+ab)}{1+a}]) & , \quad t > \dfrac{x}{1+a} \end{cases}$$

where
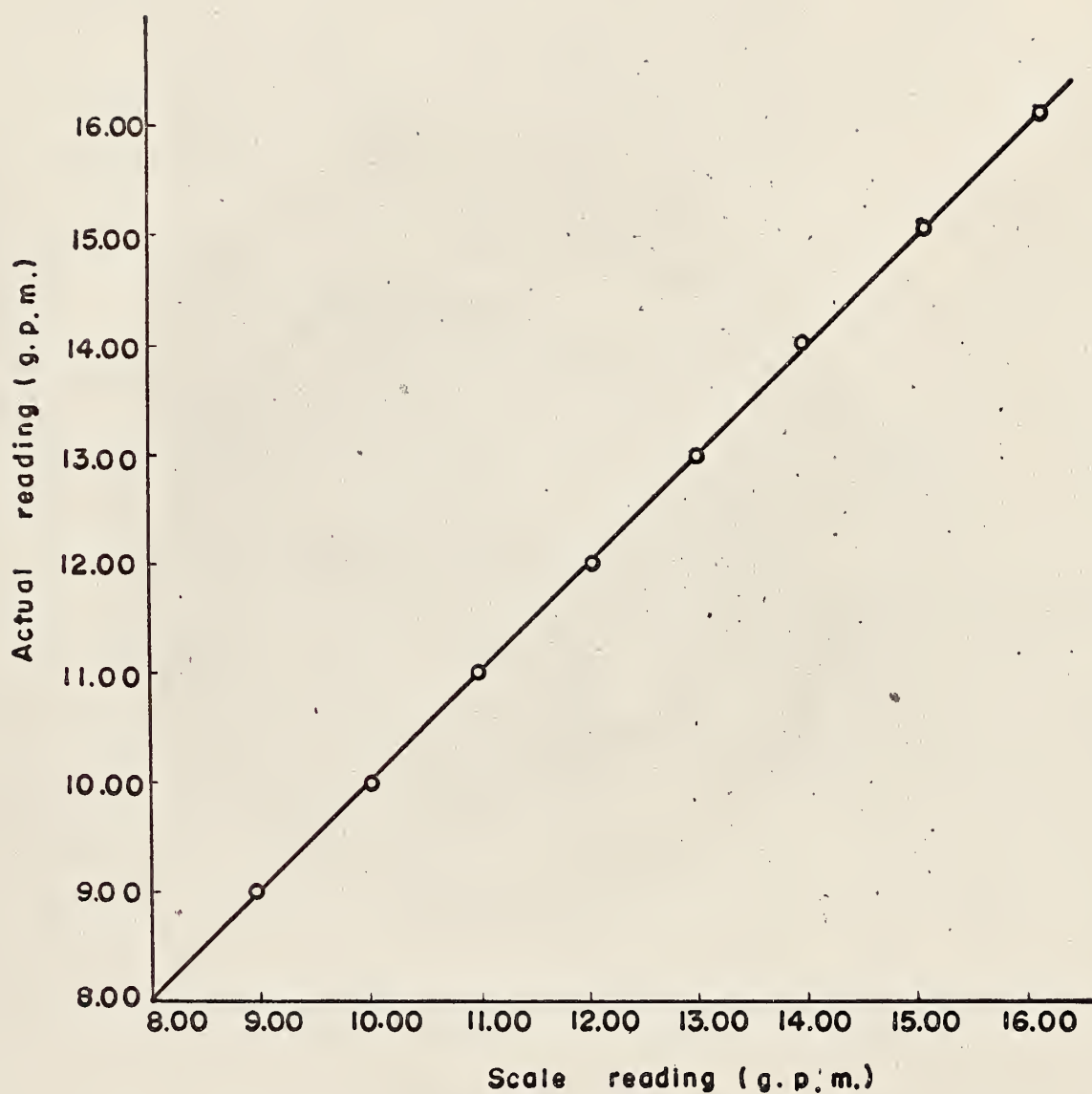
a = dimensionless magnitude of step change in flow rate

u(t) = unit step change

The effect of axial dispersion can be taken into account by modifying the governing equation to

$$\frac{\partial C}{\partial t} + E_x(t)\frac{\partial^2 C}{\partial c^2} + [1 + r(t)]\frac{\partial C}{\partial x} = -P_o[1 + b\,r(t)]C$$

where

$E_x(t)$ = the axial eispersion coefficient and is a function of time
in this case

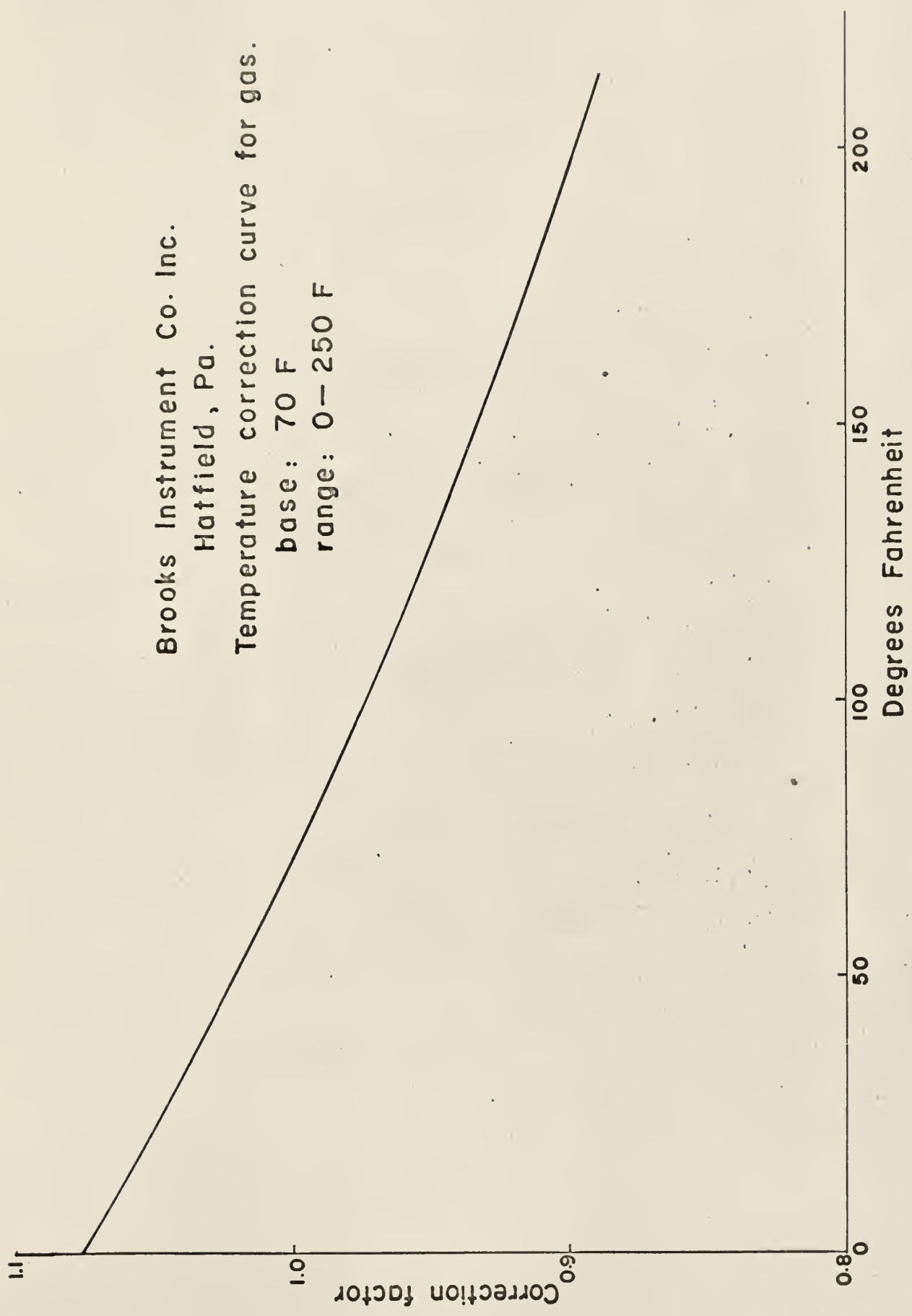Appendix I a. Rotameter I, Calibration curve (Sp. Gr.=1).
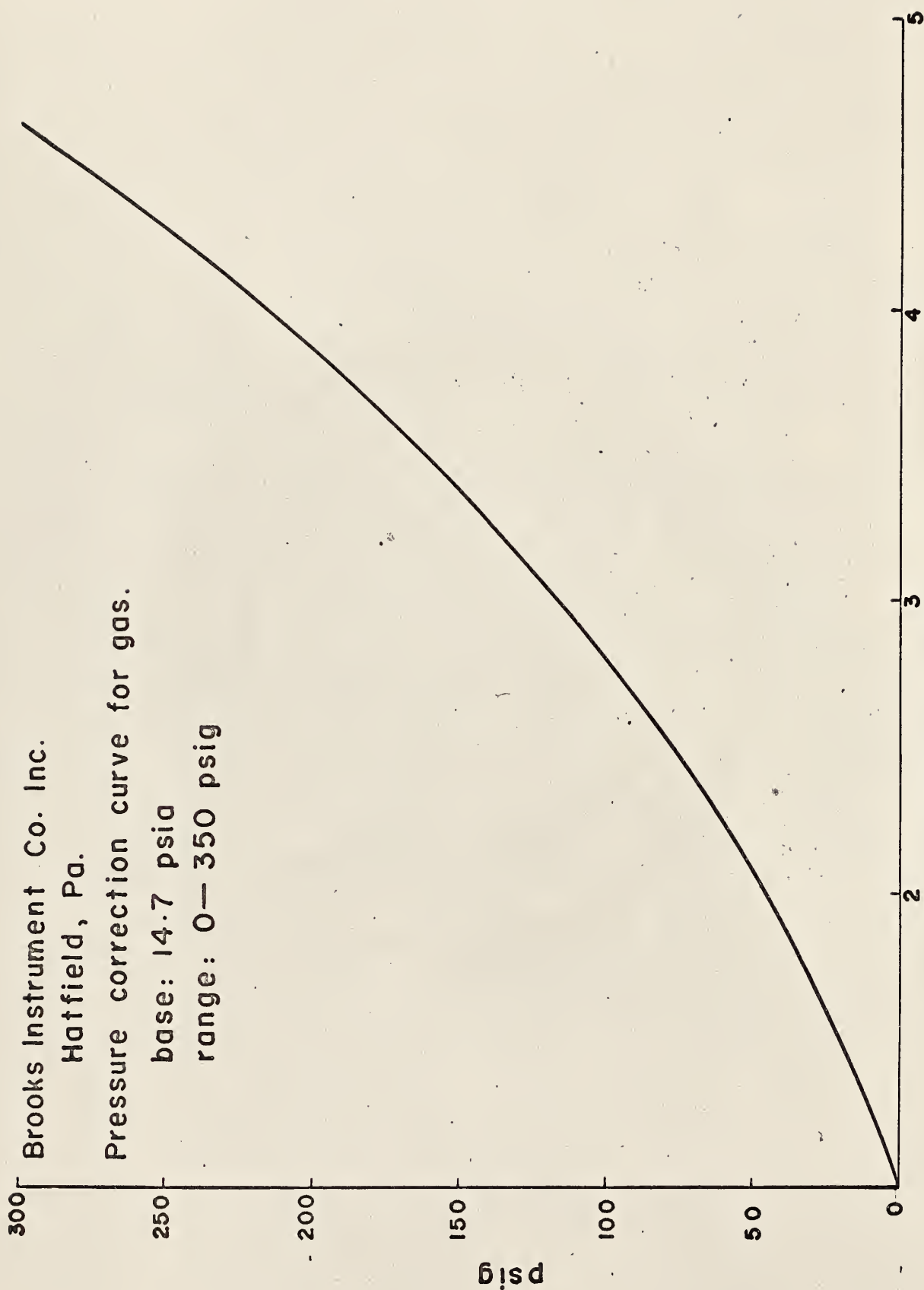
Brooks Instrument Co. Inc.
Hatfield, Pa.
Temperature correction curve for gas.
base: 70 F
range: 0–250 F

Degrees Fahrenheit

Correction factor

Appendix 2a. Temperature correction curve for gas.

Appendix 2b. Pressure correction curve for gas.

APPENDIX III

DESIGN OF THE CONDUCTIVITY INSTRUMENT SYSTEM

The conductivity measurement system used in this work were designed by the Industrial Instruments Inc., Cedar Grove, N. J.. This system contains two Type RA4 Solu Meters and two probe type conductivity cells.

The following is a brief description of the instruments and the prices:

Type RA4-WB Solu Meter, range 0-2500 micromhos/cm
specific conductance refer to 25° C with
meter 0-25 evenly divided and 0-10 mv DC
output proportional to conductivity; for
115 V 60 cycle AC operation at .... $ 231.00 ea.

Probe type conductivity cells, epoxy,
approximetely 12" long and 5 mm OD;
platinum electrodes and cell constant
of 0.50/cm at .... $ 55.00 ea.

WH: weir height , L: liquid rate

PF : percentage free area

G : gas rate

COMMENT : Shaded area for 3 levels experimental runs

Appendix 4. Proposed statistical design of the
experimental work for four level

ACKNOWLEDGEMENT

LITERATURE REVIEW

1. Johnson, J. L., Ph.D Thesis, Department of Chemical Engineering, Kansas State University, Manhattan (1966).

2. Danckwerts, P. V., Chem. Eng. Sci., 1, 1 (1953).

3. Noar, P. and R. Shinnar, I&EC Fundamentals, 2, 4, (1963).

4. Bell, R. L. and A. L. Balb, On the interpretation of measured residence time distributions in chemical process equipment. A.I.Ch.E. Reprint 22E Fifty-eight annual meeting, December 5-9 (1965).

5. Danckwerts, P. V., Chem. Eng. Sci. 2 (1958).

6. Spalding, D. B., Chem. Eng. Sci. 9, 74 (1958).

7. Zweitering, T. N., Chem. Eng. Sci 11, 1 (1959).

8. Levenspiel, O. "Chemical Reaction Engineering, John Wiley & Sons Inc., New York (1962).

9. Eguchi, W., Proc. 25th Anniv. Congress, Soc. Chem. Eng. (Japan), Nov. (1961).

10. Sater, V. E. and Octave Levenspiel, I&EC Fundamentals 5, 1 (1960).

11. Leonard, E. F., Ph.D dissertation, Department of Chemical Engineering, University of Pennsylvania, Philadelphia (1960).

12. Hay, J. R., M.S. Thesis, Department of Chemical Engineering, Vandervilt University, Nashville, Tenn (1964).

13. Hay, J. R., A.I.Ch.E. Annual meeting, Philadelphia Dec 5-9 (1965).

14. Clements, W. C. Jr., Ph.D dissertation, Vandervilt University, Nashville, Tenn. (1963).

15. Otto, R. E. and Jr. Stout, Chemical Engineering Progress Symposium Series, Process Dynamics and Control, 36, 57 (1961).

16. Moser, J. H. and C. R. Cupit, Fifty-eight National Meeting, Reprint 5D Dallas, Texas, Feb. 6-9 (1966).

17. Bishoff, K. B. and E. A. Mccraken, Principles of the interpretation of tracer tests of flow systems part 1 & 2.
    Manuscript from I&EC Research Results, Service treat as a private communication (1966).

18. Adler, R. J., "Finite Stage Modeling". Presented at the Fourth National Chemical and Petroleum Symposium of the Instr. Society of America, May (1961).

19. Kirchabum, E., "Distillation and Rectification", Trans. by M. Wulfinghoff, Brooklyn Pub. Co. (1948).

20. Nord, M., Trans. Am. Inst. Chem. Engrs., 42, 863 (1946).

21. Gatreaux, M. F., and H. E. O'Connell, Chem. Eng. Prog., 51, 232 (1961).

22. Mickley, H. S., L. A. Gould, and L. M. Schwartz, Canadian Journal of Chemical Engineering., 137, 14 (1961).

23. Oliver, E. D., and J. Marangozis, Can. J. of Chem. Eng., 36, 161 (1958).

24. Warzel, L. A., Ph.D Dissertation, University of Michigan (1955).

25. Johnson, A. I., and J. Marangozis, Can. J. of Chem. Eng., 36, 161 (1958).

26. Anderson, J. E., Sc.D. Dissertation, M.I.T. (1954).

27. Gerster, J., et.al., "Tray Efficiency in Distillation Column", Final Report from University of Delaware, A.I.Ch.E., New York (1958).

28. Welch, N. E., Ph.D Dissertation, Texas A & M University, College Station (1958).

29. Iyer, S. R. and P. S. Murti, Indian J. Technol. 3, 75 (1964).

30. Foss, A. S. et.al. A.I.Ch.E. Journal 4, 231 (1958).

31. Mutzenberg, A., Chem. Eng. Techn. 34, 542 (1962).

32. Olson, R. E. and W. J. Heidiger, University of Washington, Seattle (1962).

33. Strand, C. P., Chem. Eng. Prog. 59, 58 (1963).

34. A.I.Ch. E. "Tray Efficiencies in Distillation Columns," Final Reports of Research Committee (1958, 1959, 1960).

35. Cha, L. C., Ph.D Dissertation, Department of Chemical Engineering, Kansas State University, Manhattan (1965).

36. Perry, J. H., R. H. Perry, C. H. Chilton, and S. H. Kirkpatrick, "Perry's Chemical Engineers' Handbook." Fourth Edition, McGRAW-HILL BOOK COMPANY INC., New York (1963).

37. A.I.Ch.E. Research Committee, "Bubble Tray Design Manual" (1958).

38. Brown, G. G., "Unit Operations" Second Printing, John Wiley & Sons Inc., New York (1951).

39. Yakubovich, V. I. Ulanov, and A. V. Machinskii, Zavodsk. Lab., 29 (9), 1141-3 (1963).

40. Westerterp, K. R. and P. Landsman, Chem. Eng. Sci. $\underline{17}$, 4 (1962).

41. Woong Ki Kang (At. Energy Res. Inst., Seoul) Ta Han Hsueh Hui-Chih, 6(2), 130-2 (1962).

42. Stenhagen, E. and O. Mellander, Acta Chem. Scan. $\underline{10}$, 1317-26 (1956).

43. Prausnitz, J. M., Ph.D Dissertation, Department of Chemical Engineering, Princeton University, New Jersey (1955).

44. Manning, F. S., Ph.D Dissertation, Department of Chemical Engineering, Princeton University (1959).

45. Schlichting, H., "Boundary Later Theory" Fourth Edition, McGRAW-HILL BOOK COMPANY, INC., New York (1960).

46. 24th Meeting of the European Federation of Chemical Engineering Proceedings of the International Symposium on Distillation, Brighton, England 4/5/6 May (1960).

47. Teller, A. J. and R. E. Rood, A.I.Ch.E. Journal, July (1962).

48. Cheng, S. I., and A. J. Teller, A.I.Ch.E. Journal, $\underline{7}$, 282 (1961).

49. Rooze, J. M., Bulletin SRC 20-C-62-6, Systems Research Center, Case Institute of Technology (1962).

50. Kamman, D. T. and L. B. Koppel, I&EC $\underline{5}$, 2 (1966).

51. McALLISTER, R. A. and C. A. Plamk, A.I.Ch.E. Journal $\underline{4}$, 3 (1958).

AN EXPERIMENTAL INVESTIGATION OF LIQUID MIXING
ON A NONIDEAL SIEVE TRAY

by

TSUNG-WEN LEE

B. S., National Taiwan University, Taiwan, China, 1962

_____

AN ABSTRACT OF A MASTER'S THESIS

submitted in partial fulfillment of the

requirements for the degree

MASTER OF SCIENCE

Department of Chemical Engineering

KANSAS STATE UNIVERSITY
Manhattan, Kansas

1967

A 12 x 48" rectangular sieve tray column with rectangular downcomers was used to study liquid mixing effects on a non-ideal plate. Using the air-water system, liquid mixing tests were made by using the pulse testing technique. Sodium chloride was used as a tracer. Data were taken for a tray with one row of holes (15 holes) and three rows of holes (43 holes).

Various flow patterns were visually observed and were also photographically recorded and analyzed. By using conductivity measurements, the effect of stratification on the degree of liquid mixing was investigated. Using the technique, a tracer monitoring technique was developed. Experimental data were analyzed by using the moments method in which the values of the difference of the second moments about the mean between the input and output pulses, σ_θ^2, were calculated. The Γ-distribution model with bypassing and a modified model with a different path for bypassing were employed to fit the experimental data.

Future work has been proposed, which includes a statistical design of experimental work.